AFCRL-66-828
DECEMBER 1966
ENVIRONMENTAL RESEARCH PAPERS, NO. 241

OPTICAL PHYSICS LABORATORY PROJECT 7670
AIR FORCE CAMBRIDGE RESEARCH LABORATORIES
L. G. HANSCOM FIELD, BEDFORD, MASSACHUSETTS

An Atlas of Aerosol Attenuation and Extinction Profiles for the Troposphere and Stratosphere

L. ELTERMAN

OFFICE OF AEROSPACE RESEARCH
United States Air Force

Abstract

Light scattering measurements were carried out to determine the aerosol properties of the atmosphere. First the expression for the aerosol attenuation coefficient is derived, based on the field geometry in conjunction with Rayleigh and aerosol scattering considerations. Then the results derived from the measurements are discussed. The paper concludes with an atlas of 105 profiles for altitudes to about 35 km (the data does not exclude the presence of aerosols with low number density between 35 to 70 km). These profiles consist of aerosol attenuation and extinction coefficients as a function of altitude. Since the coefficients are proportional to aerosol number density, the profiles yield information concerning aerosol stratification. A plot for the computed mean of the 105 vertical profiles is included.

Contents

Illustrations

Tables

Symbols

A = area (normal to beam axis) of scattering volume (cm^2)

B = base line distance between projector and collector (cm)

D = diameter of projector mirror (cm)

E = irradiance ($watts/cm^2$)

E_{rp} = instrumentation response (volts)

F_d = total energy at detector (watts)

F_s = total energy of source (watts)

h = altitude (km)

$J(\phi_s)$ = intensity of angular scattered energy (watts/ster)

L = length of scattering volume (cm)

$P_p(\phi_s)$ = normalized aerosol phase function (sr^{-1})

$P_r(\phi_s)$ = normalized Rayleigh phase function (sr^{-1})

R = distance between source and scattering volume (cm)

T_d = total transmission between source and scatter volume

T_p = aerosol transmission for both slant paths

T_r = Rayleigh transmission for both slant paths

T_s = total transmission between source and scatter volume

Z = zenith angle

β_p = aerosol attenuation coefficient (km^{-1})

β_r = Rayleigh attenuation coefficient (km^{-1})

$\beta(\phi_s)$ = total volume scattering function ($cm^{-1} ster^{-1}$)

θ = beam divergence

λ = wavelength) (μ)

τ_p = aerosol optical thickness

ϕ_β = angle between beam and collector field

ϕ_d = elevation angle of detector mirror

ϕ_p = elevation angle of projector mirror

ϕ_s = scattering angle

ω = solid angle subtended by collector with apex at element of scattering volume (steradian)

An Atlas of Aerosol Attenuation and Extinction Profiles for the Troposphere and Stratosphere

1. INTRODUCTION

In nearly all problems concerned with the interaction of light with the atmosphere, the aerosol attenuation coefficient in the troposphere and stratosphere emerges as an indispensible and little known parameter. But it is an important parameter because it describes quantitatively how the aerosol content of the atmosphere effects the passage of light. Also, because of its proportionality to the aerosol number density, this parameter provides information concerning aerosol stratification. There has been much emphasis on aircraft, balloons, and rockets in the pursuit of this research discipline. However, ground-based remote sensing methods have great merit. First, they have the important capability of performing true in situ measurements. Then there is the added advantage of being able to acquire large quantities of data at relatively small cost.

In this report, the searchlight method of optical probing used in New Mexico is summarized. Although measurement capability at 0.55 micron wavelength exceeds 70 km, the altitudes of interest will be discussed up to 35 km because above this altitude the measurements show that aerosol attenuation for most purposes can be neglected. A description of the methods used was published recently (Elterman, 1966). At this time, the primary objective is to present an atlas of profiles.

(Received for publication 28 November 1966)

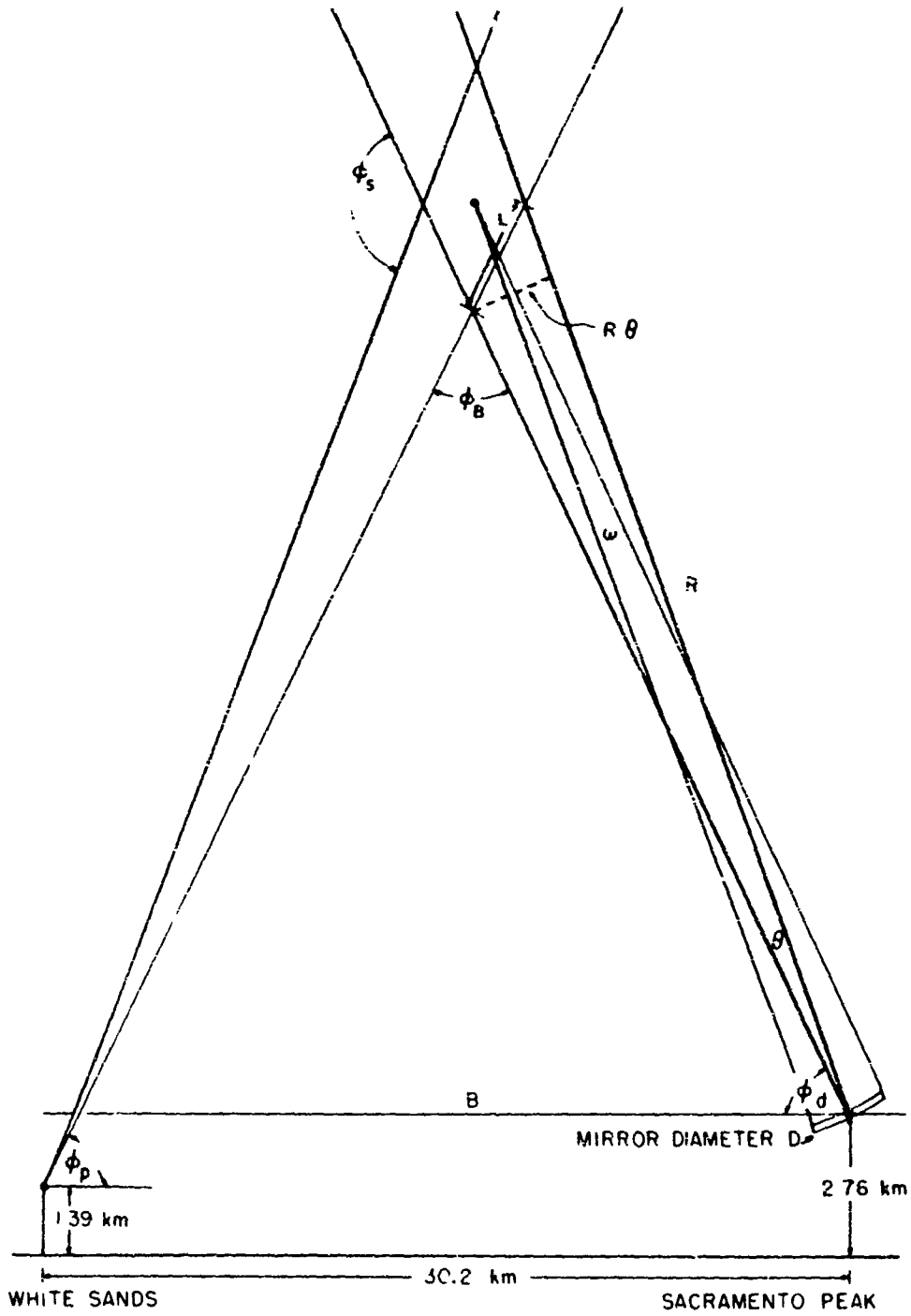

Figure 1. Searchlight Scene Geometry in New Mexico. Projector elevation angle $\phi_p = 75^o$, beam and collector field divergences are adjusted to 1.7^o and 2.0^o, respectively. Both divergences are exaggerated in this figure

Table 1. Computer Output (partial tabulation)
Measurement on 13 April 1964 at 00:18

Collector Elevation (degrees) ϕ_d	Scatter Volume Altitude (km)	Scatter Angle (degrees) ϕ_s	Detector Response (normalized) E_{rp}	Rayleigh Coefficient β_r (km^{-1})	Aerosol Coefficient β_p (km^{-1})
0	2.76	75	93.95	8.852×10^{-3}	9.50×10^{-3}
1	3.28	76	89.20	8.396	9.72
-	-	-	-	-	-
-	-	-	-	-	-
-	-	-	-	-	-
20	12.65	95	23.49	2.674	5.74×10^{-4}
21	13.14	96	22.03	2.478	5.85
22	13.63	97	20.93	2.291	7.49
23	14.13	98	19.83	2.117	8.79
24	14.63	99	19.26	1.962	1.20×10^{-3}
25	15.12	100	18.53	1.812	1.45
26	15.63	101	17.80	1.675	1.66
27	16.13	102	16.34	1.547	1.44
28	16.64	103	14.87	1.428	1.17
29	17.16	104	13.73	1.319	1.03
30	17.67	105	12.89	1.214	1.04
31	18.20	106	11.95	1.122	9.33×10^{-4}
32	18.73	107	11.17	1.031	9.09
33	19.26	108	10.23	9.491×10^{-4}	7.63
34	19.80	109	95.10×10^{-1}	8.715	7.20
35	20.35	110	88.38	7.940	7.08
36	20.90	111	81.19	7.301	6.06
37	21.46	112	73.07	6.662	4.44
38	22.03	113	66.87	6.114	3.49
39	22.61	114	62.05	5.567	3.46
40	23.20	115	55.91	5.065	2.40
-	-	-	-	-	-
-	-	-	-	-	-
-	-	-	-	-	-
57	35.28	132	10.00×10^{-1}	7.711×10^{-5}	0.00 (neglected)

2. ENERGY TRANSFER EQUATIONS

Figure 1 presents the searchlight scene geometry. The projecting mirror is parabolic with a diameter of 91.4 cm, and its elevation angle is fixed. The collecting mirror is identical, and scans up or down the beam with elevation angle ϕ_d. The beam and field of view are aligned precisely so as to be co-planar for all elevation angles. Approximately 30 minutes is required for a continuous scan of the beam over the altitude range 3.8 to 35.3 km (0 to 57° elevation). The altitude of the scattering volume is established by the intersection of the optical axis of the beam and the collector field of view. The altitude resolution averages about 1 km. A partial list of the geometrical relationships is shown in Table 1.

Since the divergences of the beam and collecting field are small, the opposing extremities of the scattering volume are nearly equal, both angularly and in length. From the scene geometry (see Figure 1), the equations for the energy transfer are:

(1) Source to Scattering Volume

$$F_s \cdot T_s = EA \tag{1}$$

where:

F_s = total energy of source (watts)

T_s = transmission (molecular + aerosol) source to scatter volume

A = area (normal to beam axis) at scattering volume, receiving incident radiation (cm^2)

E = irradiance incident on area A ($watts/cm^2$)

(2) At the Scattering Volume

$$J(\phi_s) = E\,A\,L\,\beta(\phi_s) \tag{2}$$

where:

ϕ_s = scattering angle

$J(\phi_s)$ = intensity of angularly scattered light (watts/steradian)

$\beta(\phi_s)$ = (molecular + aerosol) angular scattering function ($cm^{-1}ster^{-1}$)

L = length of scattering volume (cm)

(3) Scattering Volume to Detector

$$F_d = J(\phi_s)\,T_d\,\omega \tag{3}$$

where:

F_d = total energy at detector (watts)

T_d = transmission (molecular + aerosol) scatter volume to detector

ω = solid angle subtended by collector with apex at element of scattering volume (steridians)

Combining Eqs. (1), (2) and (3), the energy at the detector is

$$F_d = F_s\,T_s\,T_d\,L\,\omega\,\beta(\phi_s) \tag{4}$$

From Figure 1 it follows that the product $L\omega$ is constant; that is,

$$L = R\,\theta/\sin\,\phi_B \tag{5}$$

$$\sin\,\phi_B = \frac{B}{R}\sin\,\phi_p \tag{6}$$

$$\omega = \frac{\pi D^2}{4R^2} \tag{7}$$

and combining Eqs. (5), (6) and (7),

$$L\omega = \frac{\pi\ D^2\,\theta}{4B\sin\,\phi_p} = C_1 \tag{8}$$

Here $\phi_p = 75^\circ$ and C_1 is the constant.

The instrumentation response to the scattered energy is linear so that $E_{rp} = C_2\,F_d$. Also, measurements show that the variation of source intensity for each scan is small so that F_s can be assigned the constant C_3. If the constants are combined, $C = C_1\,C_2\,C_3$, and Eq. (4) becomes

$$E_{rp} = C\,T_s\,T_d\,\beta\,(\phi_s) \tag{9}$$

Rearranging the transmissions and expressing the volume scattering function by its components,

$$T_s\,T_d = T_r\,T_p \tag{10}$$

and

$$\beta\,(\phi_s) = \beta_r P_r(\phi_s) + \beta_p\,P_p\,(\phi_s) \tag{11}$$

where:

T_s = total transmission source to scatter volume

T_d = total transmission detector to scatter volume

T_r = Rayleigh transmission for both slant paths

T_p = Aerosol transmission for both slant paths

β_r = Rayleigh attenuation coefficient (cm^{-1})

β_p = Aerosol attenuation coefficient (cm^{-1})

$P_r(\phi_s)$ = normalized Rayleigh phase function ($steradian^{-1}$)

$P_p(\phi_s)$ = normalized aerosol phase function ($steradian^{-1}$)

Equation (9) takes the form

$$E_{rp} = C\, T_r\, T_p\, [\beta_r \cdot P_r(\phi_s) + \beta_p \cdot P_p(\phi_s)] \tag{12}$$

where:

E_{rp} = instrumentation response (volts)

C = proportionality constant (volt cm steradian)

3. AEROSOL SCATTERING EQUATION AND ITS SOLUTION

Equation (12) has the limitation that the constant C is unknown. The procedure for evaluating C is demonstrated by referring to Figure 2 which represents a set of measurements obtained 8 May 1964 at 03:05. The ordinate is designated as the relative response since these values are normalized to unity at 35.3 km. Also shown is the calculated Rayleigh response for identical conditions. As in other measurements, the curves nearly converge over the last few kilometers. Accordingly, at about 35 km, aerosol scattering is assumed to be sufficiently small so that it can be neglected. Then Eq. (12) for these conditions becomes

$$E_{rp}(35) = C\, T_r(35)\, T_p(35)\, \beta_r(35)\, P_r(132^\circ) \tag{13}$$

Here 132° corresponds to the scattering angle for the 35.3 km altitude. Combining Eqs. (12) and (13), the altitude variation of the aerosol attenuation coefficient is expressed by

$$\beta_p(h) = \frac{E_{rp}(h)}{E_{rp}(35)} \cdot \frac{T_r(35)}{T_r(h)} \cdot \frac{T_p(35)}{T_p(h)} \cdot \beta_r(35) \cdot \frac{P_r(132^\circ)}{P_p(\phi_s)} - \beta_r(h) \cdot \frac{P_r(\phi_s)}{P_p(\phi_s)} \tag{14}$$

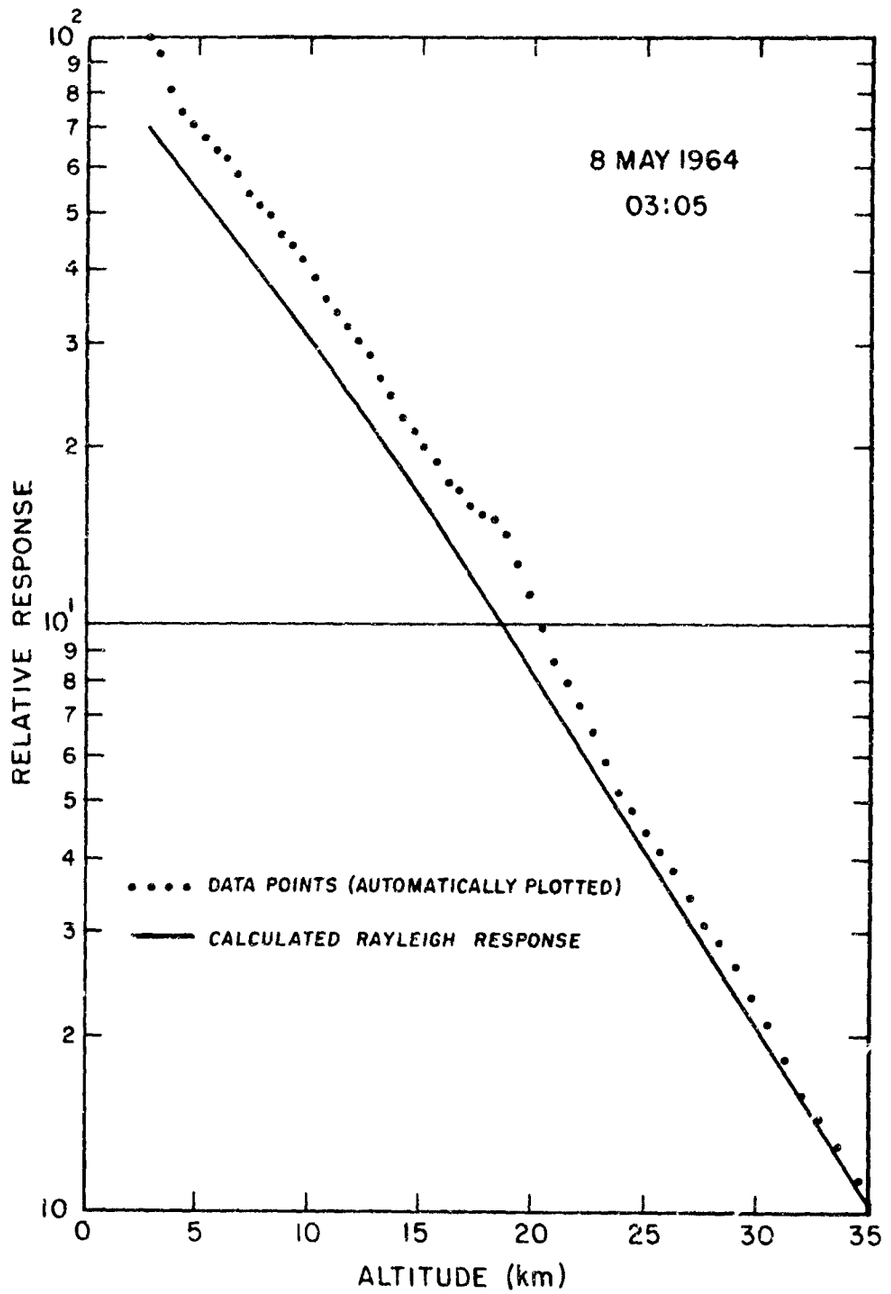

Figure 2. Instrumentation Response of Single Scan and Corresponding Rayleigh Values; Wavelength is 0.55 Microns

As mentioned, the terms $E_{rp}(h)$ and $E_{rp}(35)$ are obtained from the measurements. All the Rayleigh terms are calculated by using the Atmospheric Attenuation Model tabulations (Elterman, 1964) for 0.55 μ wavelength. The Rayleigh phase function is $P_r(\phi_s) = 0.75\ (1 + \cos^2 \phi_s)$. Assuming for the present that the aerosol phase function is established, then Eq. (14) has one unknown because $T_p(h)$ can be expressed in terms of $\beta_p(h)$

$$T_p(h) = \exp - \sum_{2.76}^{h} \bar{\beta}_p(h)\, \Delta h \sec Z(h) \qquad (15)$$

where:

$\bar{\beta}_p$ = mean value of β_p for the atmospheric layer (km^{-1})

Δh = layer thickness (km)

sec Z(h) = sum of the secants of the zenith angles for the beam and collector field slant paths

Since β_p exists in the transmission term as an exponent, the solution of Eq. (14) is not analytic. The method used is an iterative-convergent procedure. The iteration is started by using the Atmospheric Attenuation Model (Elterman, 1964) for 0.55 μ to calculate an initial series of aerosol transmission values, $T_p(h)$, applicable to the field geometry. Having done this, the Model values of $T_p(h)$ have no further function. The iteration proceeds as shown in Figure 3 until convergence is attained. Equation (11) then yields a final set of $\beta_p(h)$.

As to the choice of the aerosol phase function, $P_p(\phi_s)$, the literature is extensive with both computational and experimental studies. Here must be considered the work of Waldram (1945), Reeger and Siendentopf (1946), Bullrich and Moeller (1947 and 1964), Foitzik and Zschaeck (1952), Deirmendjian (1964), Fraser (1960), Barteneva (1960) and others who made important contributions to this area of research. The criteria finally considered for the choice of the phase function were (a) its derivation should be from field measurements with a meteorological range of at least 30 km, and (b) the phase function should permit Eq. (14) to converge within a reasonable number of iterations. The results of Reeger and Siedentopf (and there are others) readily meet these criteria. The aerosol phase function was derived from their measurements (see Figure 4).

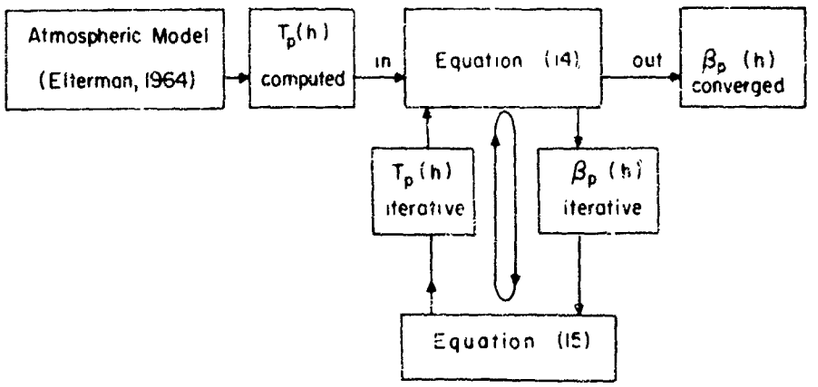

Figure 3. Iteration Procedure. T_p is aerosol transmission. β_p is aerosol attenuation coefficient

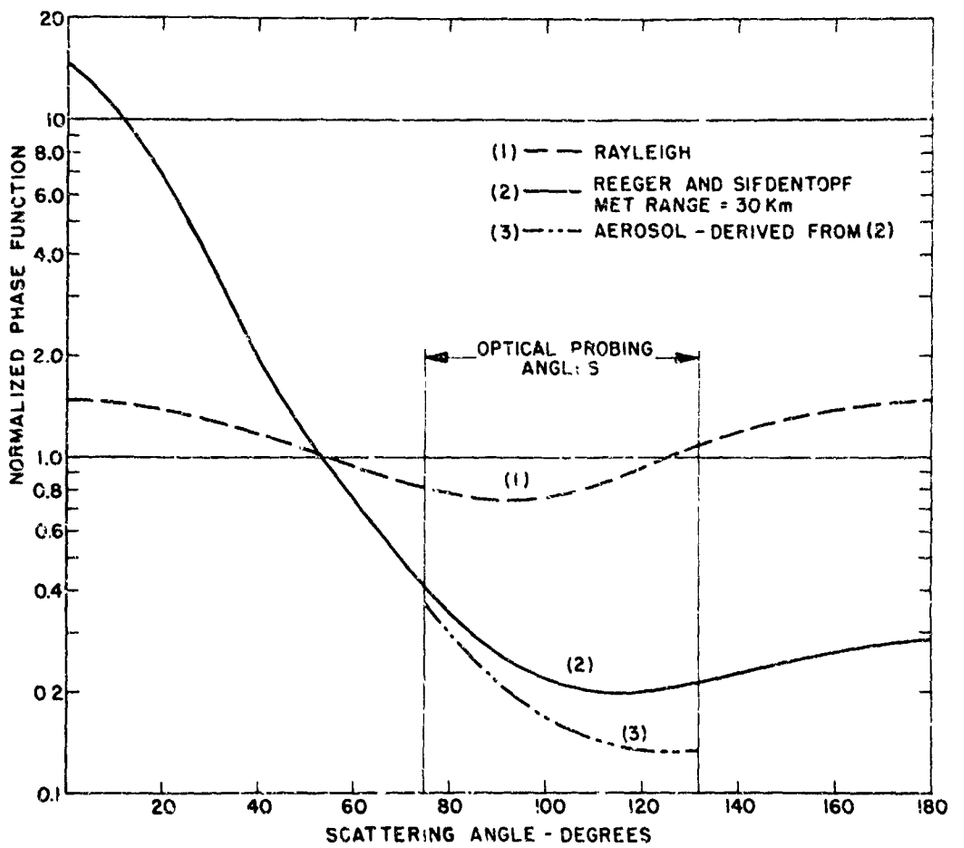

Figure 4. Normalized Phase Functions

4. INSTRUMENTATION

The methods follow those used previously (Elterman 1962, and Elterman et al 1964), but with considerable modification. The beam intensity is modulated by a shutter mechanism fronting the searchlight, Figure 5. The modulation, 20 cycles/second, represents a compromise between a desired high modulation frequency and the mechanical spin limitation of the shutters. An auxiliary detector, mounted on the beam modulator, monitors the source intensity and generates a signal which is synchronous with the modulation. The synchronous signal is transmitted to a site 30.2 km distant, where the optical collector, synchronous detector and amplifier are located. The collector mirror and the photomultiplier assembly comprise the sensing device. The detector-filter response peaks at 0.55 microns and has a wavelength bandwidth at the half-amplitude response approximating 550 Angstroms.

5. SKY BACKGROUND

The measurements were conducted during moonless nights so that the sky background would be minimized. Although modulation of the beam contributes greatly to isolating the desired scattering from the sky background and other spurious sources, it does not completely effect isolation. The sources of the background level are: (a) the star field and airglow (direct and scattered), (b) secondary and higher order scattering from the beam, and (c) instrumentation noise.

Probably the major source is direct and scattered light from the star field and the night airglow. Beam modulation with synchronous rectification is effective in suppressing these sources, but not entirely so. The incidence of modulated and unmodulated energy on the photomultiplier results in a shot noise spectrum, part of which is passed by the bandwidth of the amplifier (0.02 cycles/second). Secondary and higher order scattering from the beam enters the field of the collector mirror for the most part at low altitudes (regions of relatively high atmospheric molecular density), but is considered small due to the 30.2 km separation of the sites. Finally the photomultiplier dark current and other instrumentation noise contribute to the signal background. The signal-to-noise ratio at 35 km exceeds 20, and increases rapidly at lower altitudes.

6. OBSERVATIONS AND RESULTS

The data obtained is in the form of a continuous trace on the chart recorder. The elevation angle, ϕ_d, is recorded automatically on the chart along with the

Figure 5. Modulating Shutters with Drive Motors Below. Detector assembly for synchronous rectification mounted near the top

response to the scattered light. Subsequently, the response is digitized at 1^{o} intervals as in Table 1. The results based on sampling of a year's measurements show that it is convenient to categorize the aerosol distributions derived from the data, into "moderate-structured", "medium-structured", and "full-structured" profiles.

Following through on the measurements discussed in Figure 2, the response values were used in Eq. (14), and the resulting aerosol attenuation coefficients were plotted automatically from the punch card computer output as shown in Figure 6. The Rayleigh coefficients and the extinction coefficients (Rayleigh + aerosol) are included. The character of the aerosol curve places it in the category of a "medium-structured" profile. Since the aerosol coefficients primarily are proportional to the aerosol number density, examples of these categories will be discussed. The diminution of the aerosol density values over the lowest few kilometers occurs frequently. A region of aerosol concentration is evident with a maximum at 18 km. For the region 2.8 km down to sea level,

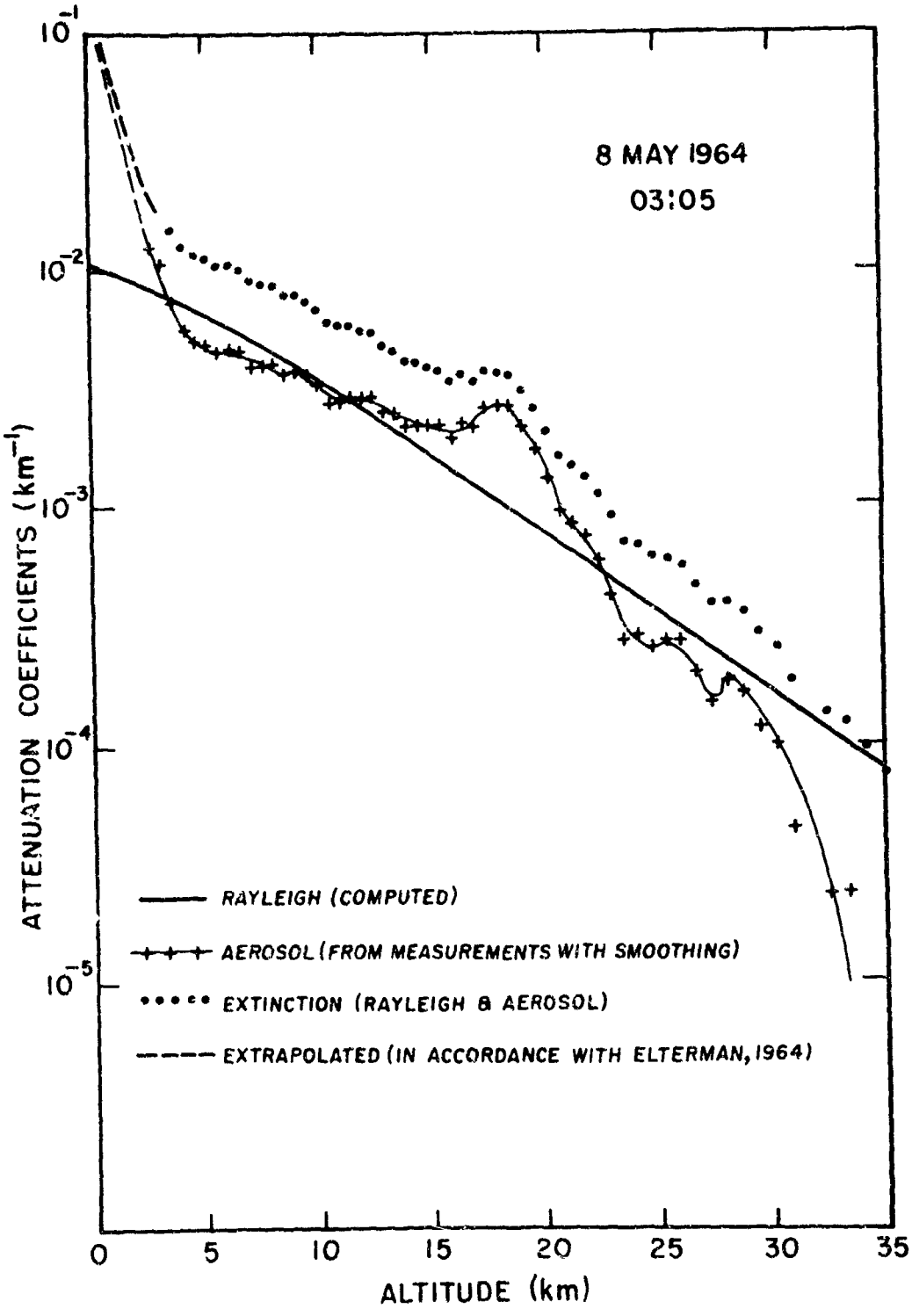

Figure 6. Aerosol and Related Parameters. The aerosol profile represents the "medium-structured" category

extrapolation was carried out to conform with the 0.55 μ tabulations of the Atmospheric Attenuation Model (Elterman, 1964).

The profiles in Figure 7 are examples from the "moderate-structure" category. Here the aerosol number densities between 2.76 and about 14 km show relatively little change. The identity of the 20 km layer is fairly evident.

The staggered scale presentation in Figure 8 shows a series of profiles taken over a six-hour period. These profiles are categorized as "full-structured". This body of data was obtained consecutively except for periods of interim activity pertaining to operational requirements. The low altitude concentration shows a maximum at 5 km in profiles A, B, and C. During the night, the maximum becomes less defined and in profile E acquires a simple logarithmic distribution (2.8 to 6.5 km). Next a tropopause concentration with a maximum at about 9 km is evident, but this region increasingly loses its identity in profiles D and E. There follows a region of aerosol concentration above the tropopause (12 to 23 km) which persists through the night, and is identified with the 20 km aerosol layer determined by the direct measurements of Junge, Chagnon and Manson (1961). Finally, a 26 km maximum shows surprising temporal integrity. Above 28 km, the decreasing values indicate a quasi-Rayleigh atmosphere.

The usefulness of the $\beta_p(h)$ profile for obtaining quantitative information can be readily demonstrated. In Figure 8 profile C, the aerosol concentration usually designated as the 20 km layer can be examined with considerable detail. It is well-defined, asymmetrical and extends in altitude from 12.7 to 23.2 km (Table 1). The median of the layer occurs at 18.2 km where $\beta_p = 9.33 \times 10^{-4}$ km^{-1} and the turbidity factory, $\beta_p/\beta_r = 0.83$. The maximum aerosol density, however, occurs at 15.6 km where $\beta_p = 1.66 \times 10^{-3}$ km^{-1} and the turbidity factor is 0.99. The aerosol optical thickness of the layer is determined by

$$\tau_p = \sum_{12.7}^{23.2} \overline{\beta}_p (h)\, \Delta h \qquad (16)$$

where:

$\overline{\beta}_p(h)$ is the mean aerosol attenuation coefficient (km^{-1}) for each altitude increment

Δh is the altitude increment (km) as designated in Table 1.

This leads to the value $\tau_p = 0.01$ which is modest but important in applications requiring large zenith angles. The slant path transmissions through the layer due to Rayleigh and aerosol attenuation were obtained with Eq. (15) and are shown in Figure 9.

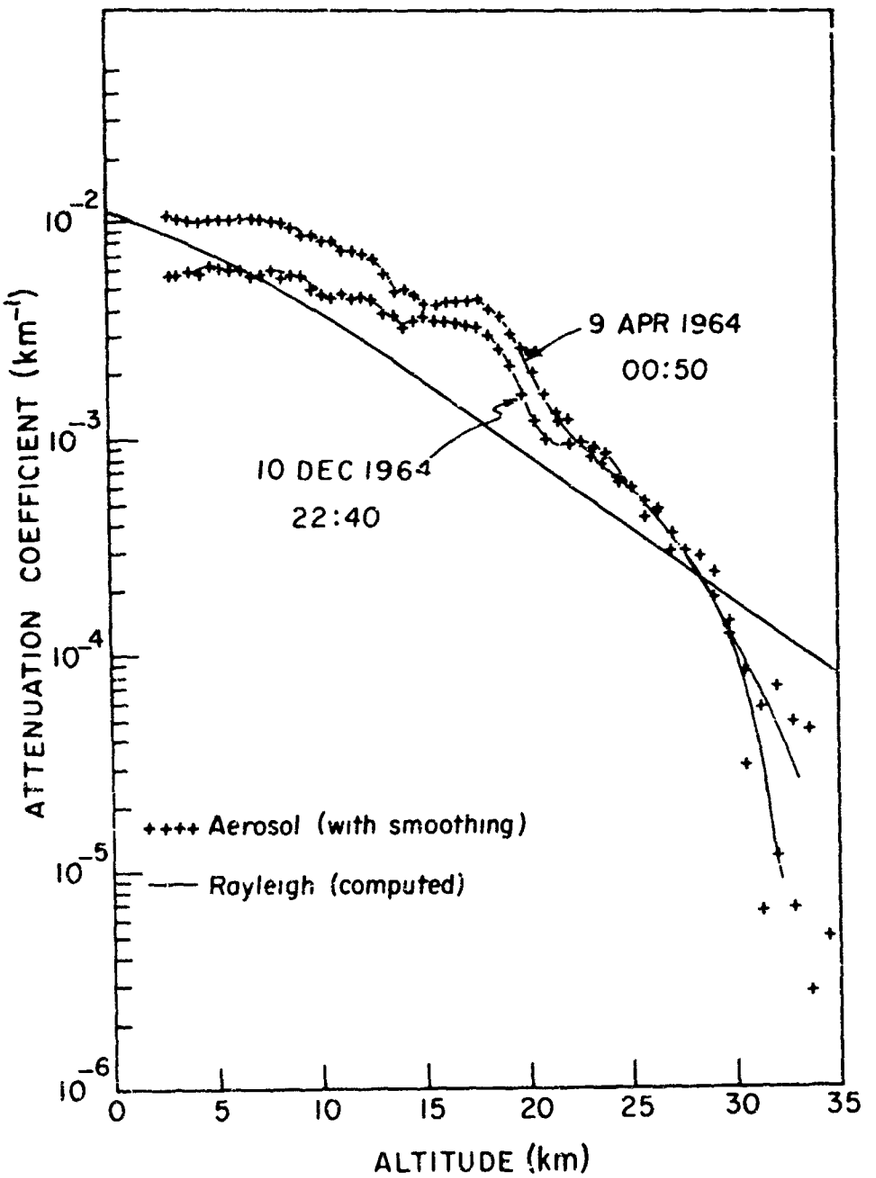

Figure 7. Aerosol Profiles Representing the "Moderate-Structured" Category

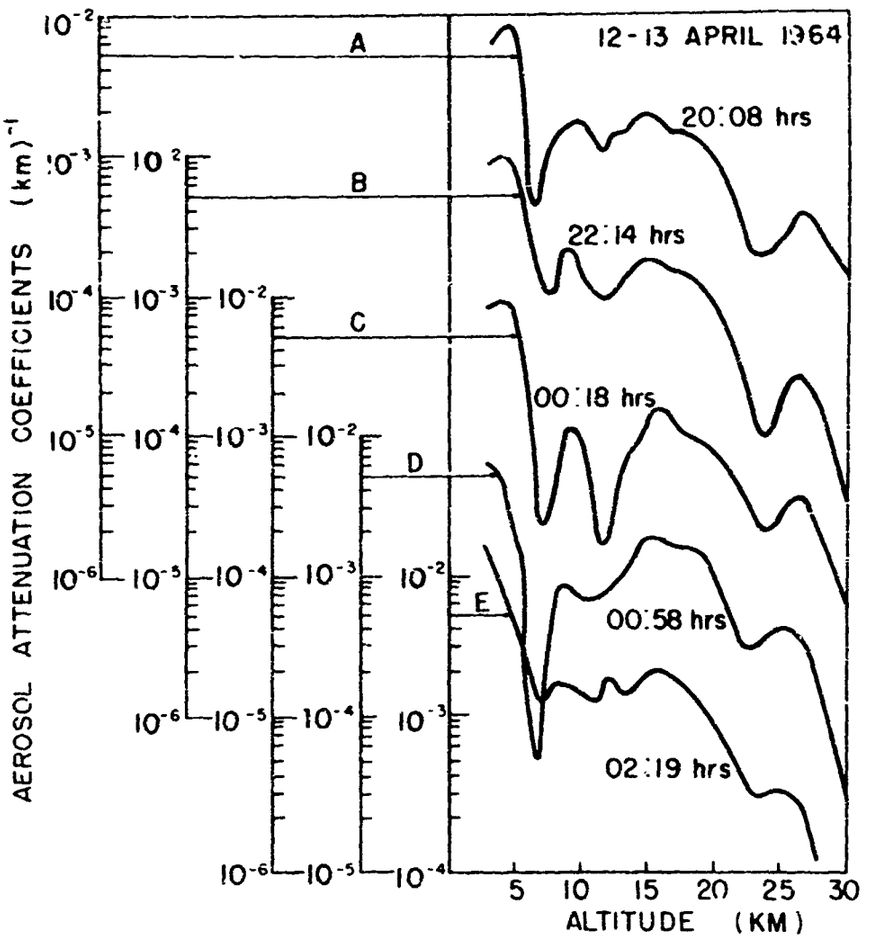

Figure 8. Aerosol Profiles Representing the "Full-Structured" Category Showing Variations Over a Period of About Six Hours

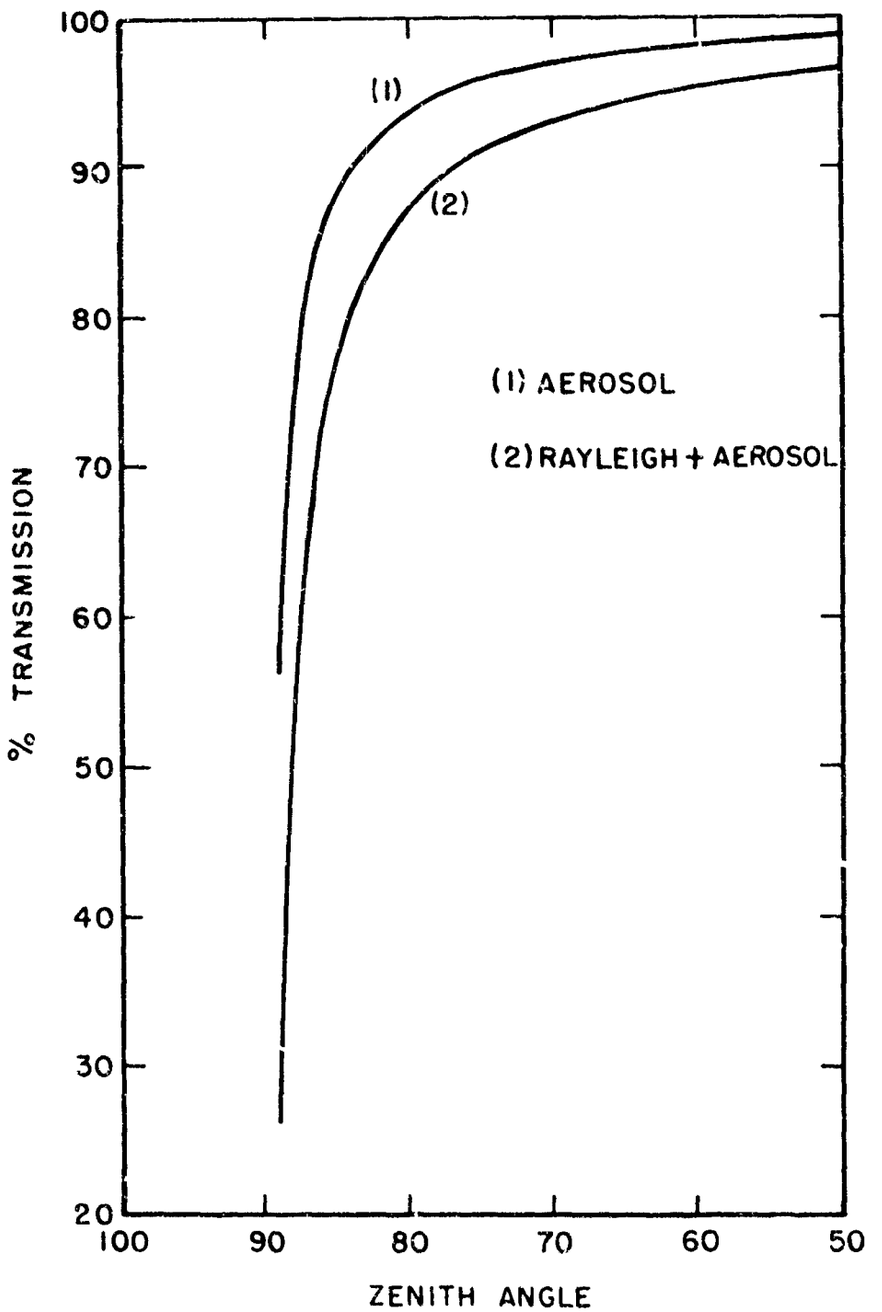

Figure 9. Slant Path Transmission (0.55 microns) Through 20 km Aerosol Layer. 13 April 1964 at 00:18

7. ERROR CONSIDERATIONS

Here, it will be convenient to designate a set of measured values, $E_{rp}(h)$, as the input profile and the computed aerosol attenuation coefficients, $\beta_p(h)$, as the output profile.

Examination of Eq. (14) shows that the term, $E_{rp}(35)$, can bear significantly on the accuracy of the results. It is necessary, therefore, to consider the effect of noise and background on this term. If the background level causes $E_{rp}(35)$ to increase, then some negative values in the output profiles may result. Also, the measured and Rayleigh curves (as shown in Figure 2) are nearly converged between 30 and 35 km. The presence of noise then may cause the measured value to be less than the corresponding Rayleigh value, which is an unacceptable condition. Accordingly, the procedure was adopted where the input profile is smoothed for the last few kilometers. The computer then examines the derived $\beta_p(h)$ values after the first iteration for the presence of negative values. Routinely, the instrumentation is set so that the measured value of $E_{rp}(35)$ is near unity. If for $h<35$ km any negative values of β_p are present, $E_{rp}(35)$ is reduced by 0.001 repeatedly until only positive values of $\beta_p(h)$ exist. The iteration then continues with no further adjustments until convergence is obtained. This procedure corrects $E_{rp}(35)$ for noise and background.

The angular pointing error, when scanning the beam upward or downward, approximates $\pm$ 0.1 degree. This is equivalent to an error of 0.05 to 0.09 km, depending on the altitudes of measurement.

The February 1964 data above 22.6 km may be questionable due to uncertain operating procedure.

It is reasonable to estimate that the other functional aspects of the measurements can result in about 5 or 6 percent error in the $E_{rp}(h)$ values. If systematic (always negative or positive), then this percentage applies to the entire input profile, and the resulting output profile will be unaffected because we are dealing with ratios, $E_{rp}(h)/E_{rp}(35)$. However, a part of the input profile subjected to a 5 percent change results in considerable error due to the summation procedure, Eq. (15). This is demonstrated by choosing a severe example of error simulation; that is, increasing the $E_{rp}(h)$ values over a substantial portion of the input profile (approximately 27 km of Table 1). If these are increased by 5 percent, the output profile values of β_p change 28 percent at 2.76 km and 40 percent at 29.7 km. A corresponding 6 percent increase results in changes of β_p from 33 to 48 percent.

In instances where convergence cannot be attained, the data is abandoned. Usually failure to converge is due to high values of $E_{rp}(h)$ for altitudes under 5 km, caused by heavy dust or thin cloud

8. CONCLUDING REMARKS

Five major factors determined the number of profiles acquired during the period

(1) The operational time that could be allowed was limited.

(2) Operations were conducted only during moonless nights in order to keep noise background at a minimum.

(3) Operations were cancelled when meteorological conditions were unfavorable. This included high winds as well as cloudy skies. July and August seasonally are months when both dust storms and cloudy skies occur daily in New Mexico.

(4) Equipment difficulties accounted for absence of data in January 1964 and at other times.

(5) Failure of site facilities, especially telephone lines, resulted in considerable loss of time. Synchronous rectification and amplification depended on transmittal of the synchronizing signal by telephone.

During the period 12 December 1963 through 12 December 1964, a total of 105 useful profiles were acquired, listed as follows:

Month	Profiles	Month	Profiles
Dec 1963	22	July 1964	3
Jan 1964	--	Aug 1964	--
Feb 1964	12	Sept 1964	2
Mar 1964	6	Oct 1964	6
April 1964	28	Nov 1964	4
May 1964	9	Dec 1964	5
June 1964	8		

The atlas of profiles that follow suggests that characteristic stratifications exist. Although these are designated as layers, they do not appear to be discrete. Rather, the profiles indicate an aerosol continuum having greater or lesser concentrations. Although results are presented for altitudes up to about 35 km, the data acquired does not exclude the presence of aerosol with low number density between 35 and 70 km. A computed mean of 105 profiles comprising the atlas is shown in Figure 10.

As mentioned, the measurements were conducted at 0.55 microns. If for exploratory calculations, aerosol attenuation coefficients are desired for other wavelengths, one can consider using the results in conjunction with an empirical relationship such as $\beta_p \sim \lambda^{-1}$.

The salient purpose of this paper is to make a substantial number of profiles available, possibly for use in various disciplines. At this time it is left to the reader to cull, tabulate, compare, and contemplate this body of material. We plan to continue evaluation and further study of these results.

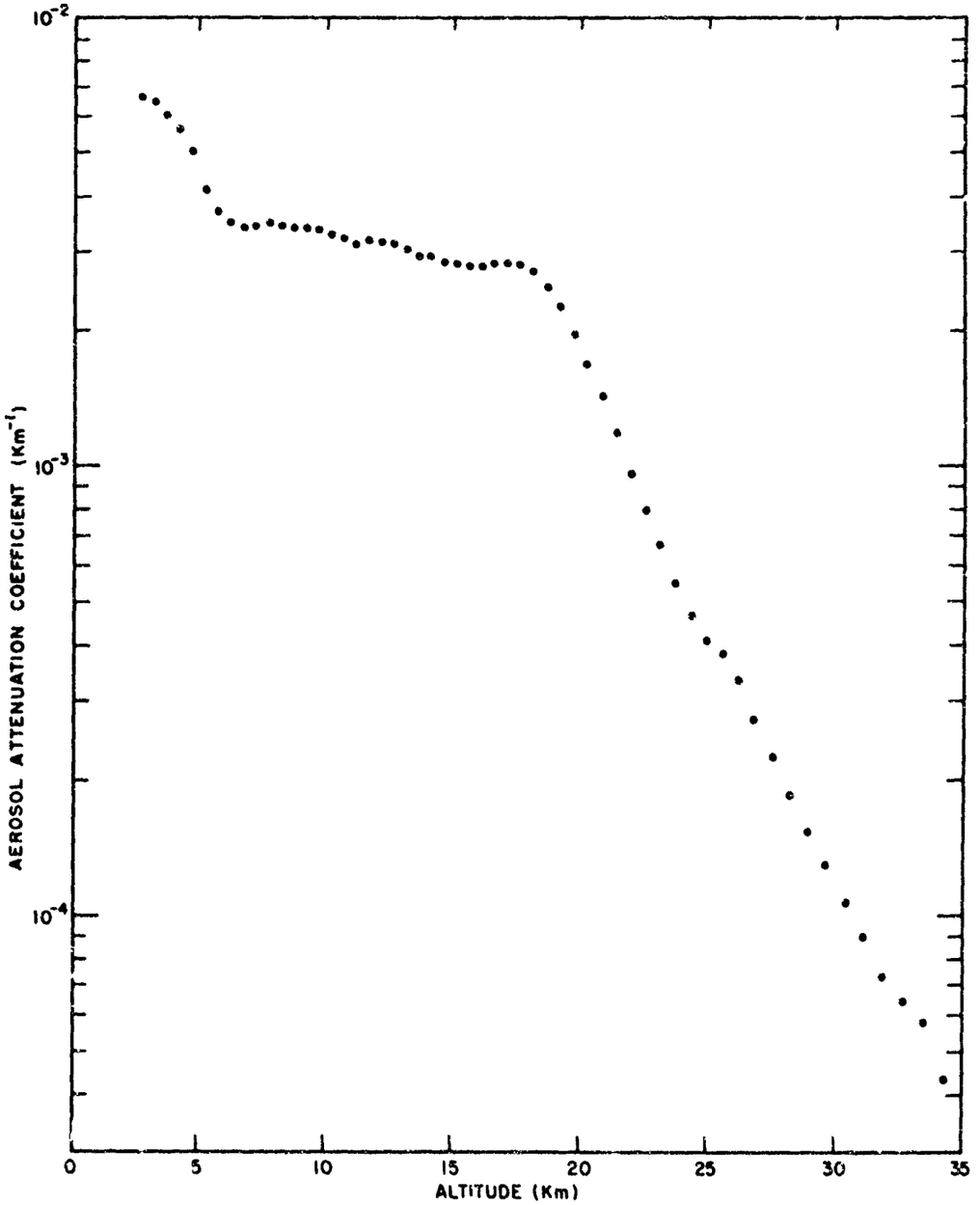

Figure 10. Computed Mean Aerosol Attenuation Coefficient of 105 Profiles Comprising the Atlas

Acknowledgments

The author would like to acknowledge the fine assistance with instrumentation afforded by A. B. Campbell and J. R. Yoder, the helpful review provided by R. Penndorf, R. W. Fenn and R. G. Walker, the able assistance by M. Jones with field activities. His appreciation is extended also to J. V. Dave for contributing a long afternoon of discussion during our 1964 visit to Leningrad, to C. Atwood and others who assisted with data reduction, to M. G. Hurwitz, R. Hoffman, and J. Fusco for their participation with computer programming, and to W. Daunt, J. Lee, H. Bass, and M. M. Kielman who were dedicated to acquiring every minute of useful data.

References

Barteneva, O. D. (1960) Bull. Acad. Sci. USSR, Geophys. Ser. 1: 1852.

Bullrich, K., and Moeller, F. (1947) Optik 2: 301.

Bullrich, K. (1964) Advan. Geophys. 10: 99.

Deirmendjian, D. (1964) Appl. Opt. 3: 157.

Elterman, L. (1962) Searchlight probing technique for upper atmosphere measurements in Encyclopaedic Dictionary of Physics, J. Thewliss, Ed., Pergamon Press, Inc., New York.

Elterman, L. (1964) Atmospheric Attenuation Model, 1964, in the Ultraviolet, Visible and Infrared Regions for Altitudes to 50 km, AFCRL-64-740, Bedford, Mass.

Elterman, L. and Campbell, A. B. (1964) J. Atmospheric Sci. 21: 457.

Elterman, L. (1966) Appl. Opt. 5: 1769.

Foitzik, L., and Zschaeck, H. (1952) Zeit. Meteorol. 7: 1.

Fraser, R.S. (1960) Scattering Properties of Atmospheric Aerosols, AFCRC-TN-60-256, Bedford, Mass.

Junge, C.E., Chagnon, C.W., and Manson, J.E. (1961) J. Meteorol. 18: 81.

Reeger, E. and Siedentopf, H. (1946) Optik 1: 15.

Waldram, J.M. (1945) Quart. J. Roy. Meteorol. Soc. 71: 319.

Atlas of Profiles

This section contains a series of 105 useful profiles, for altitudes to about 35 km, acquired during the period 12 December 1963 through 12 December 1964.

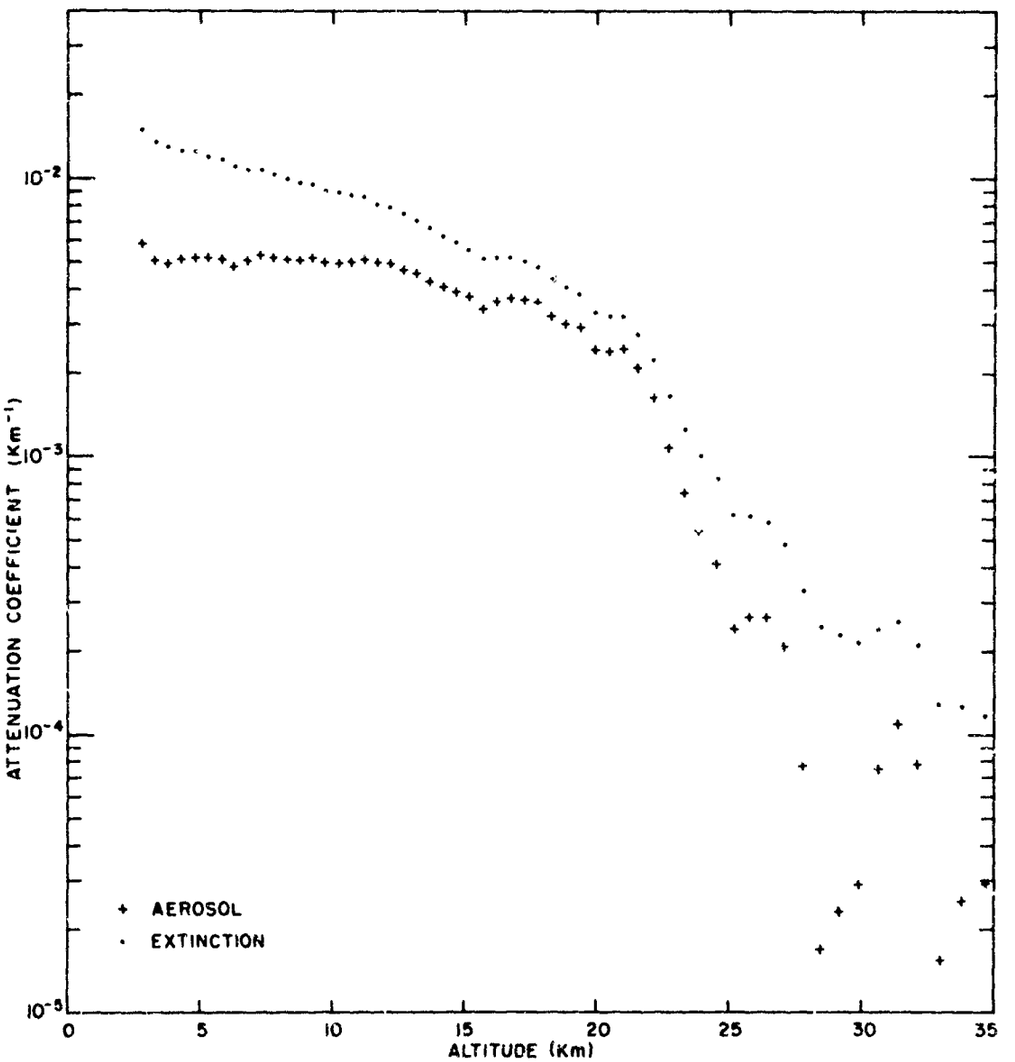

Profile 1. 12 December 1963. Time 01:03

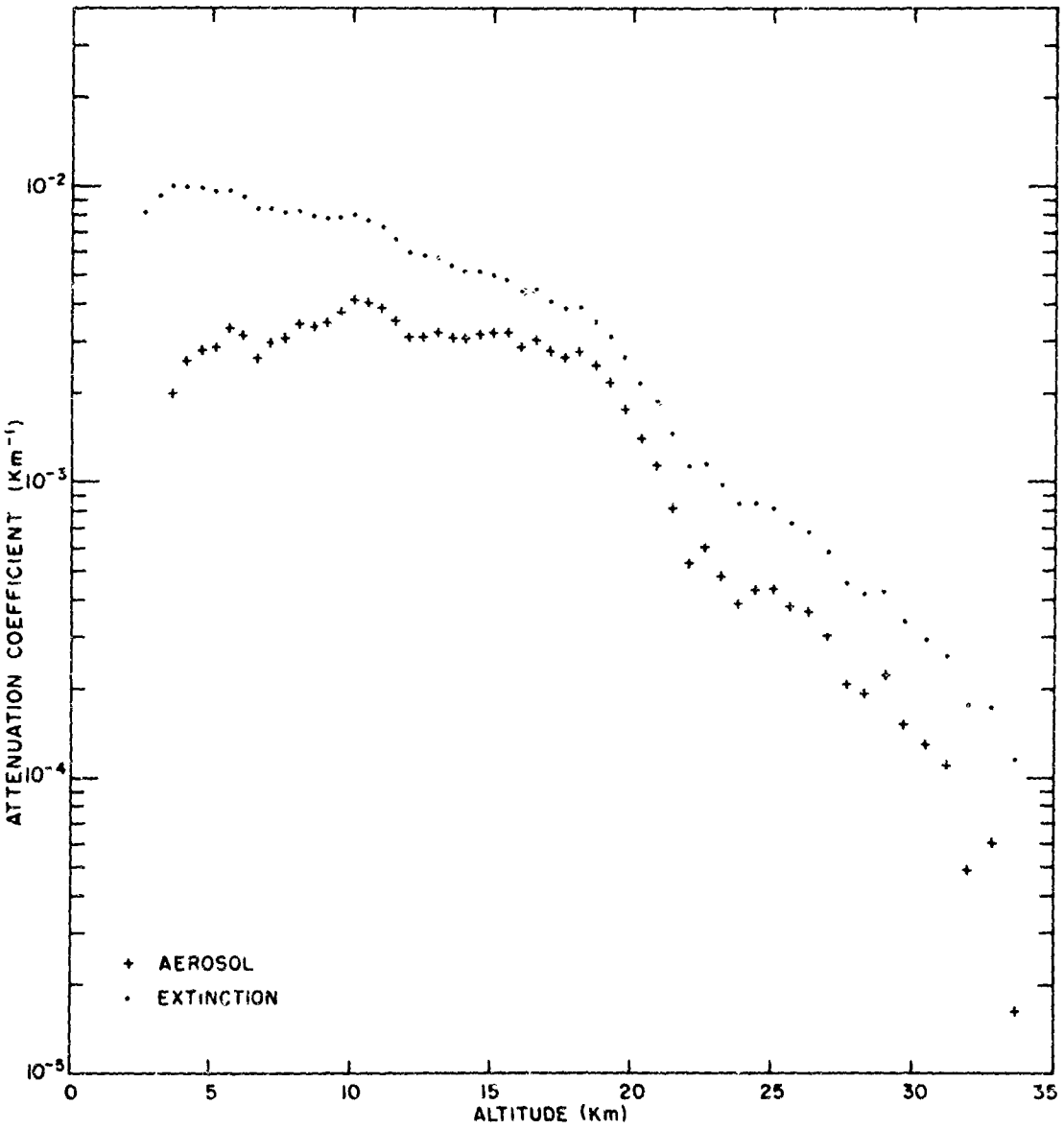

Profile 2. 12 December 1963. Time 22:42

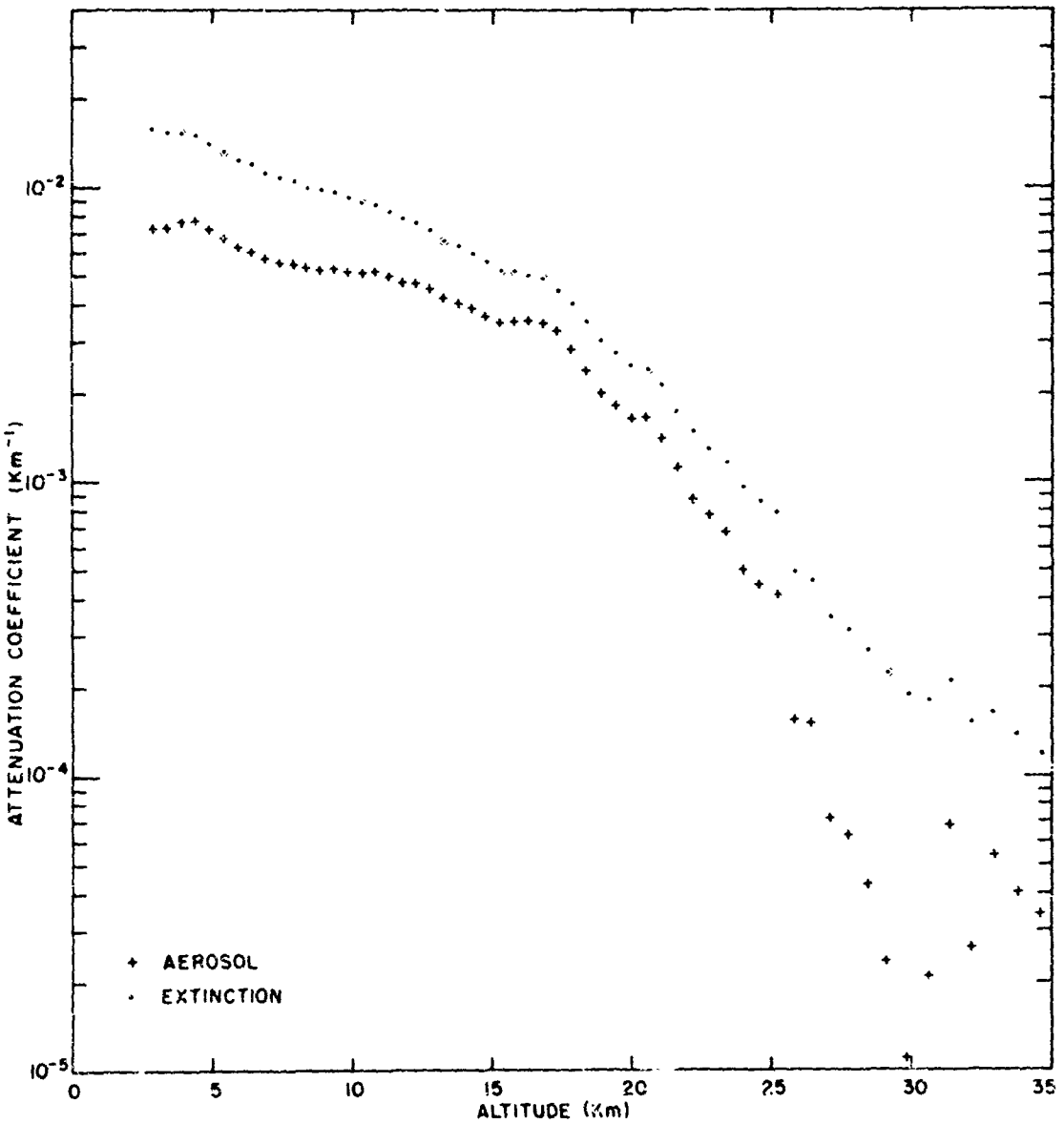

Profile 3. 15 December 1963. Time 03·35

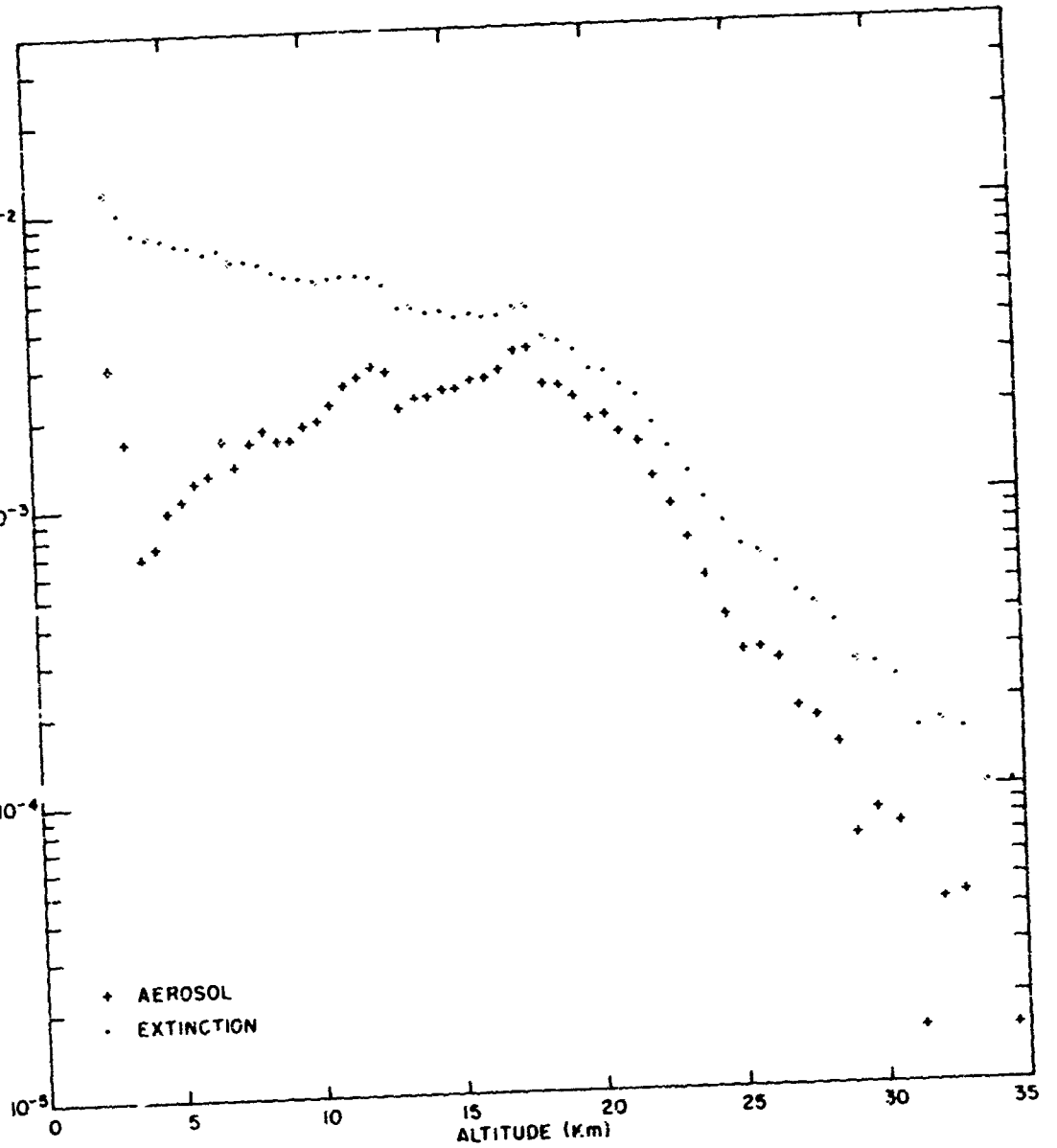

Profile 4. 16 December 1963. Time 20:20

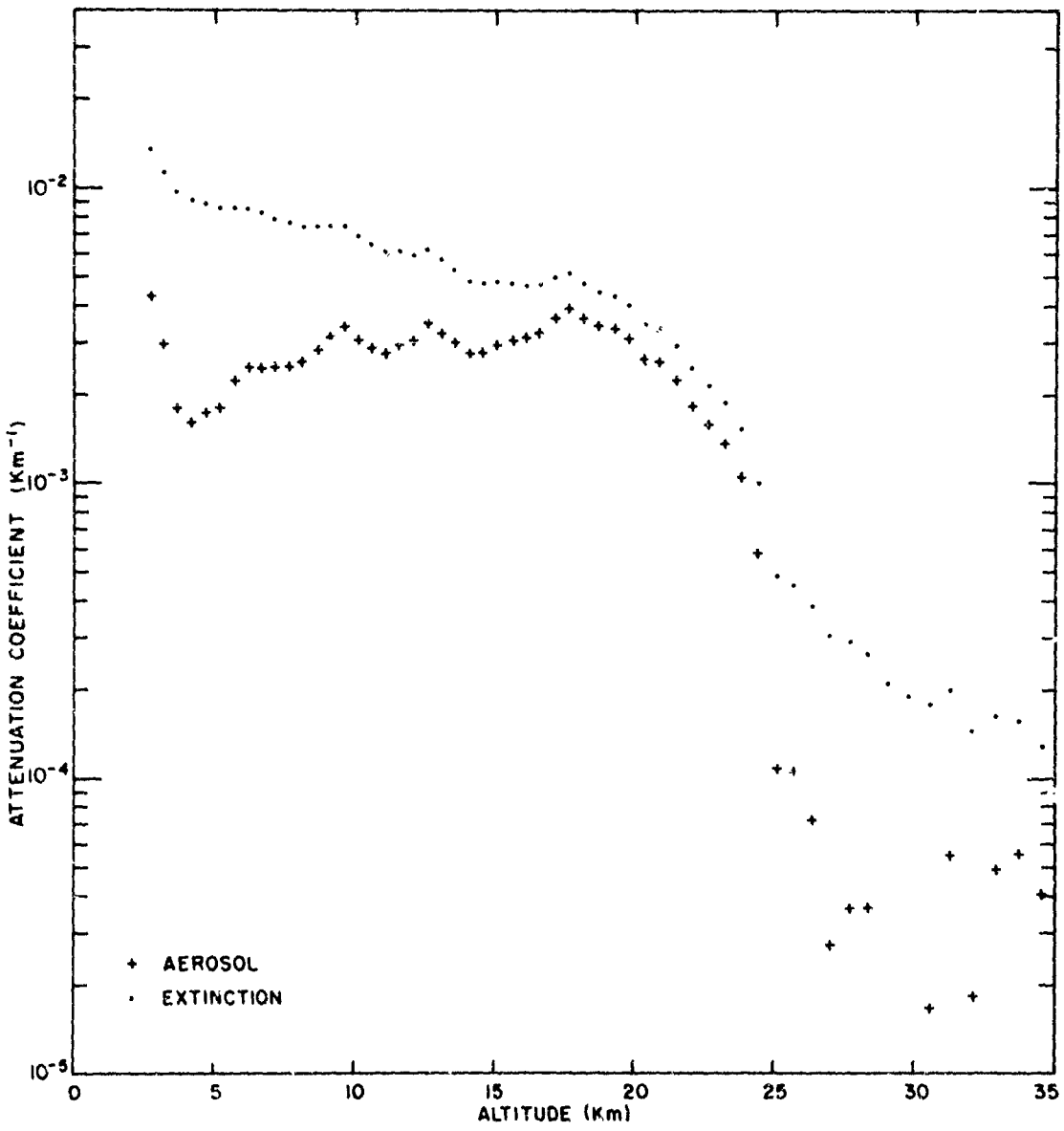

Profile 5. 16 December 1963. Time 21:23

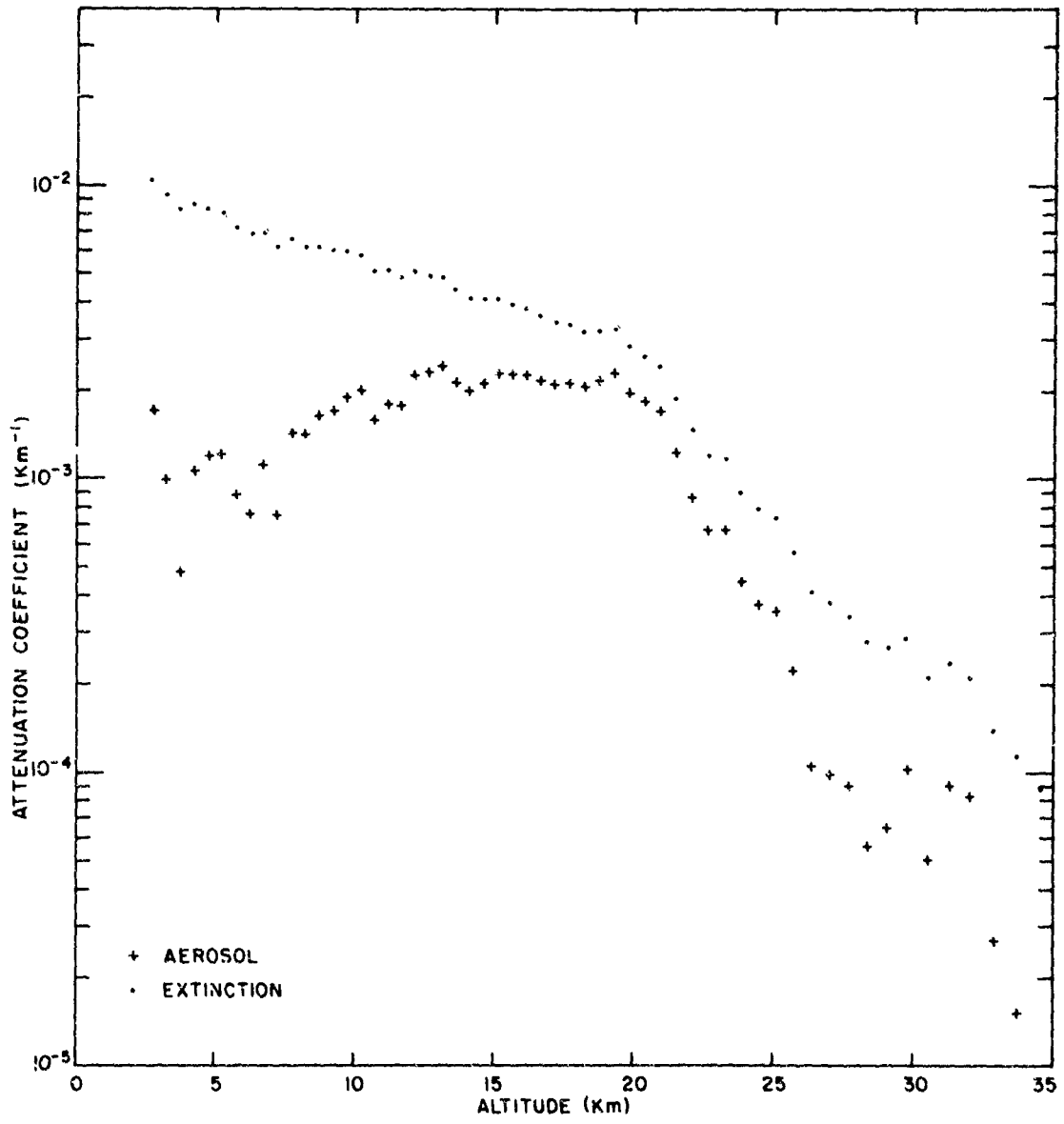

Profile 6. 16 December 1963. Time 22:17

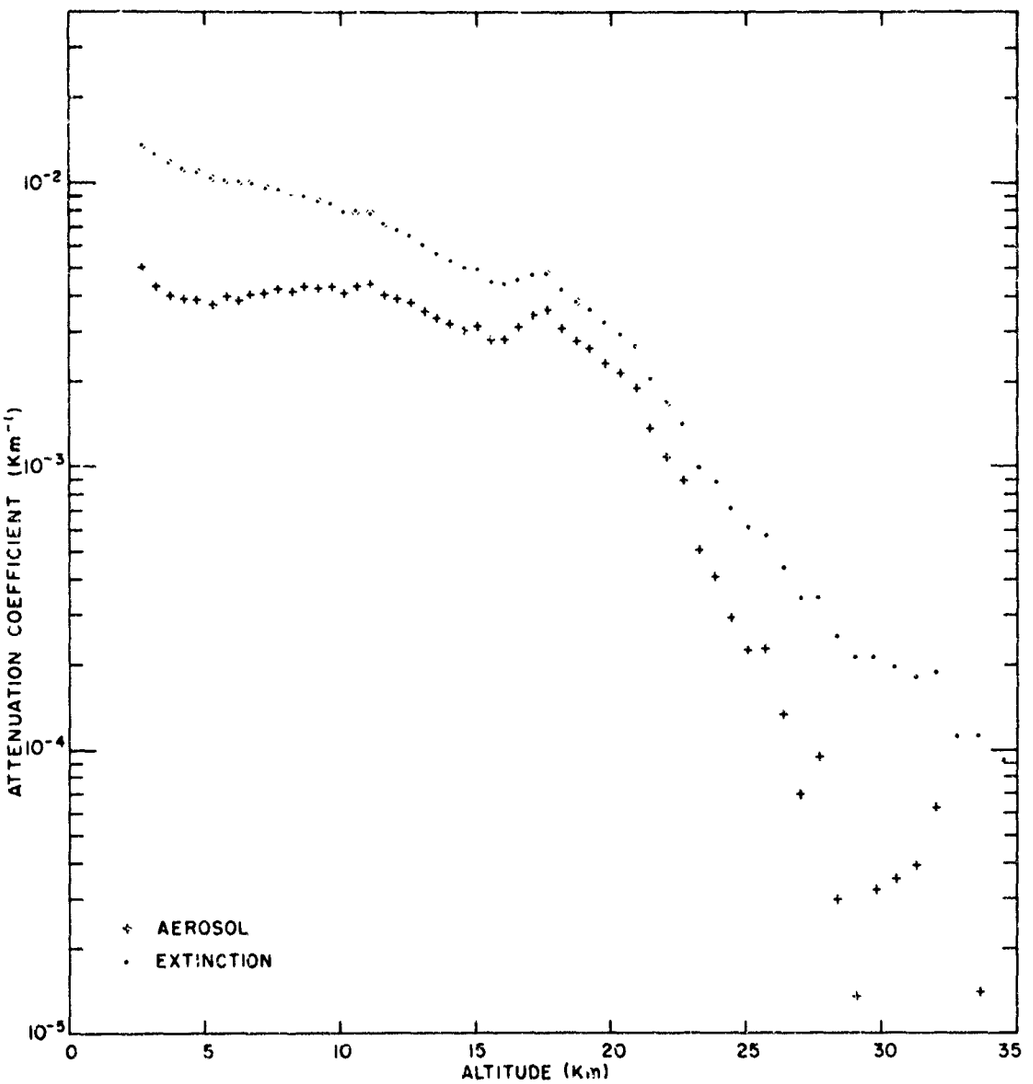

Profile 7. 17 December 1963. Time 00:07

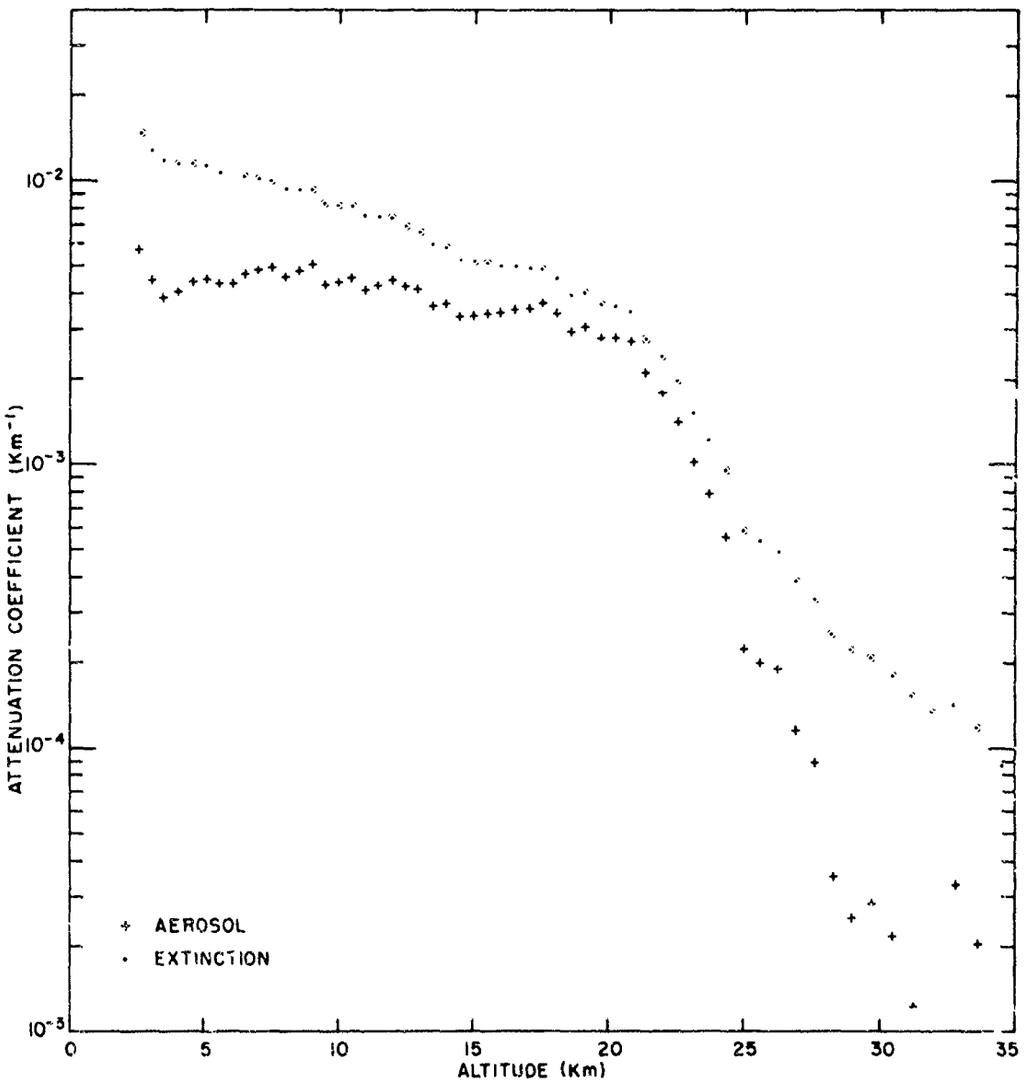

Profile 8. 17 December 1963. Time 02:00

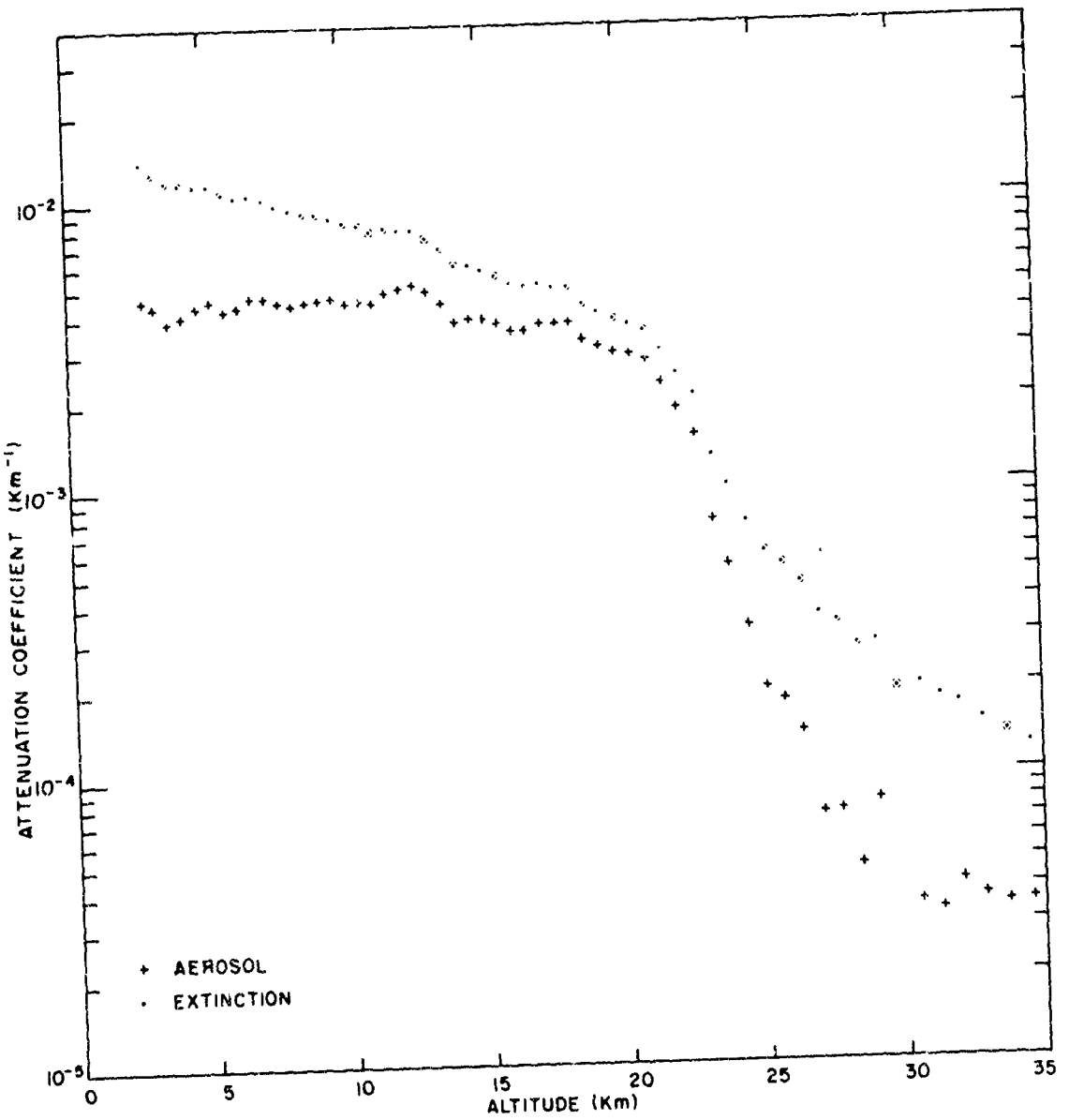

Profile 9. 17 December 1963. Time 02:56

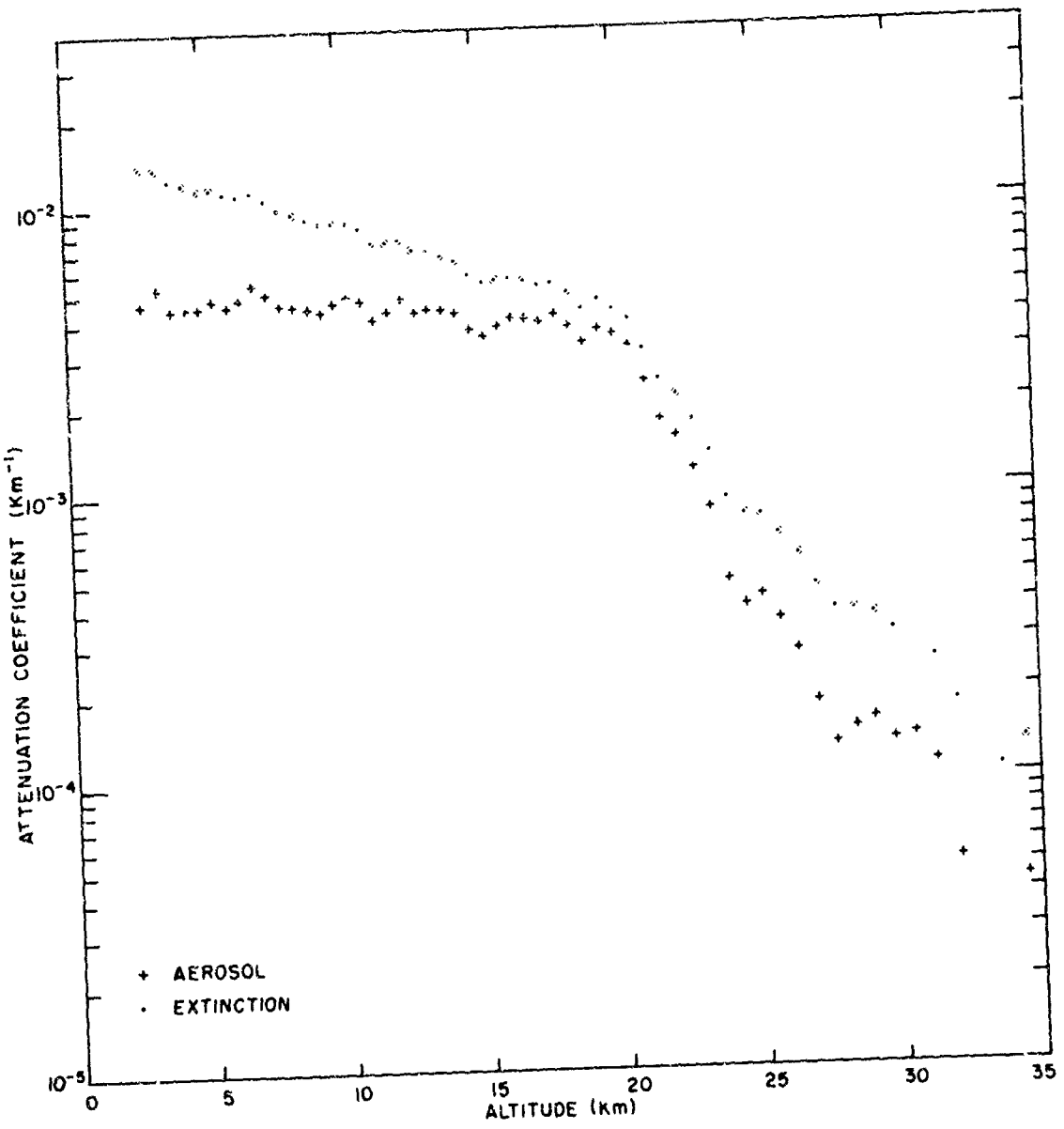

Profile 10. 17 December 1963. Time 21:42

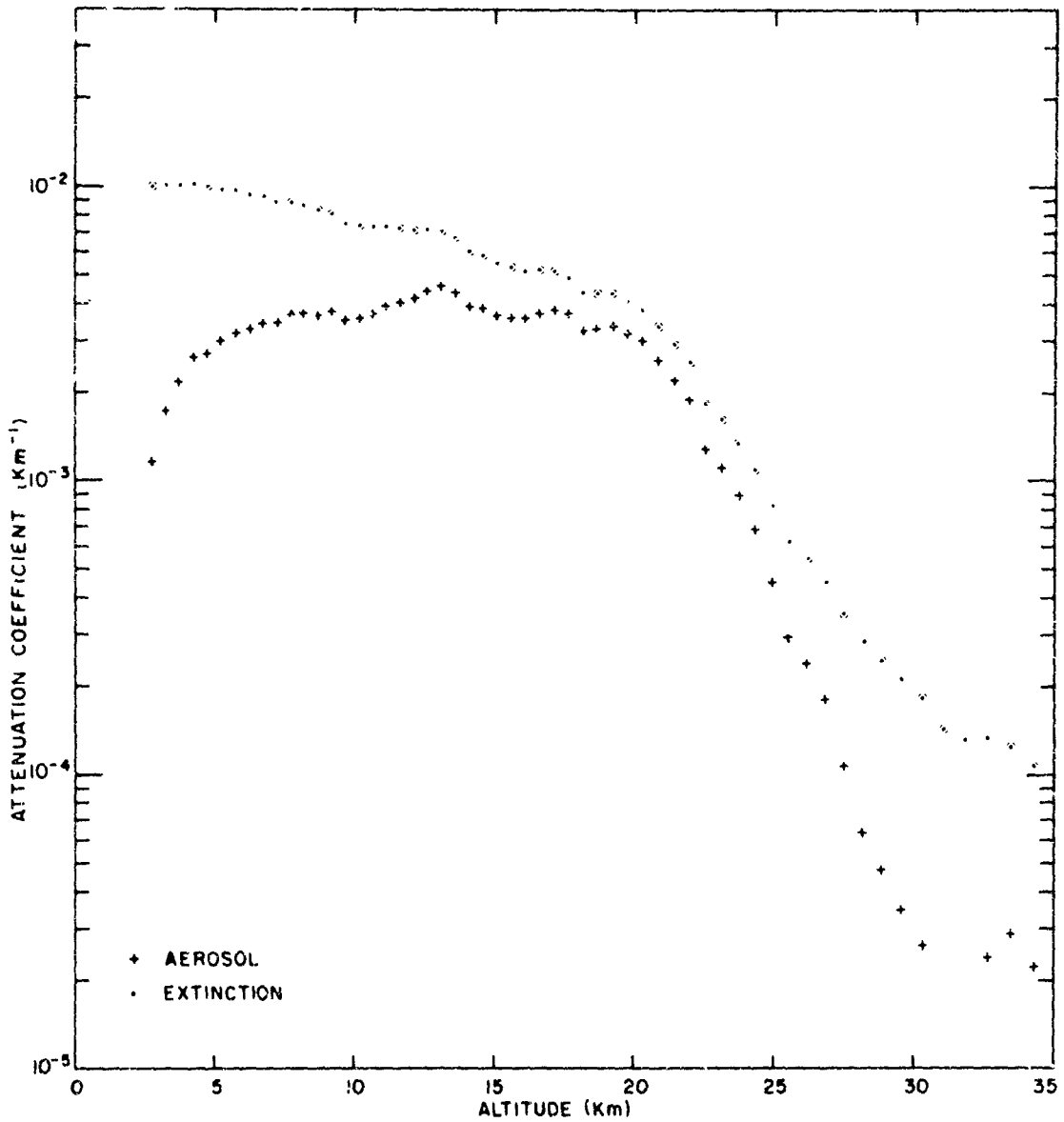

Profile 11. 17 December 1963. Time 22:30

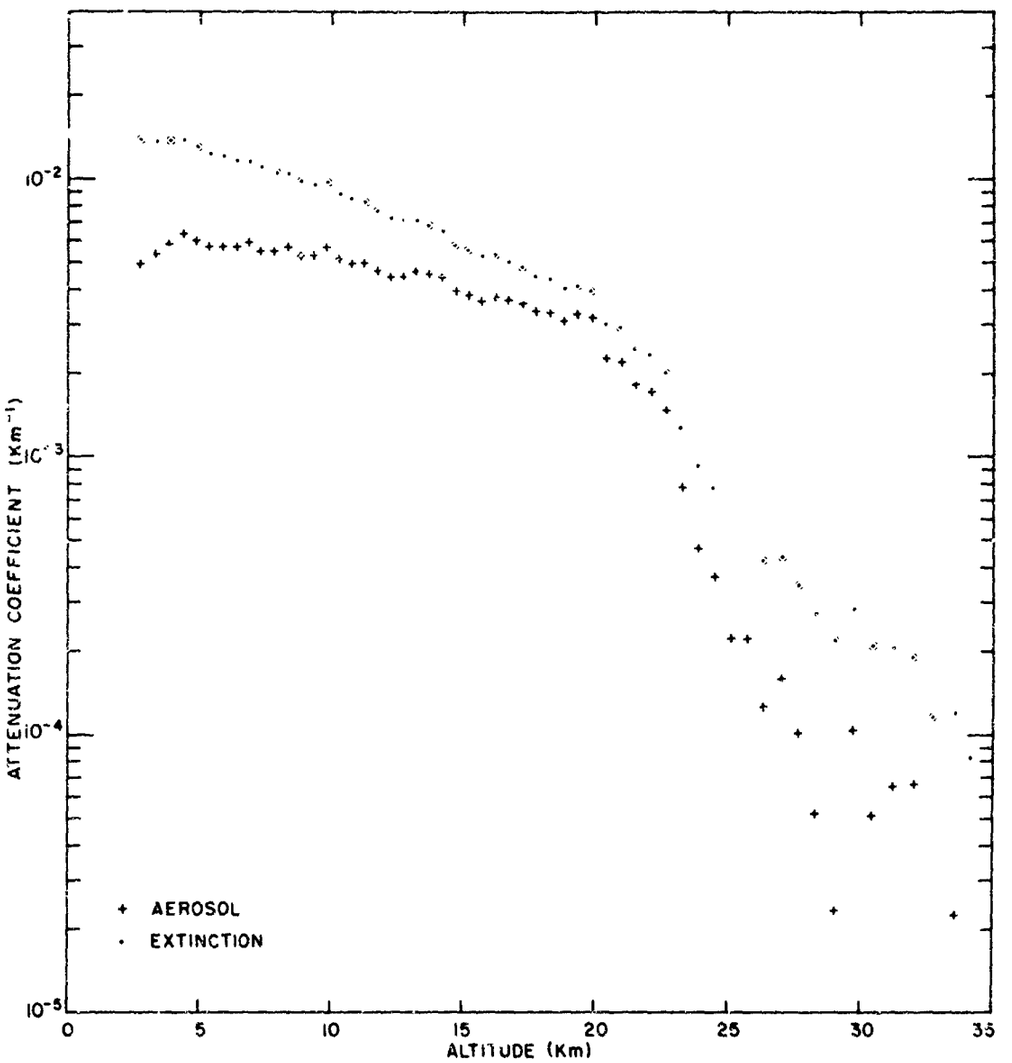

Profile 12. 17 December 1963. Time 23·40

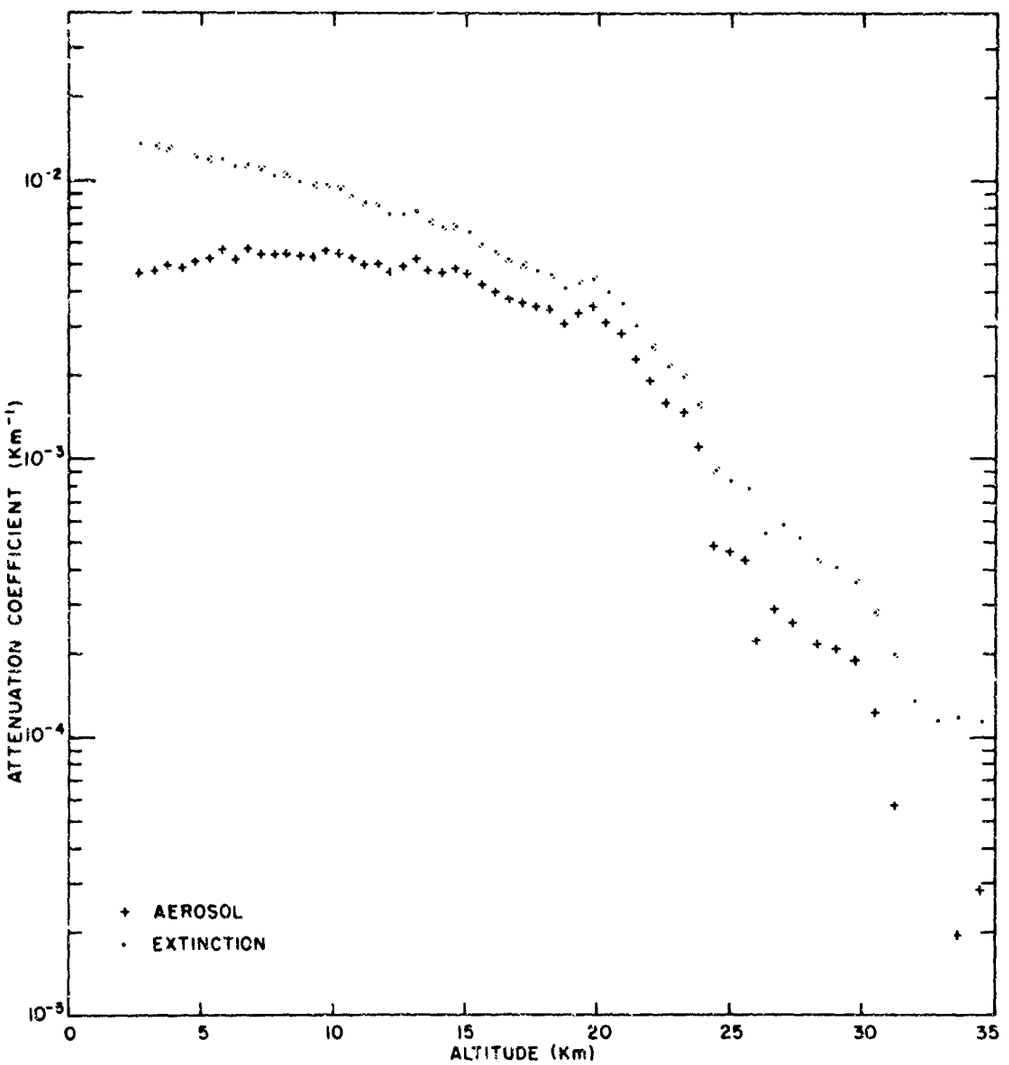

Profile 13. 18 December 1963. Time 00:36

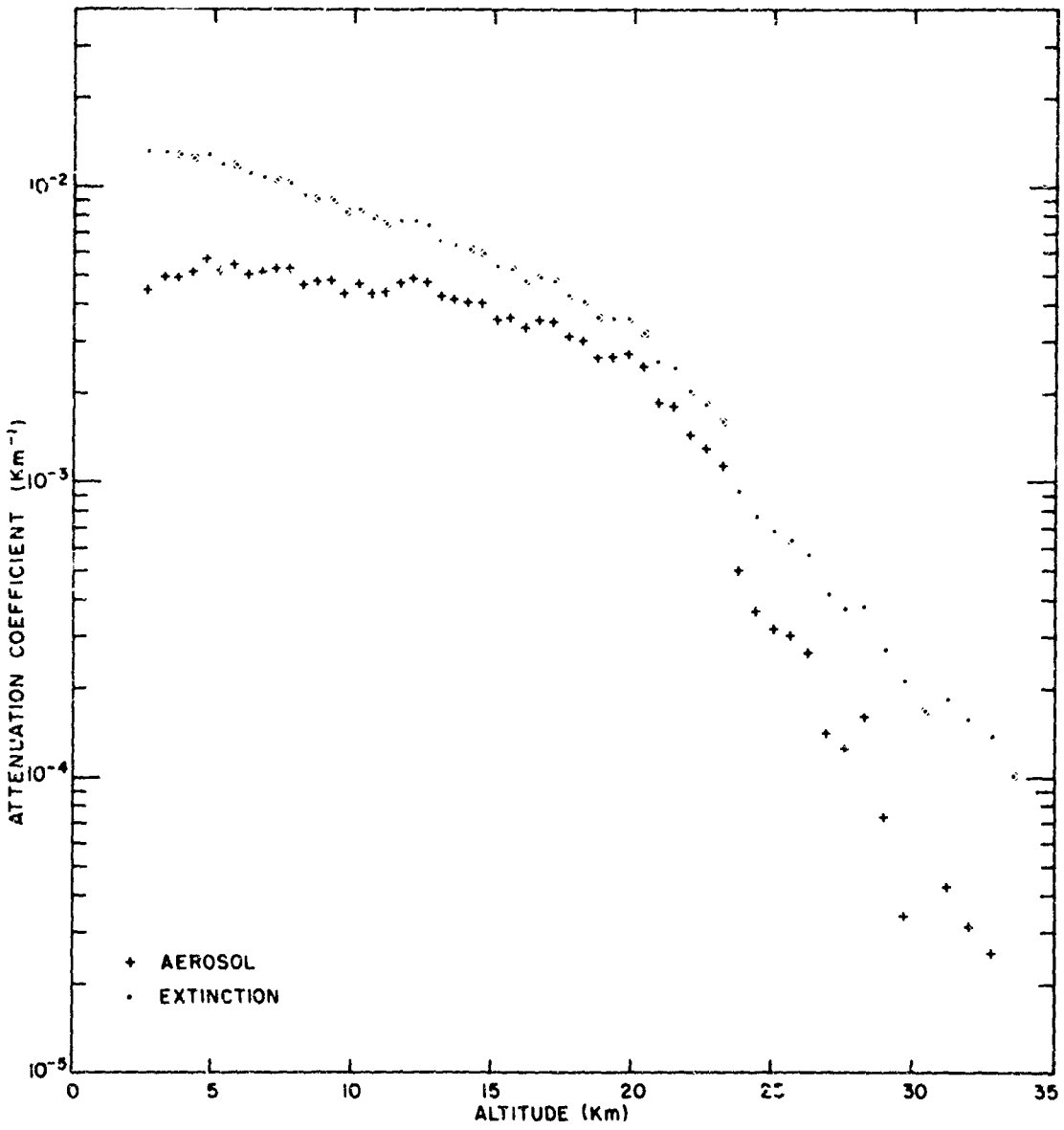

Profile 14. 18 December 1963. Time 01:35

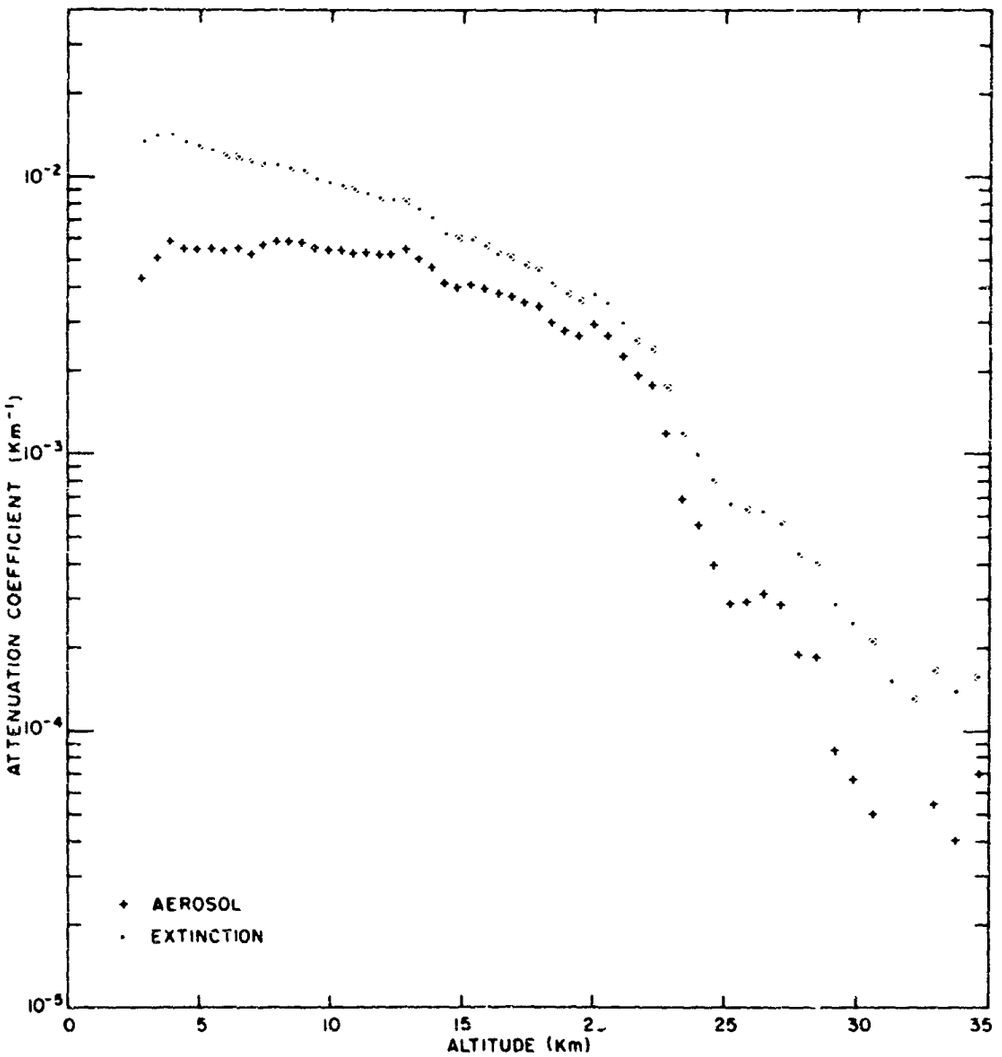

Profile 15. 18 December 1963. Time 02:31

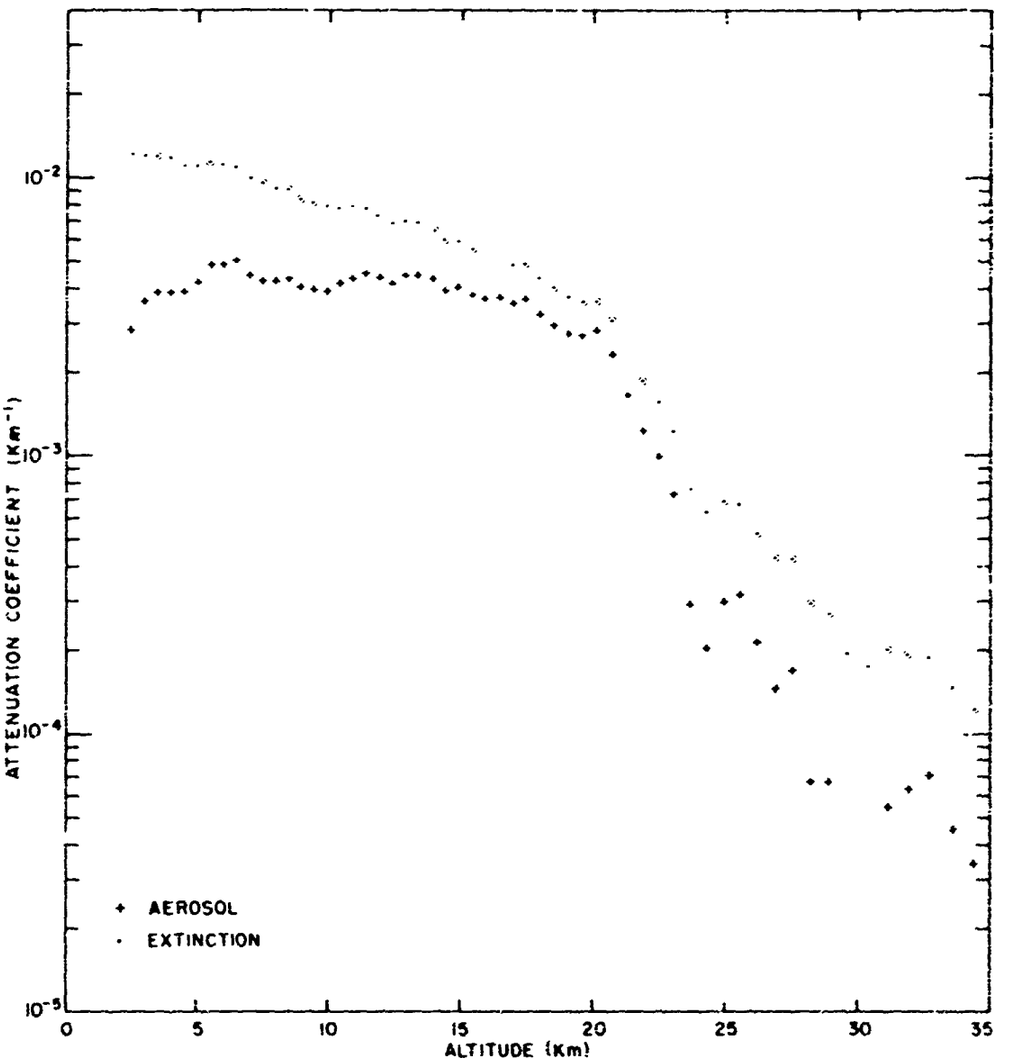

Profile 16. 18 December 1963. Time 20:40

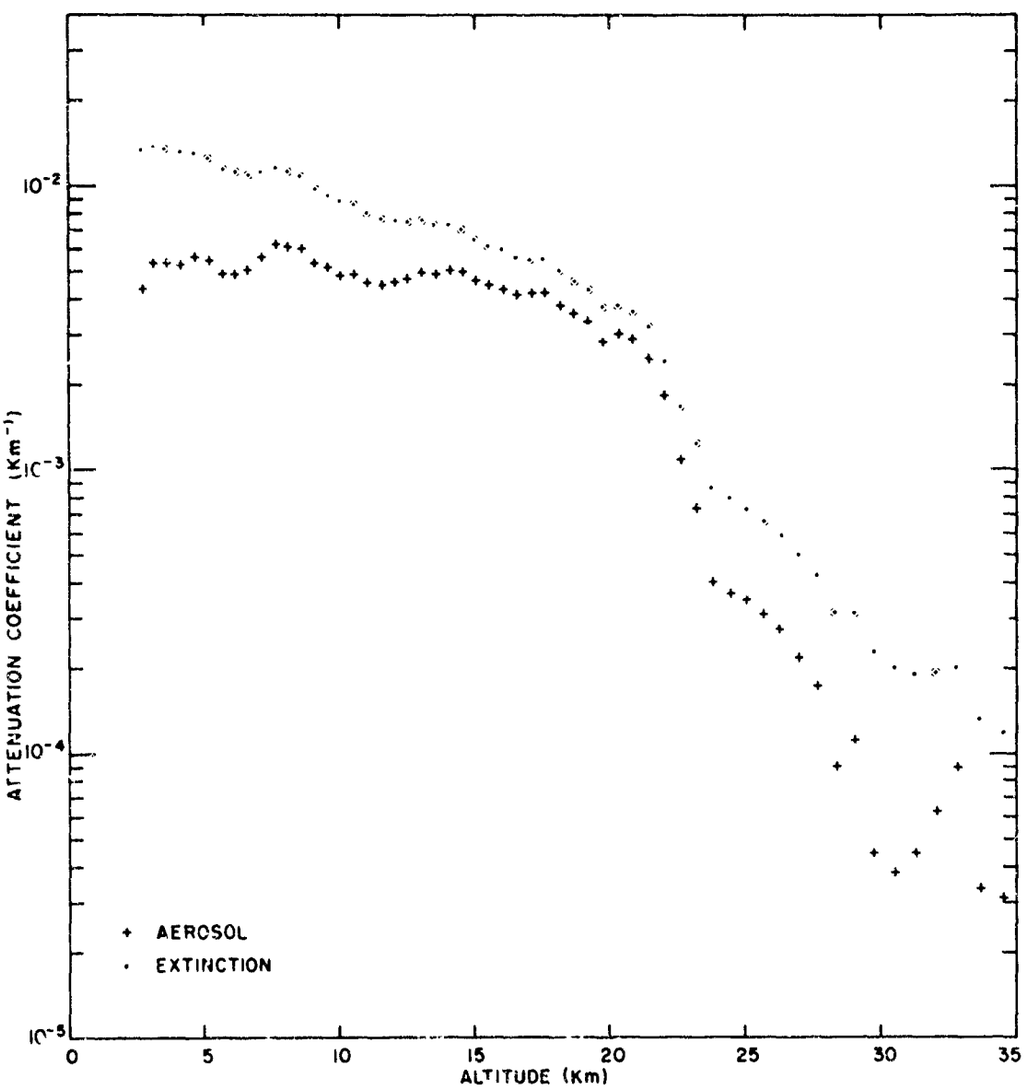

Profile 17. 18 December 1963. Time 21:00

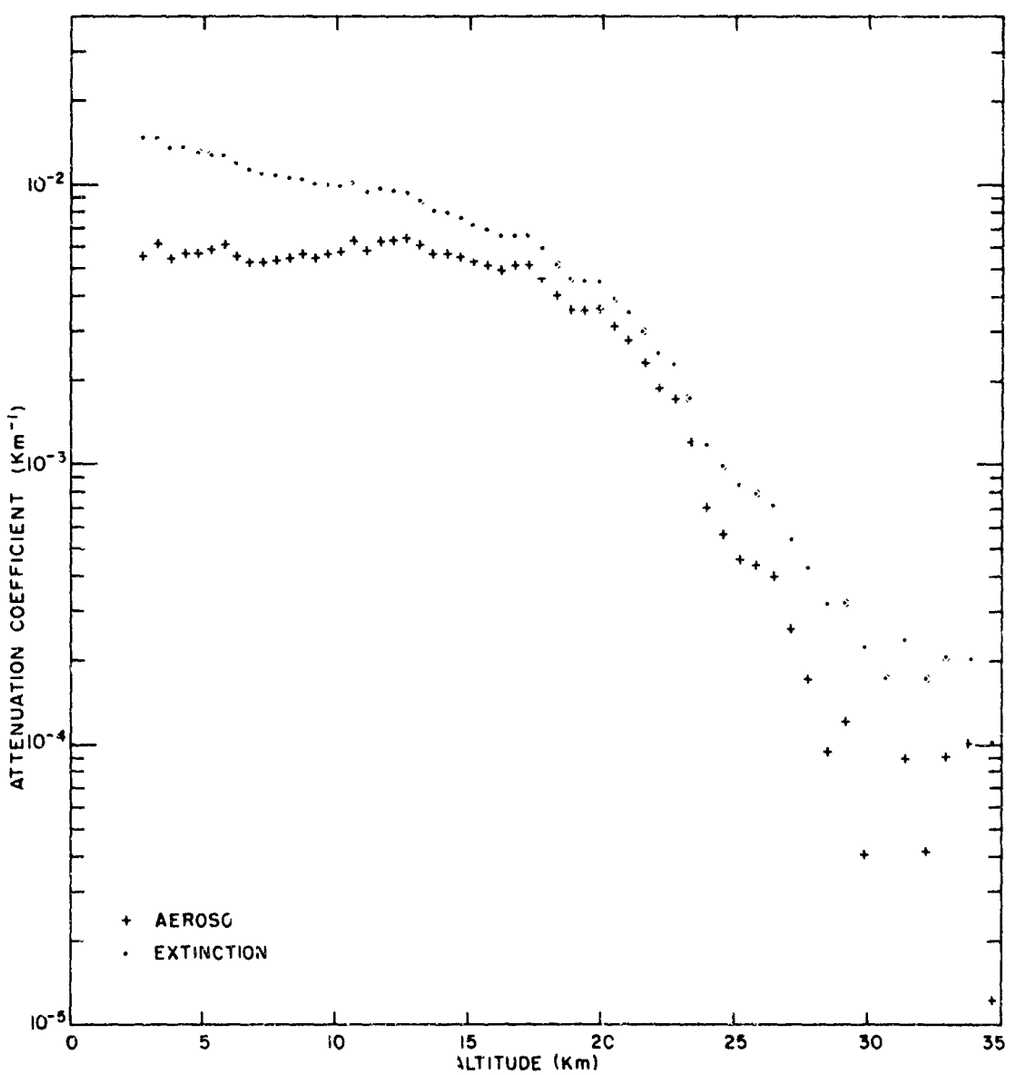

Profile 18. 18 December 1963. Time 22:05

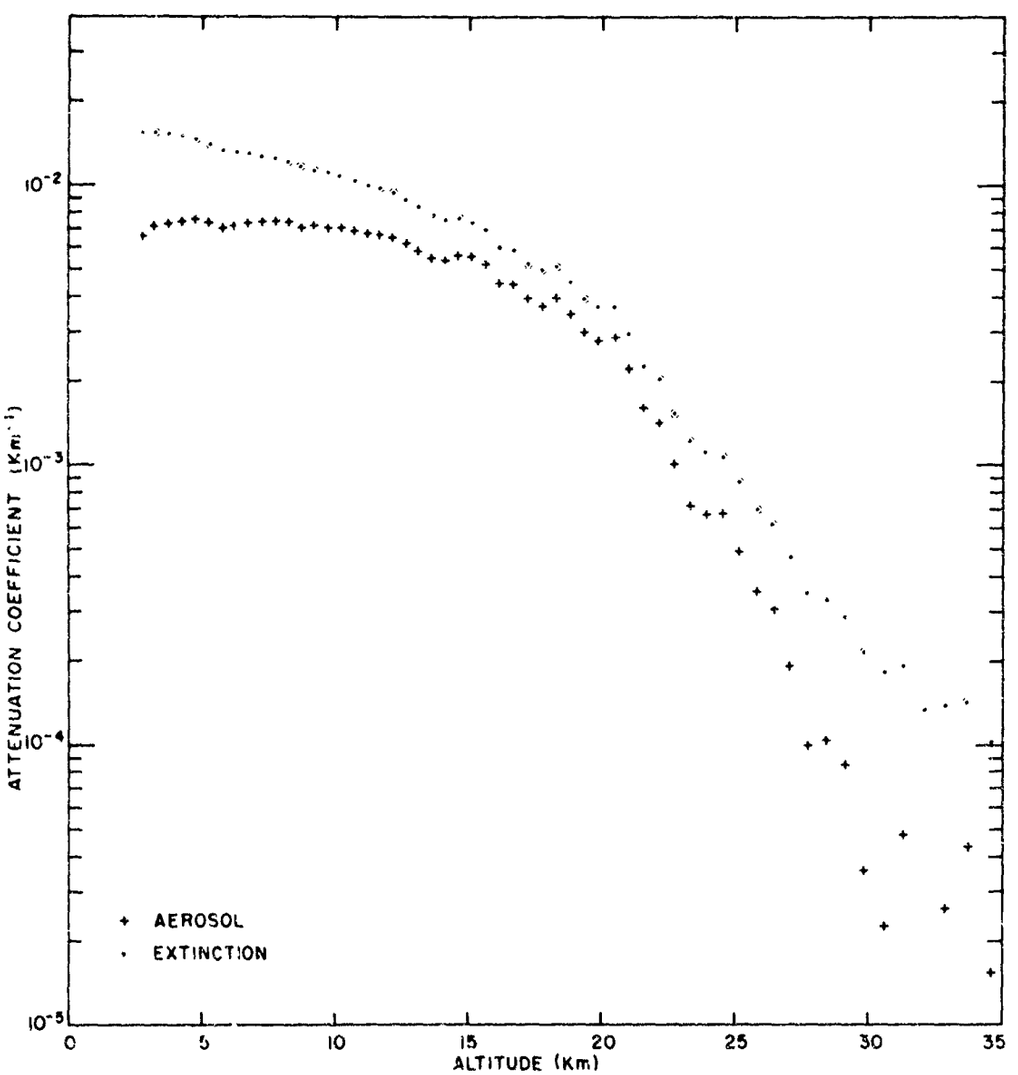

Profile 19. 19 December 1963. Time 00:47

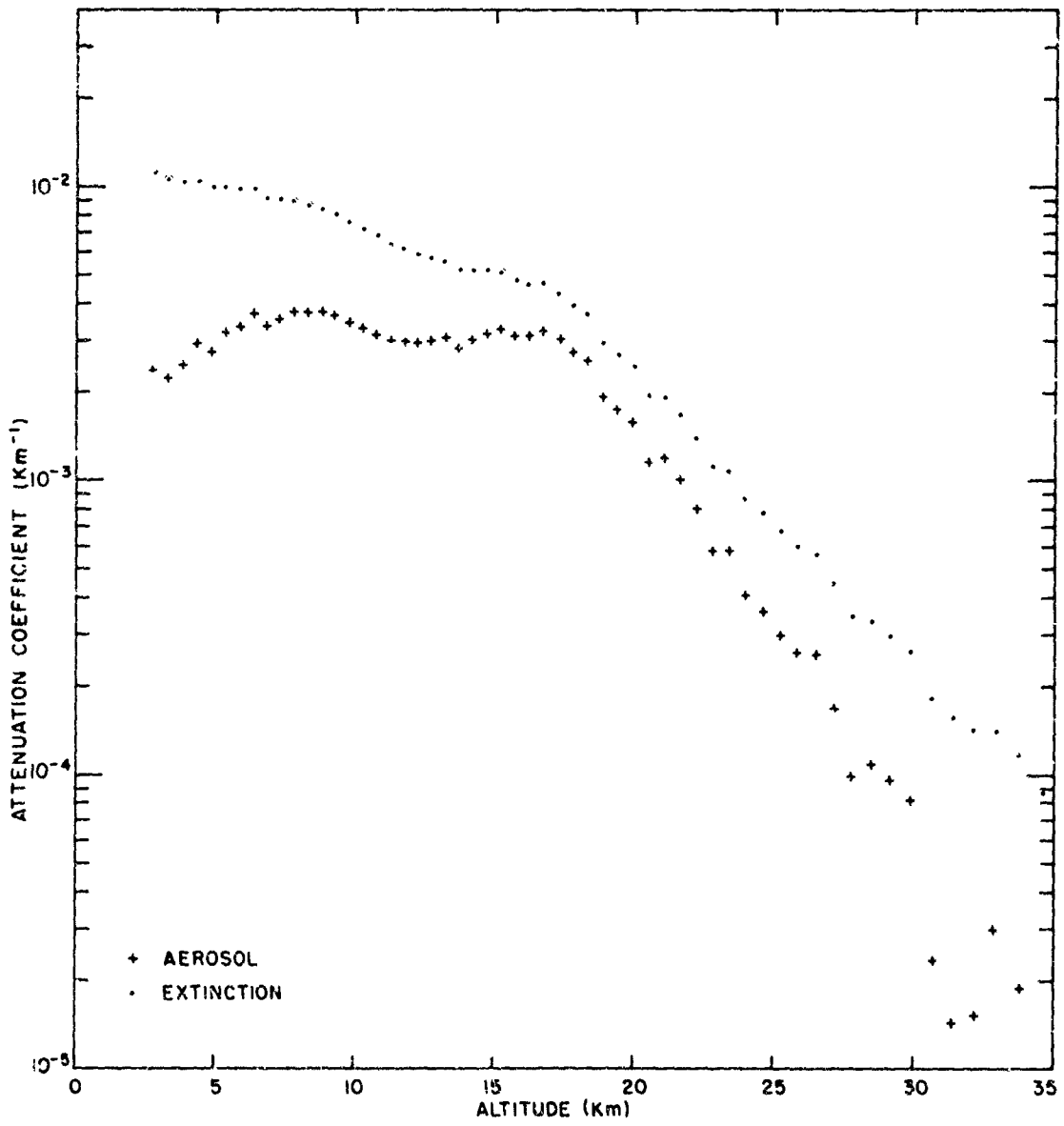

Profile 20. 19 December 1963. Time 02·15

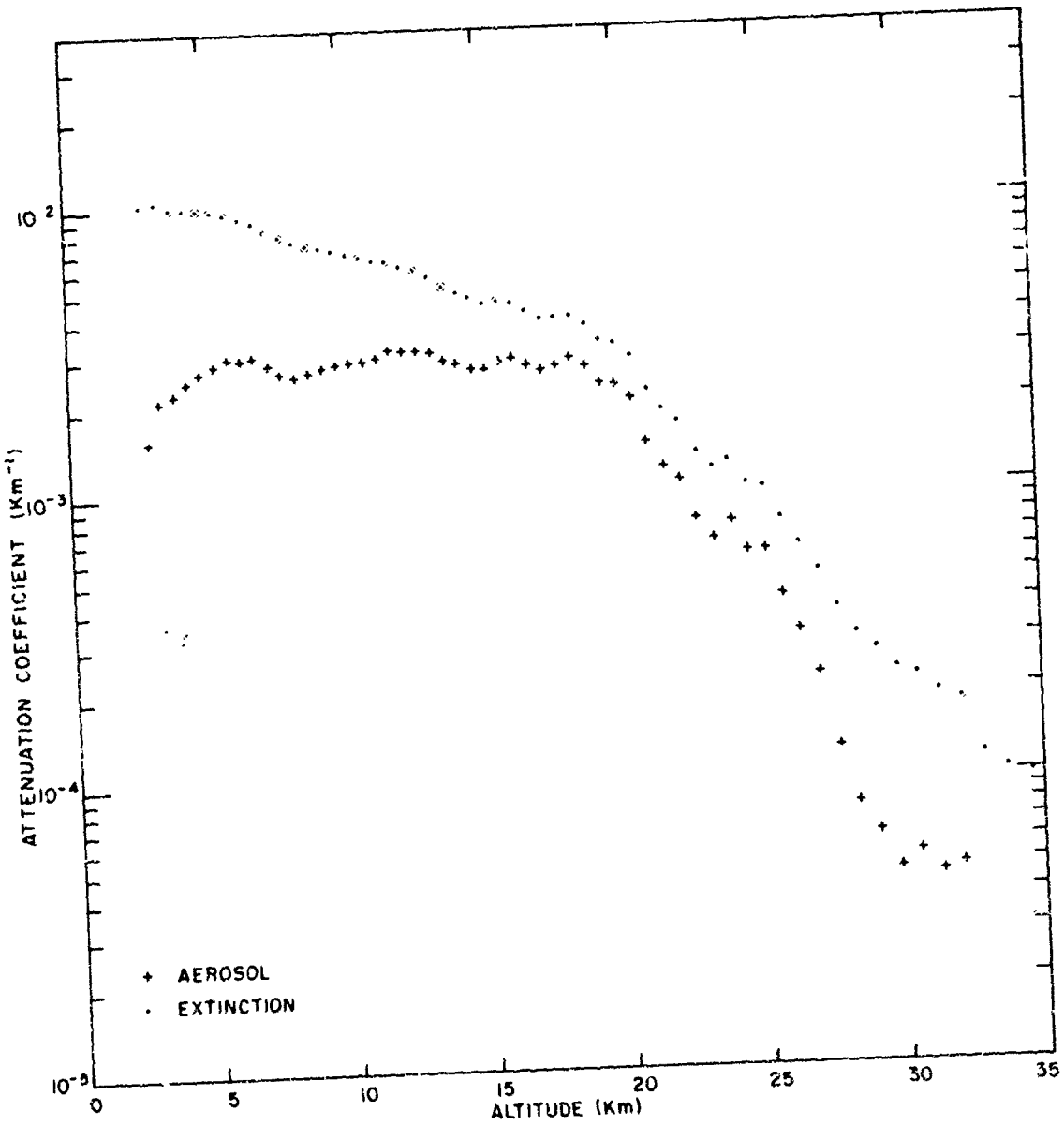

Profile 21. 19 December 1963. Time 03:03

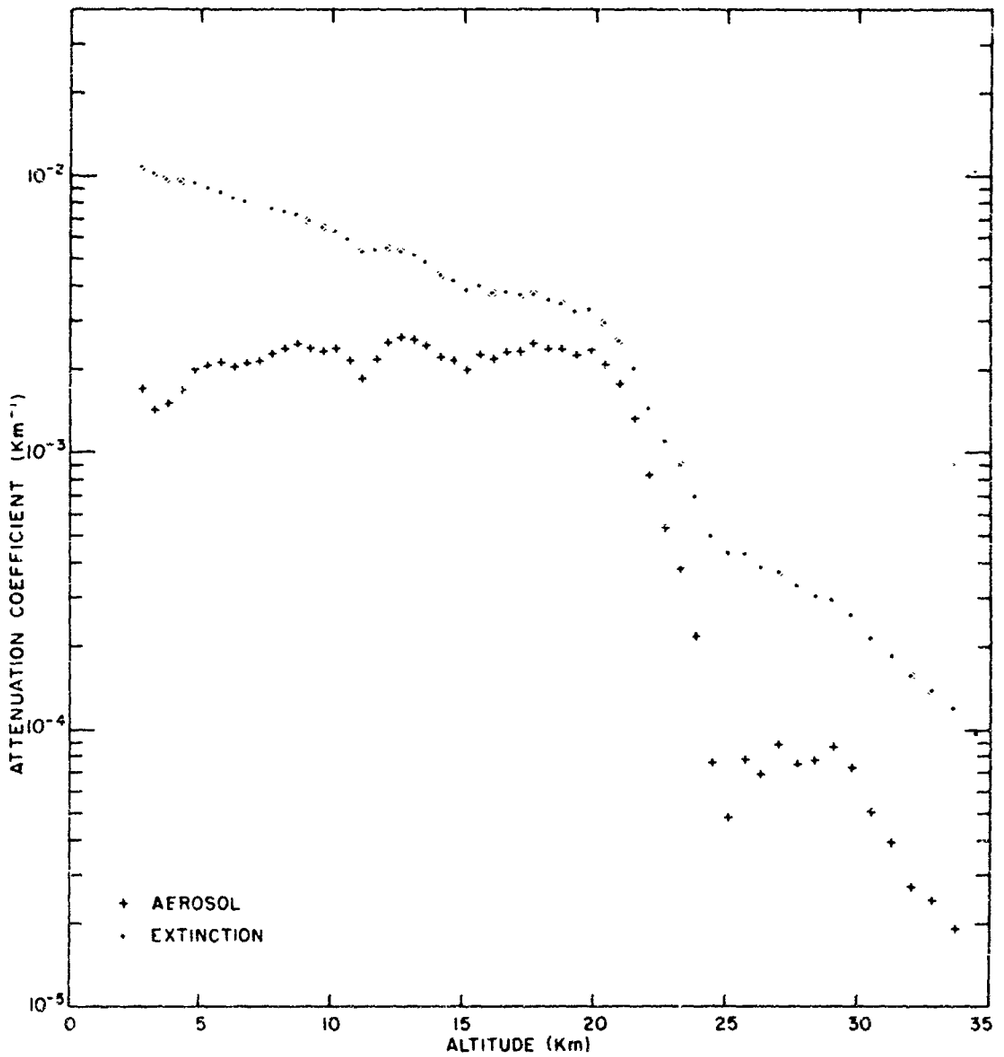

Profile 22. 19 December 1963. Time 04:25

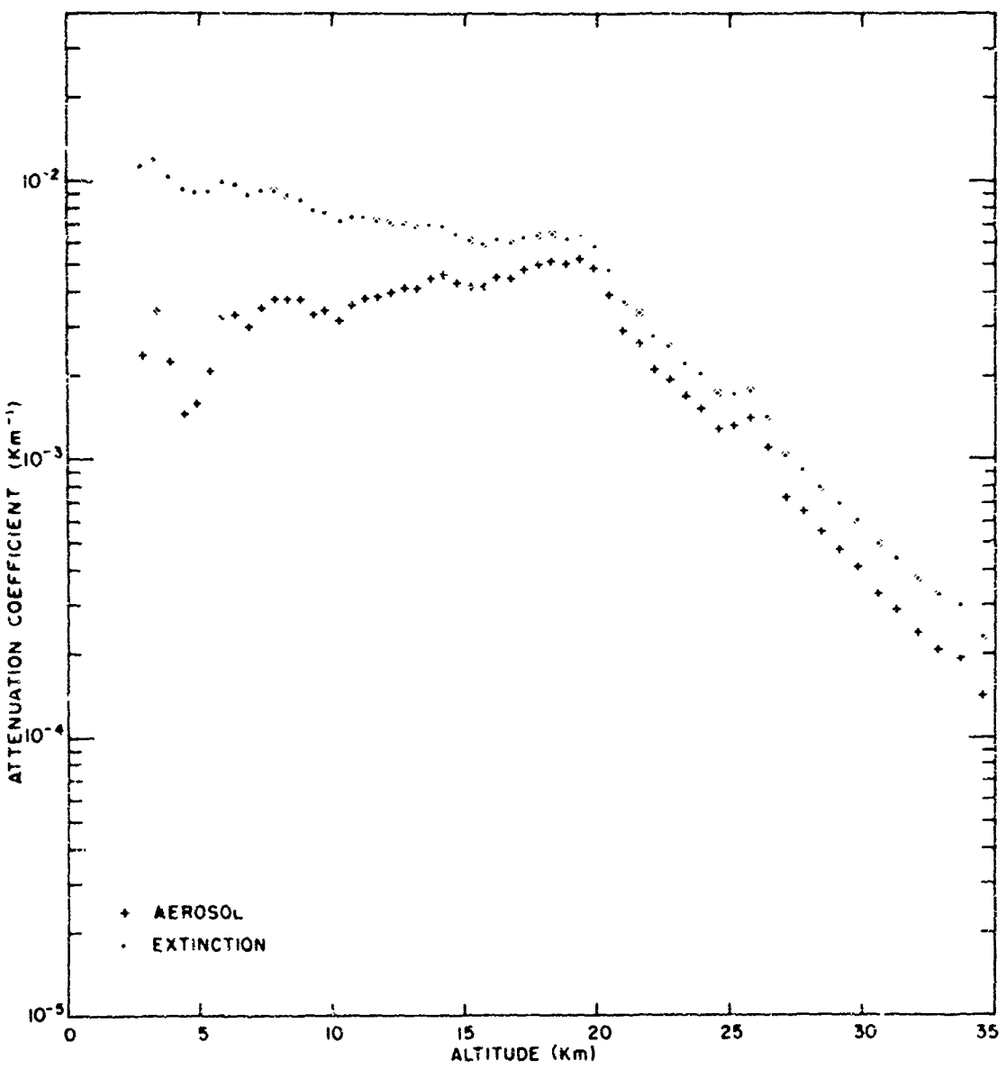

Profile 23. 13 February 1964. Time 21:30

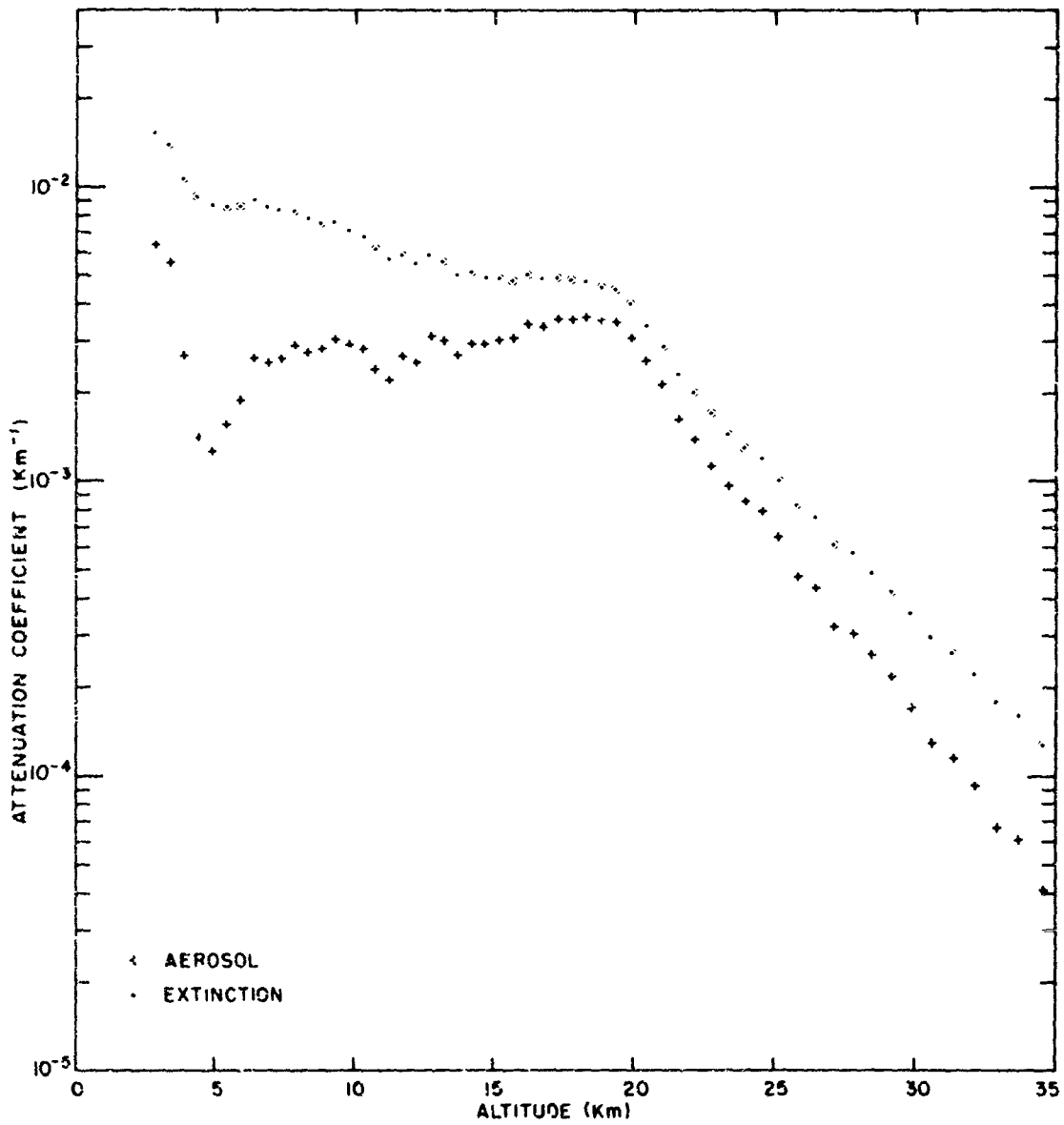

Profile 24. 13 February 1964. Time 23 30

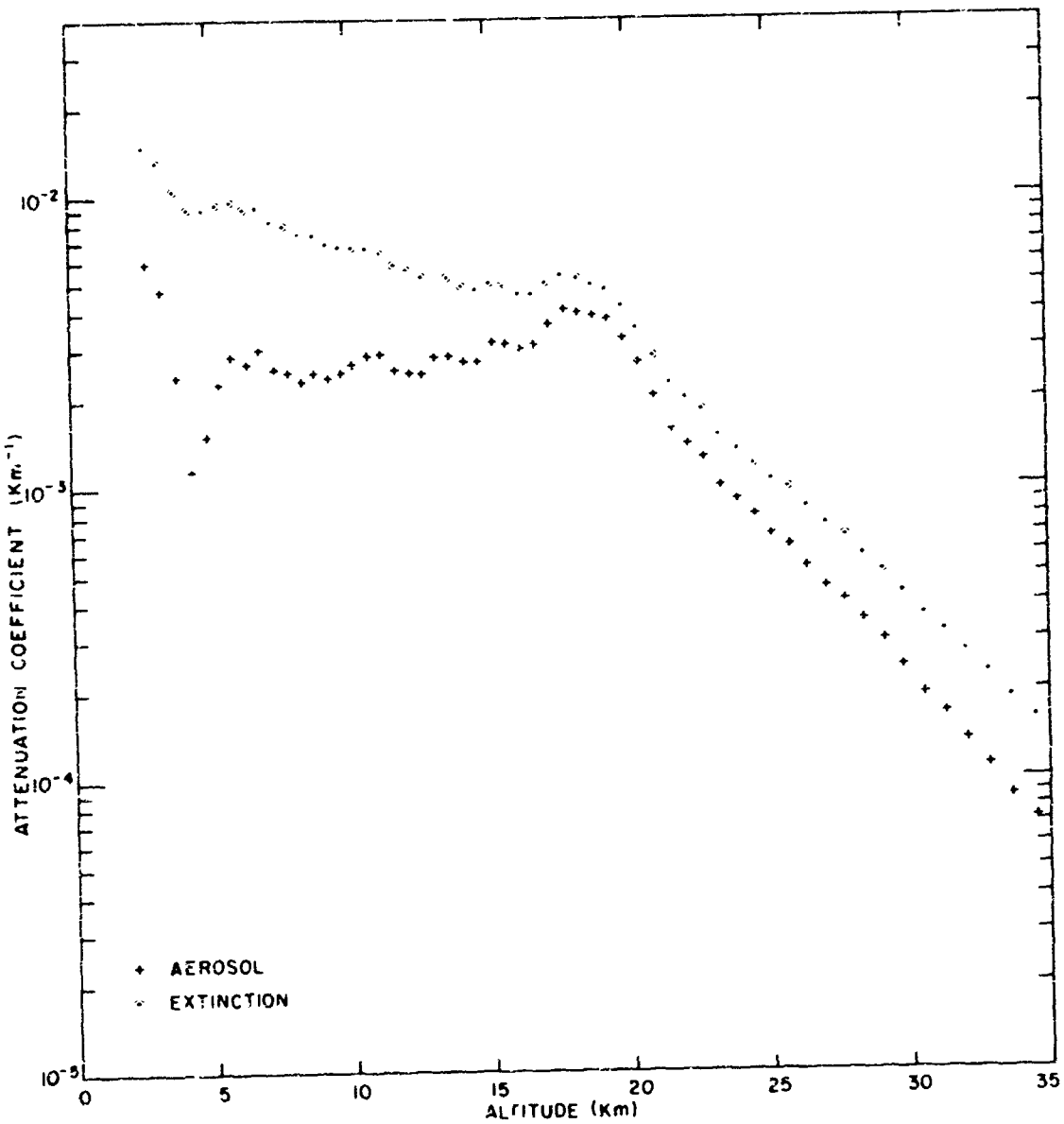

Profile 25. 14 February 1964. Time 00:56

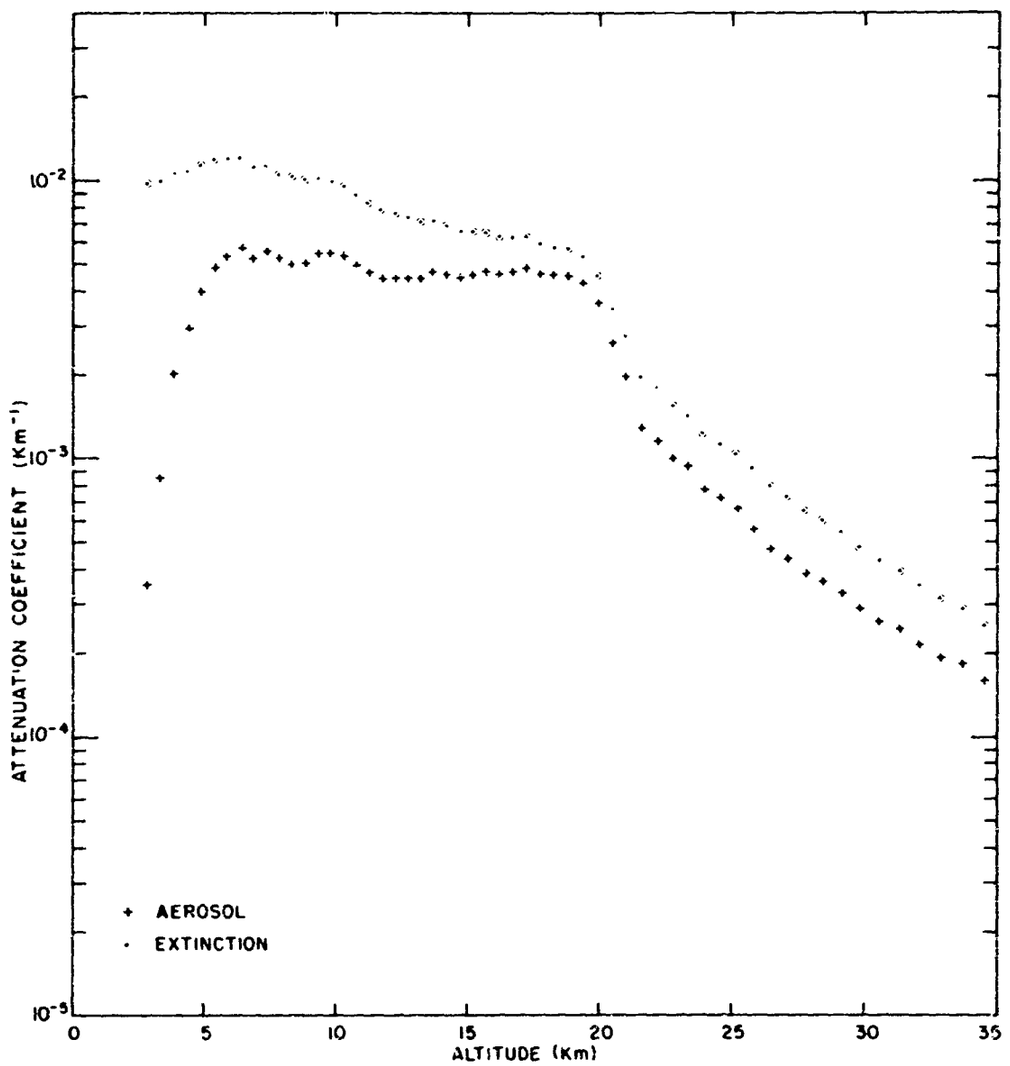

Profile 26. 14 February 1964. Time 02·38

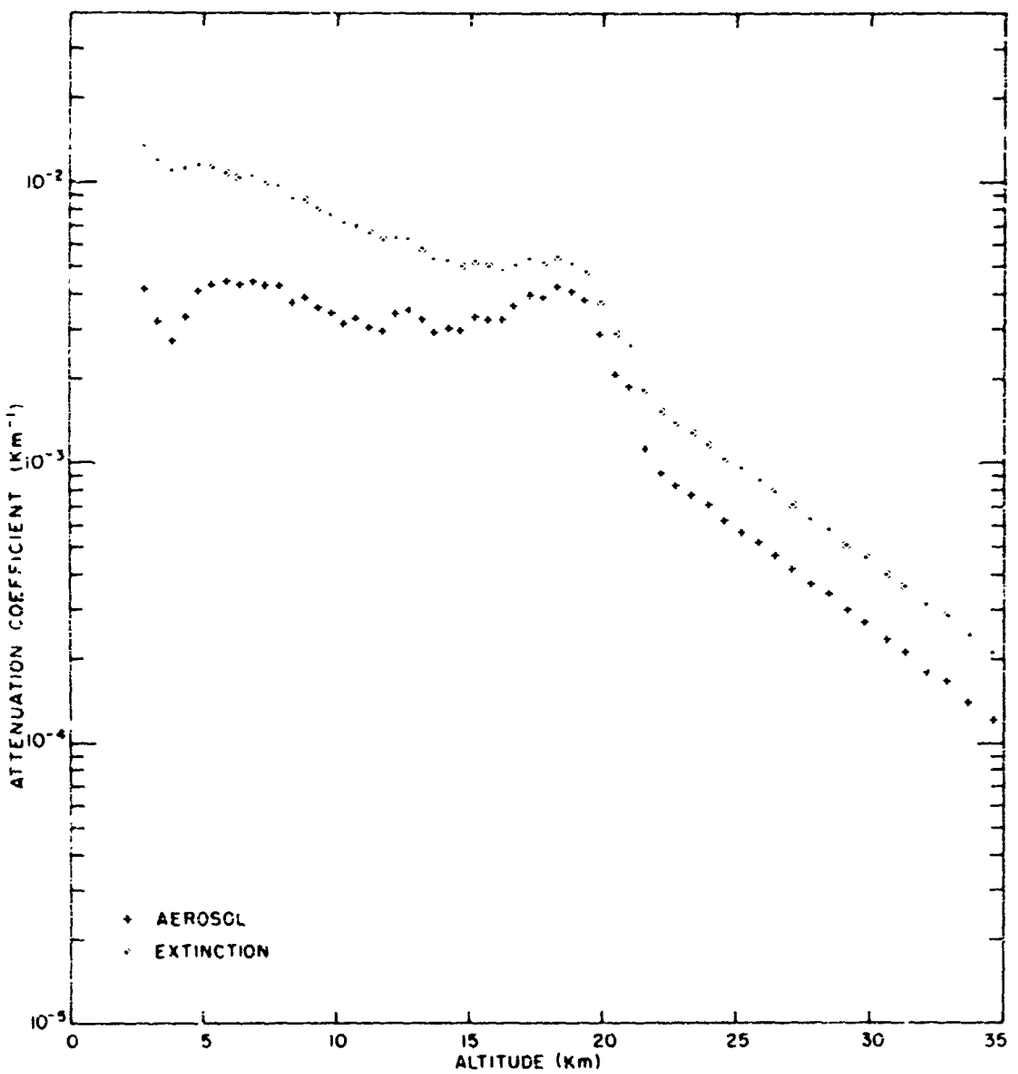

Profile 27. 14 February 1964. Time 03 36

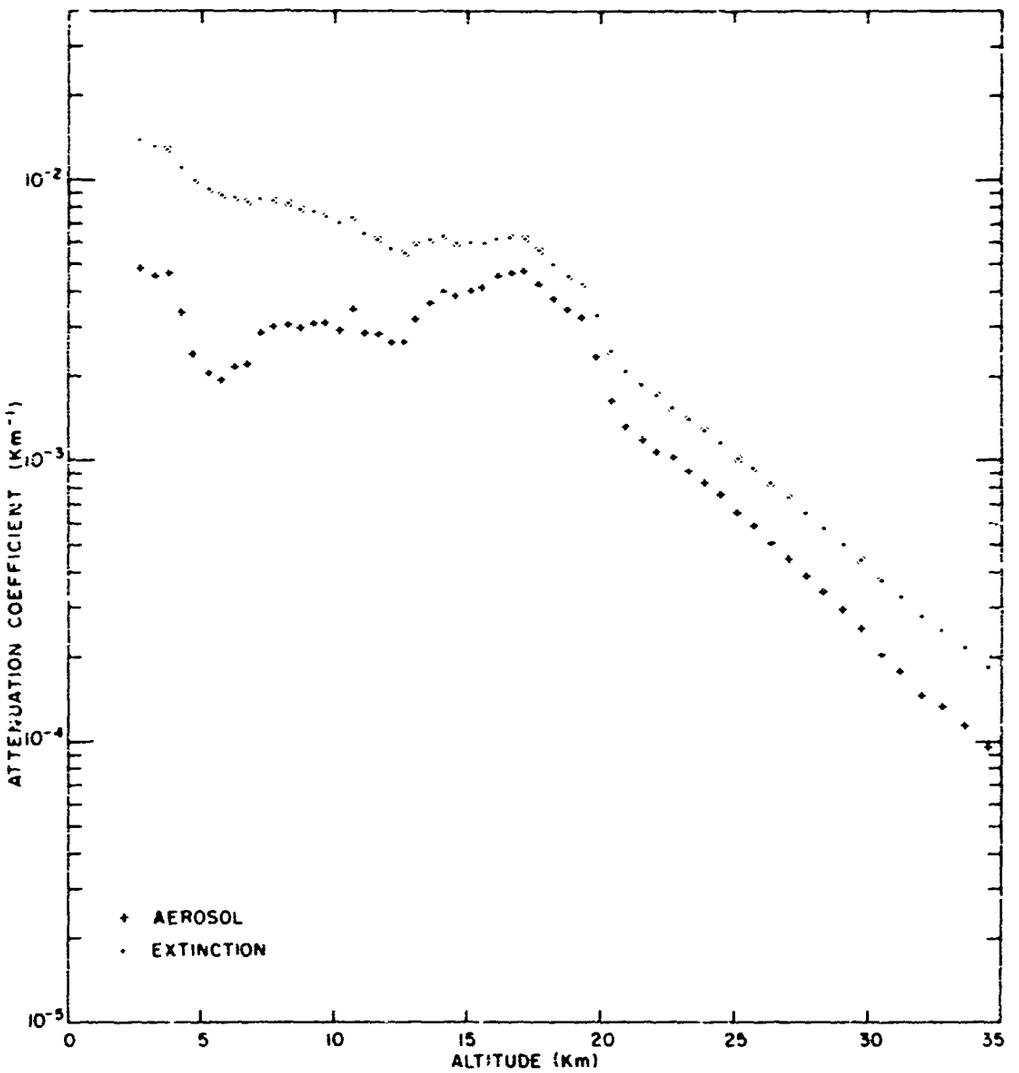

Profile 28. 14 February 1964. Time 23·04

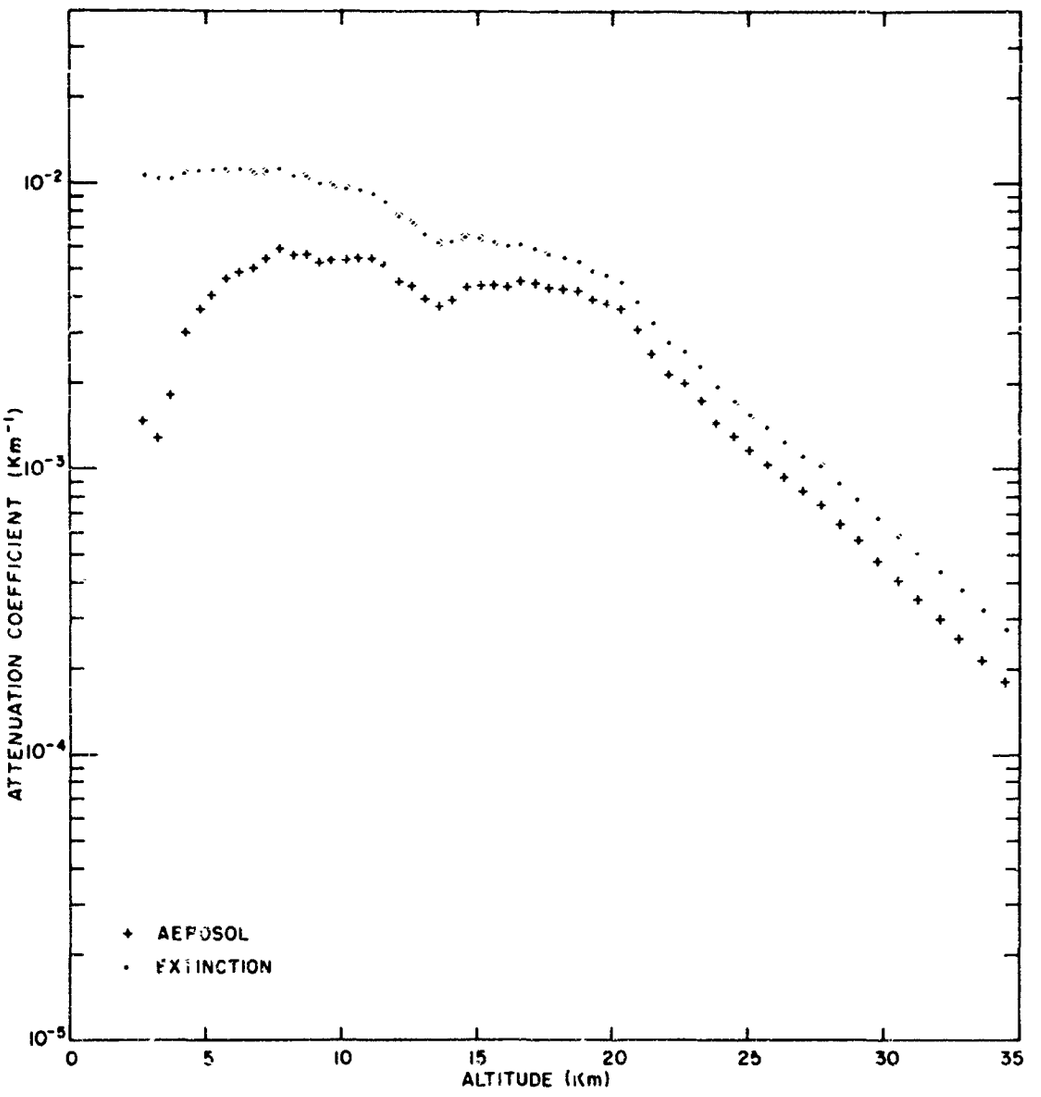

Profile 29. 16 February 1964. Time 03:05

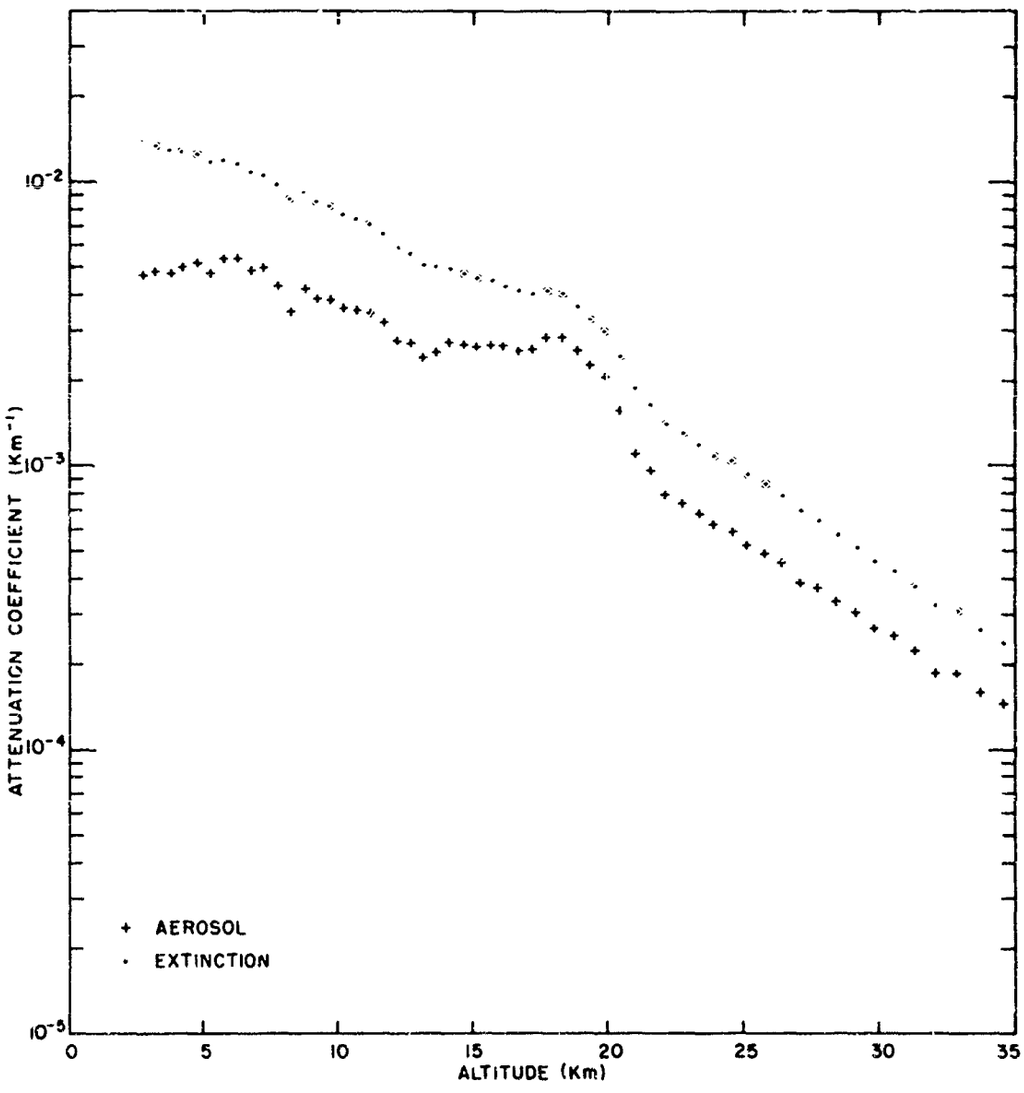

Profile 30. 16 February 1964. Time 03:53

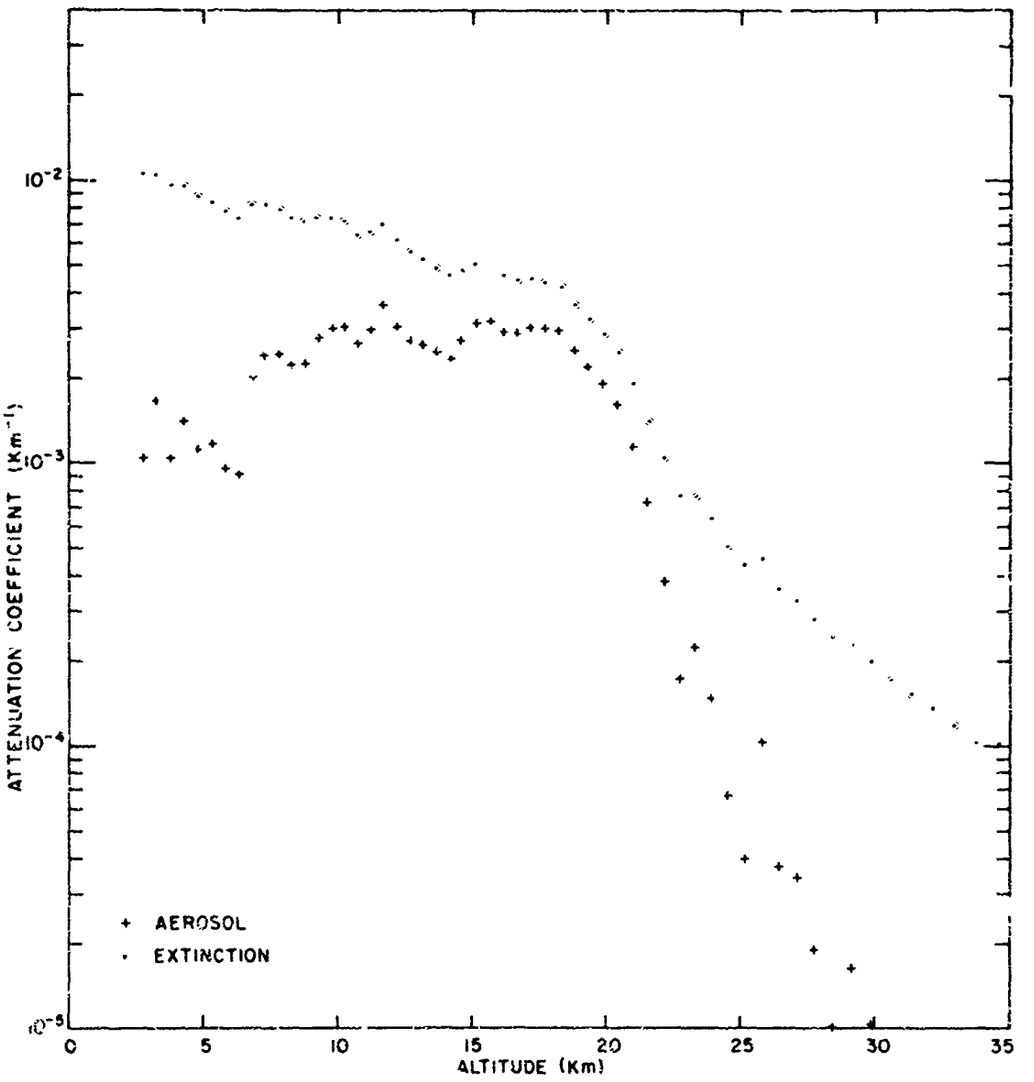

Profile 31, 16 February 1964, Time 20:33

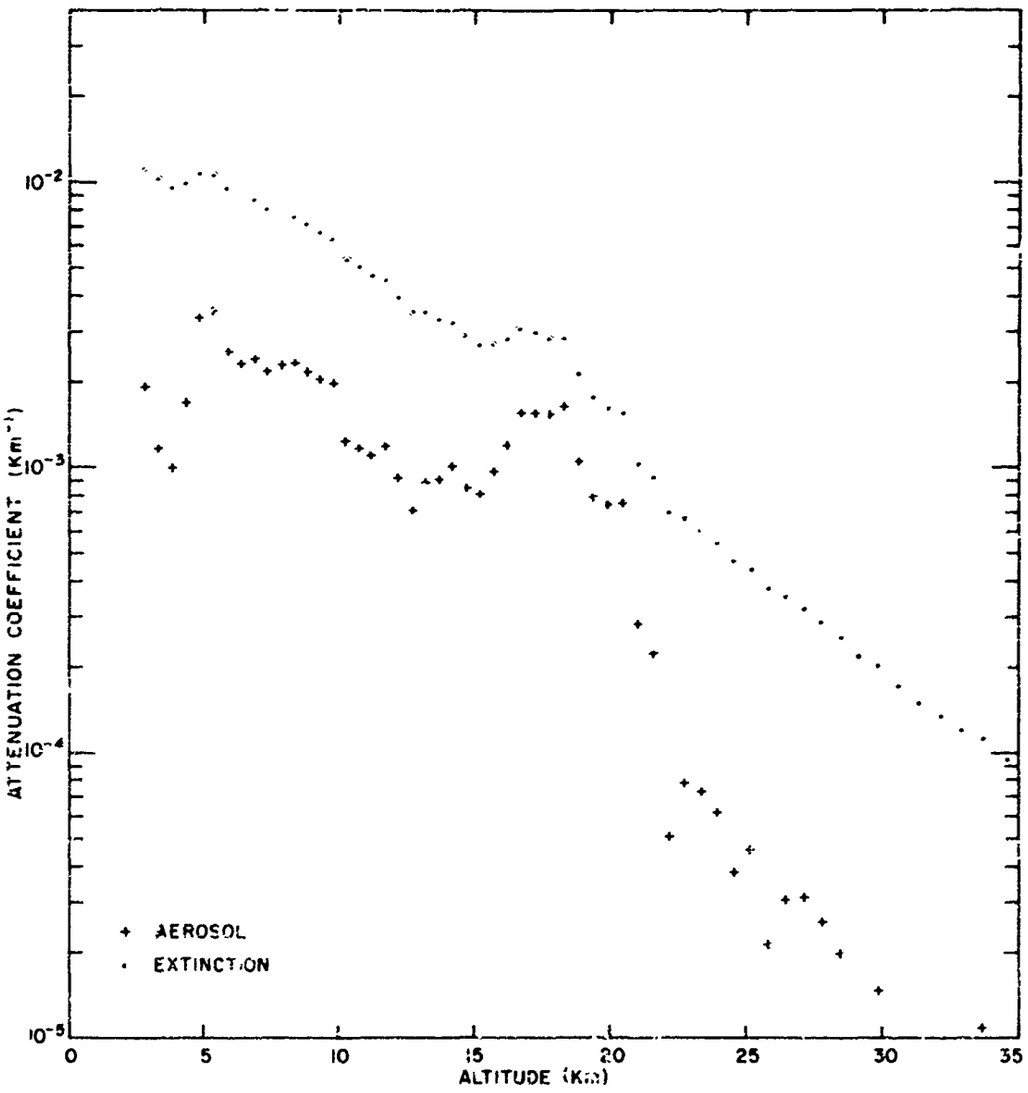

Profile 32. 17 February 1964. Time 23:27

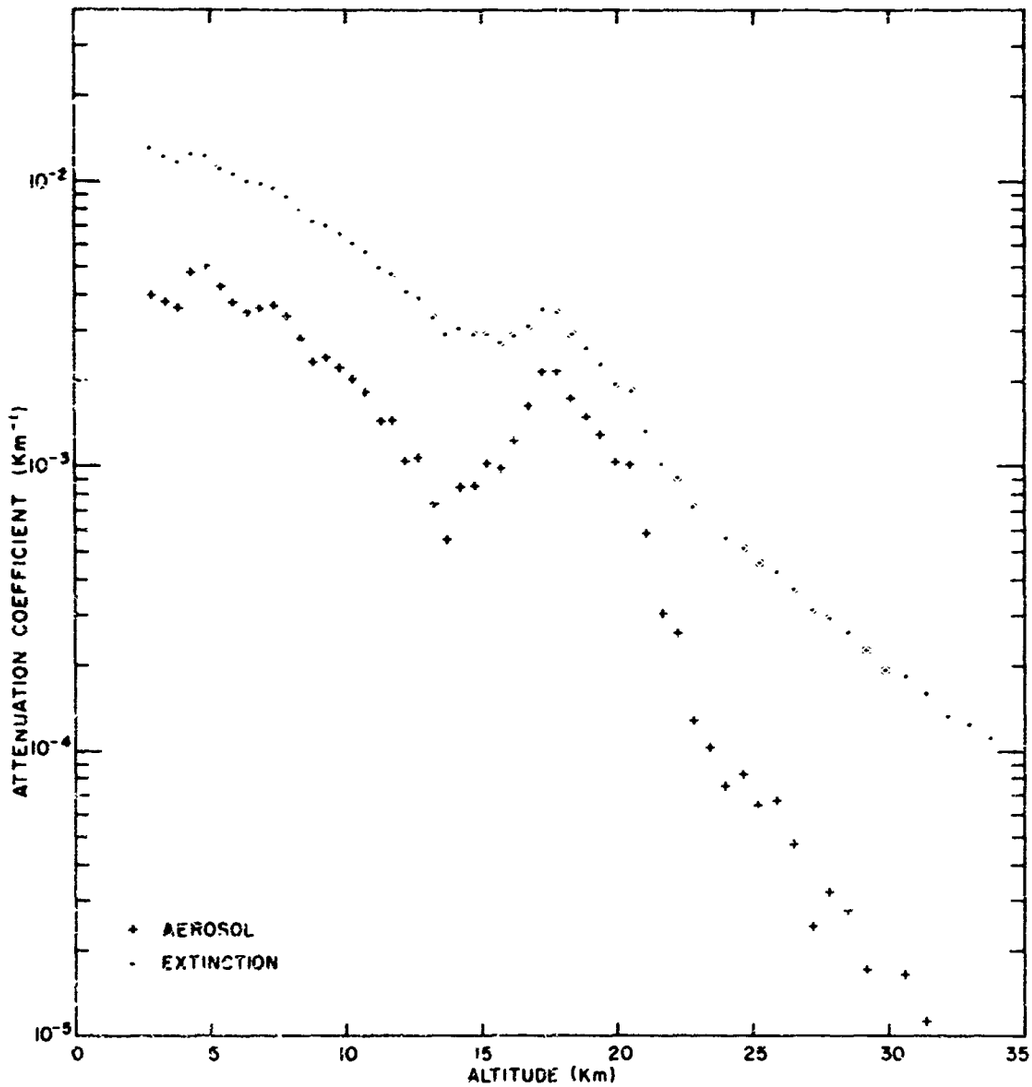

Profile 33. 18 February 1964. Time 01:15

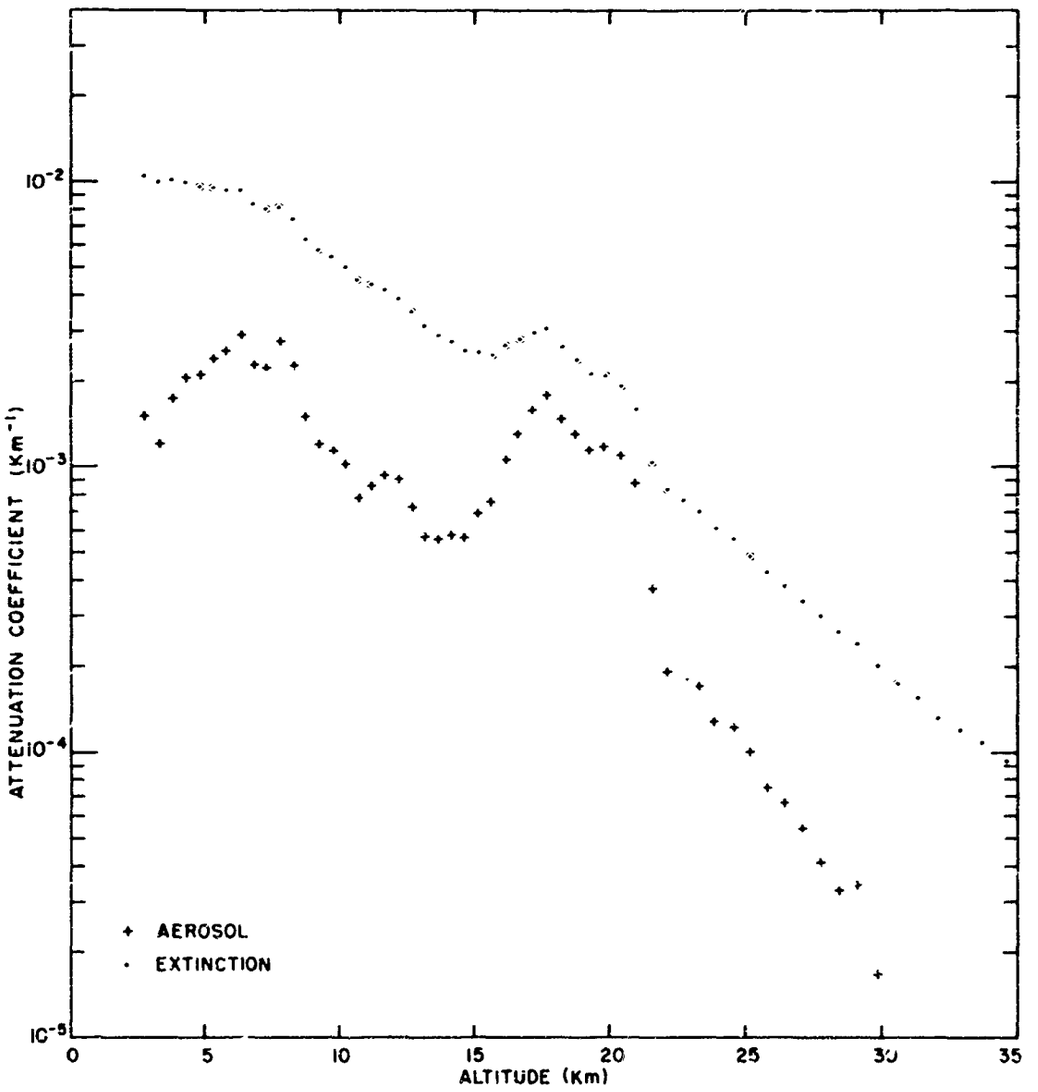

Profile 34. 18 February 1964. Time 03:04

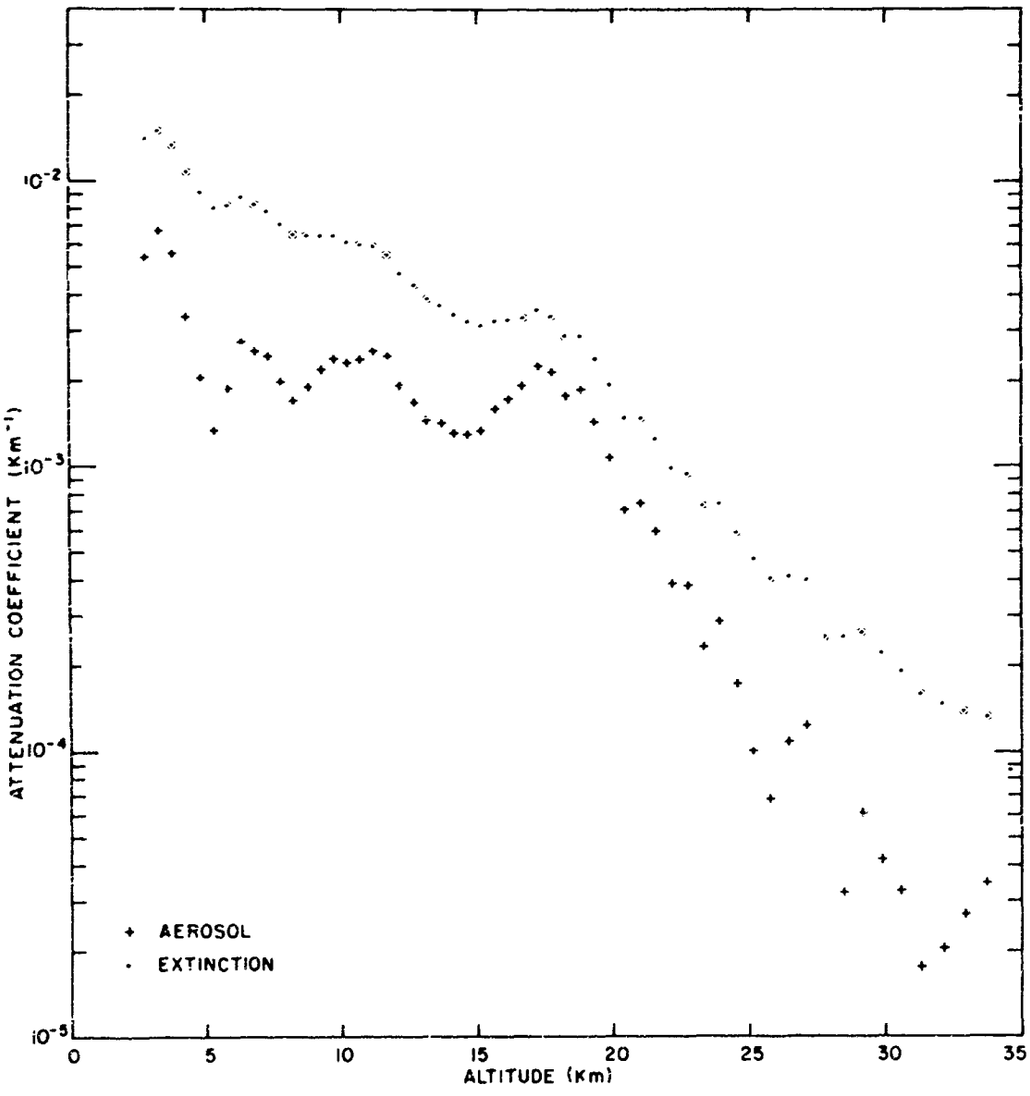

Profile 35. 14 March 1964. Time 01:20

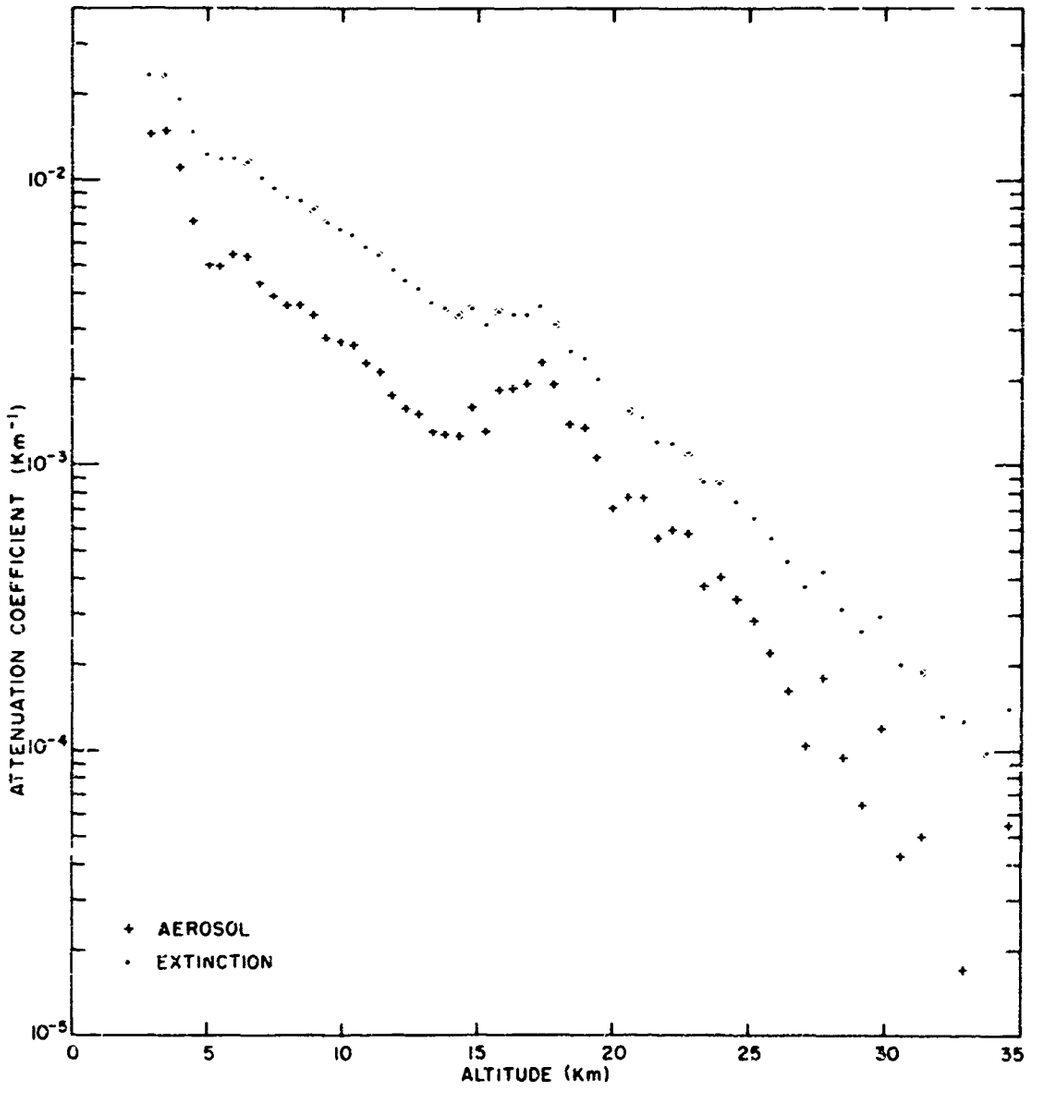

Profile 36. 14 March 1964. Time 02:00

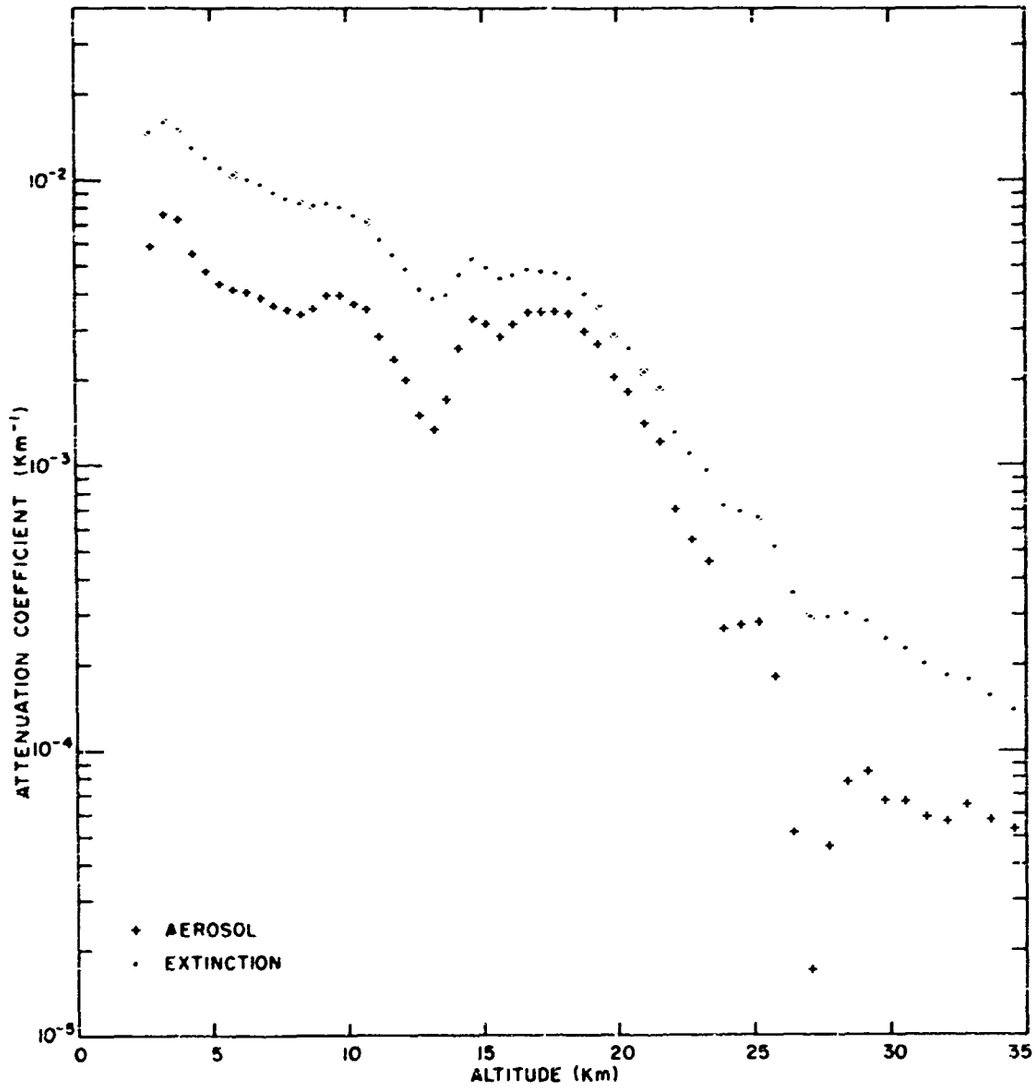

Profile 37. 14 March 1964. Time 20:45

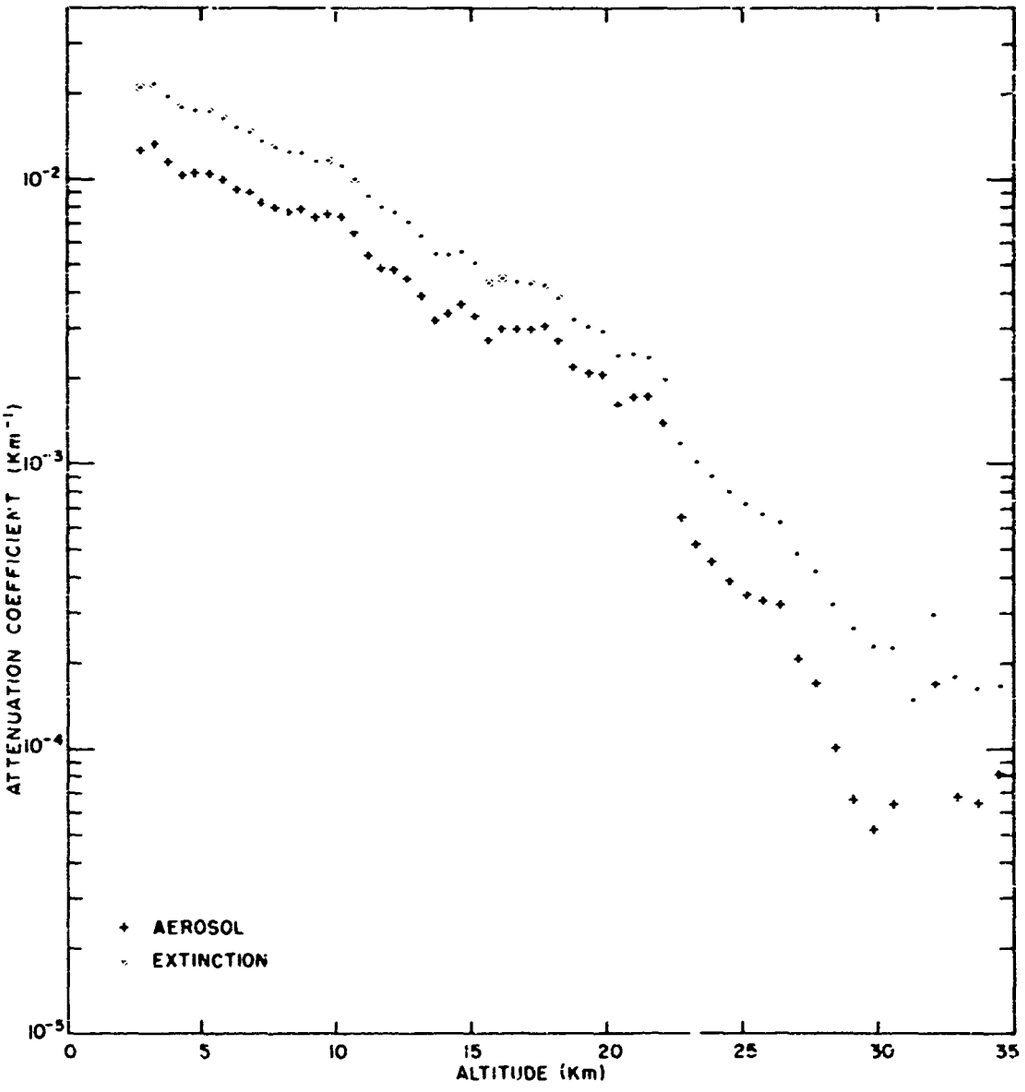

Profile 38. 14 March 1964. Time 22:25

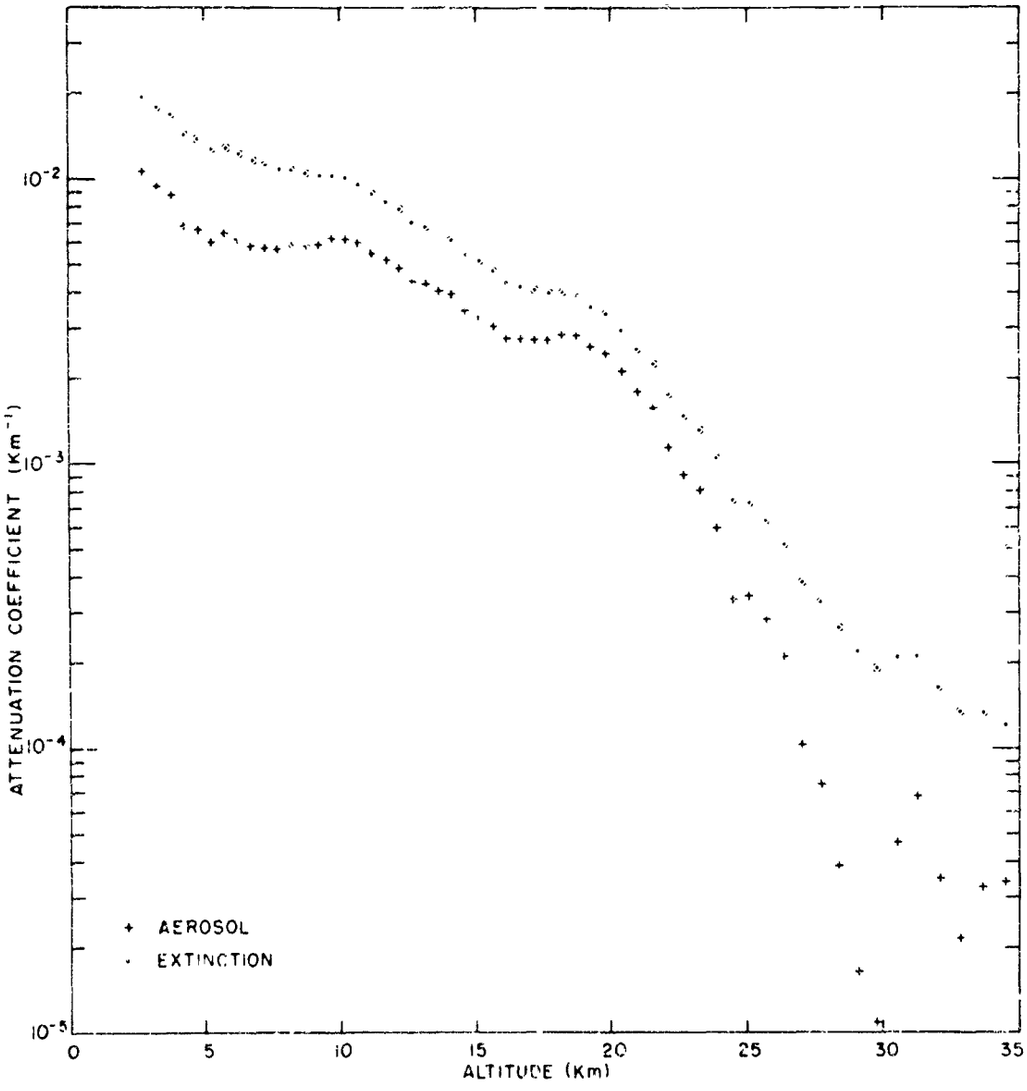

Profile 39. 15 March 1964. Time 02:35

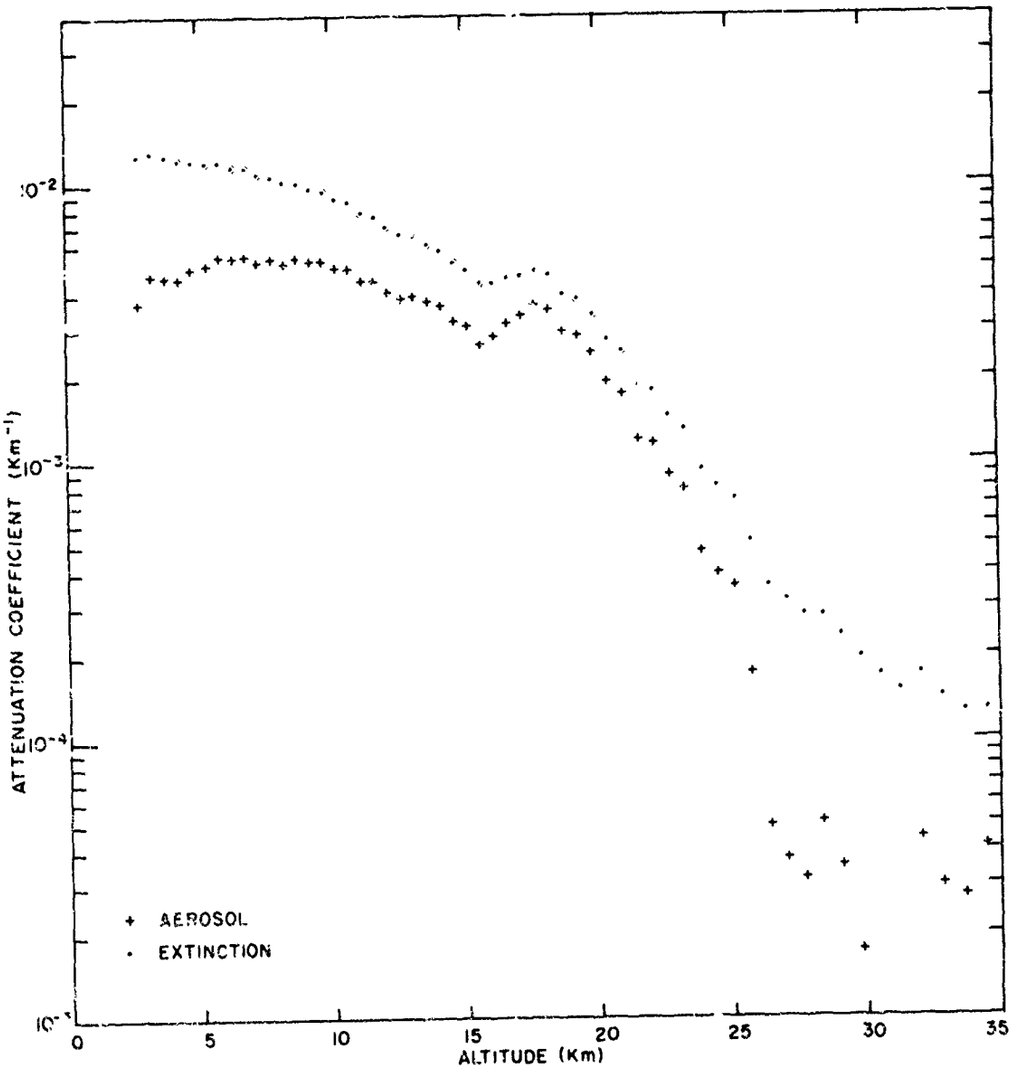

Profile 40. 15 March 1964. Time 04:03

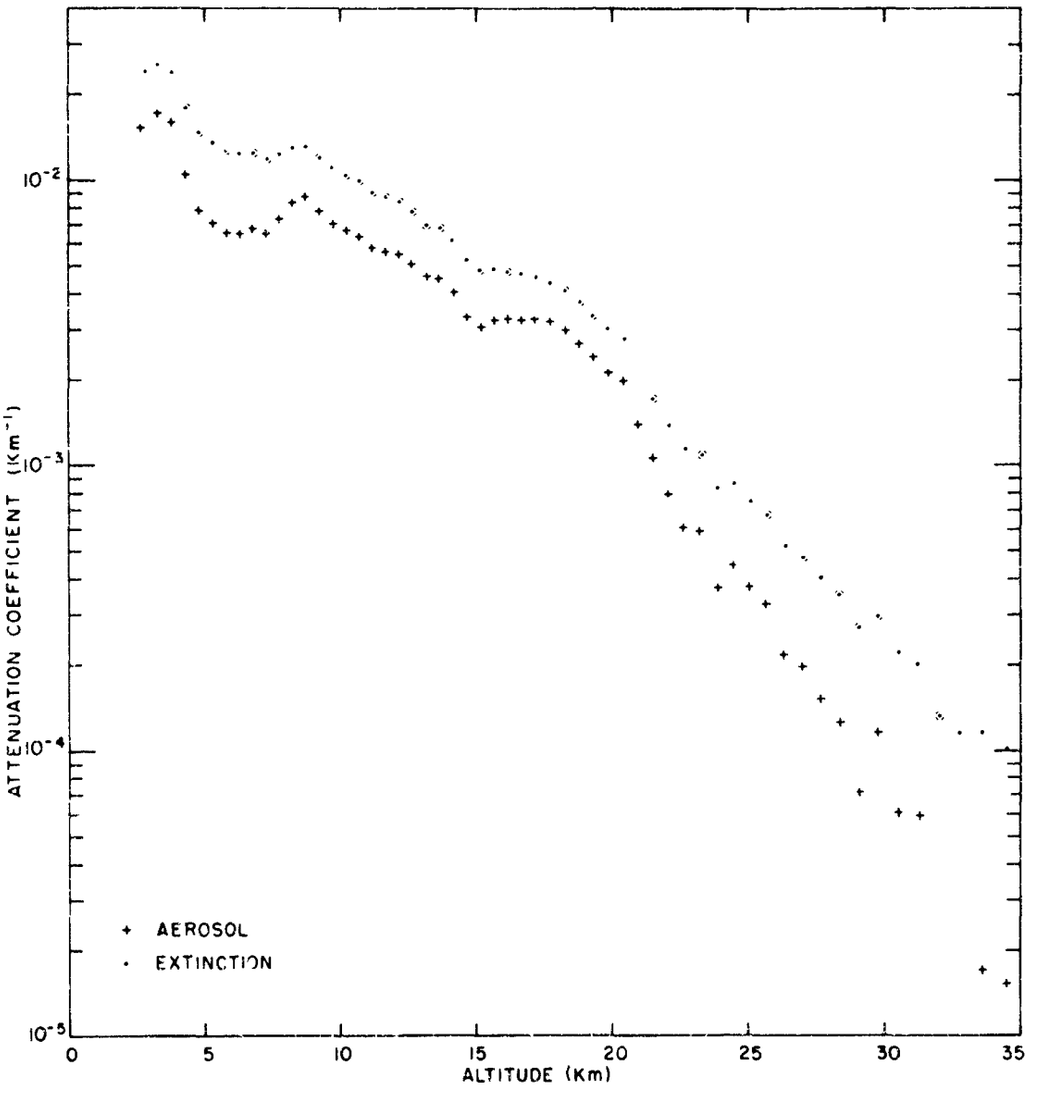

Profile 41. 8 April 1964. Time 22·38

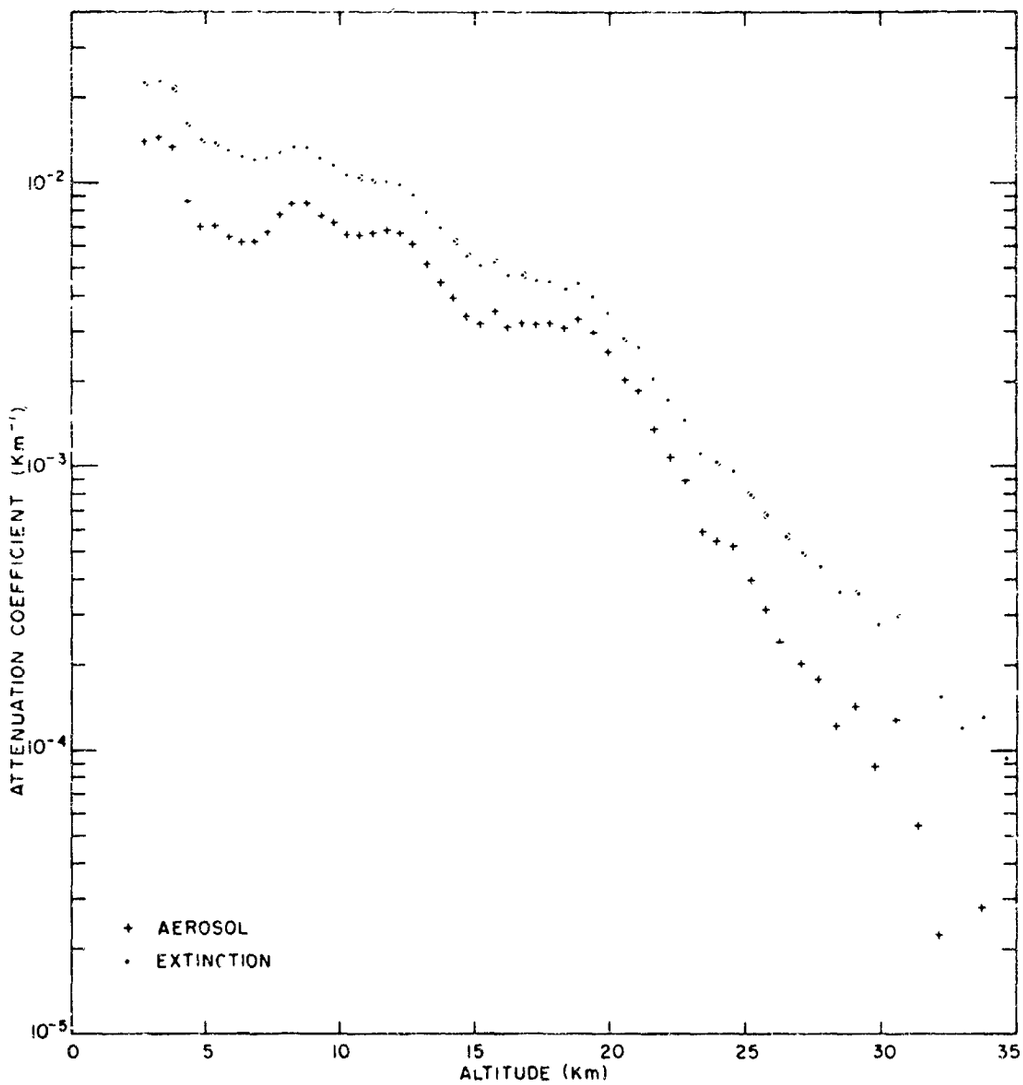

Profile 42. 8 April 1964. Time 23:43

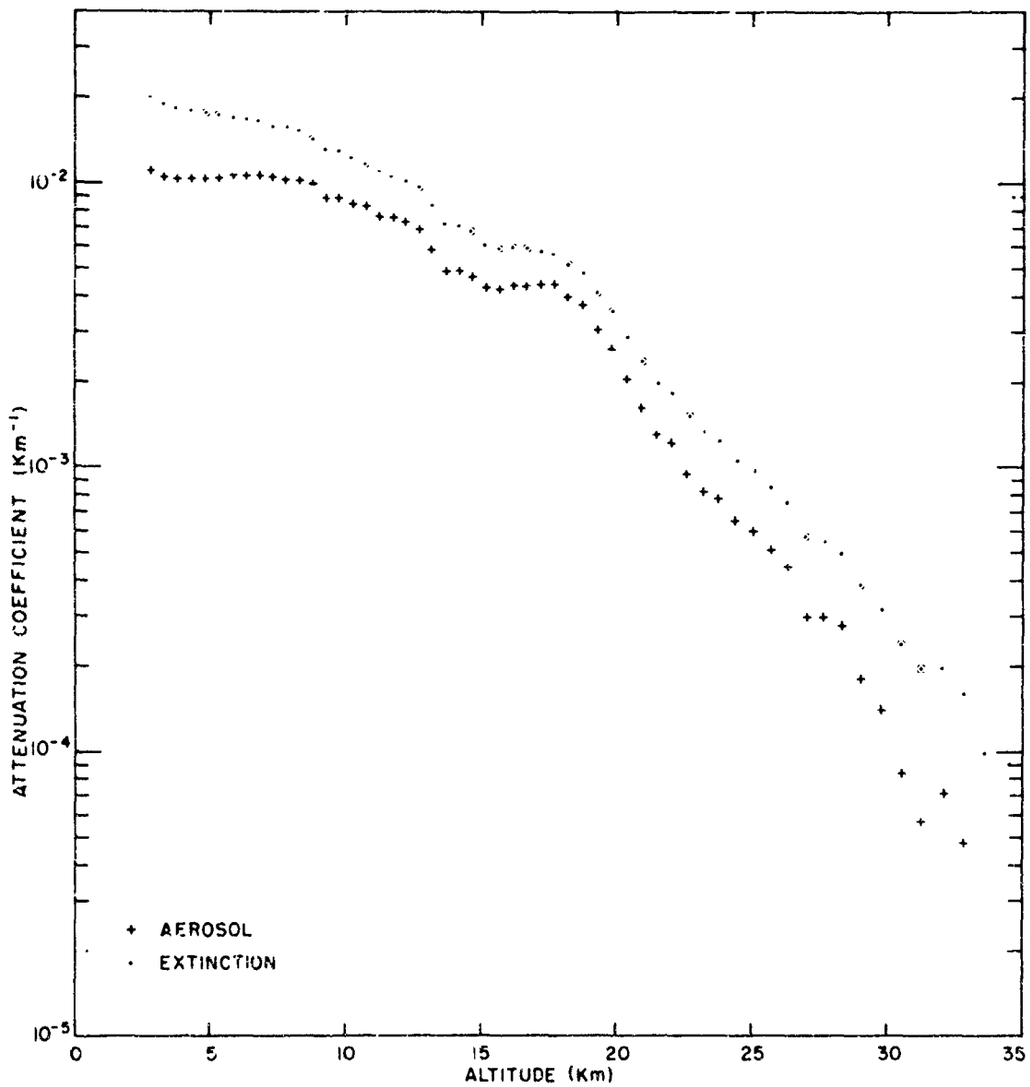

Profile 43. 9 April 1964. Time 00·50

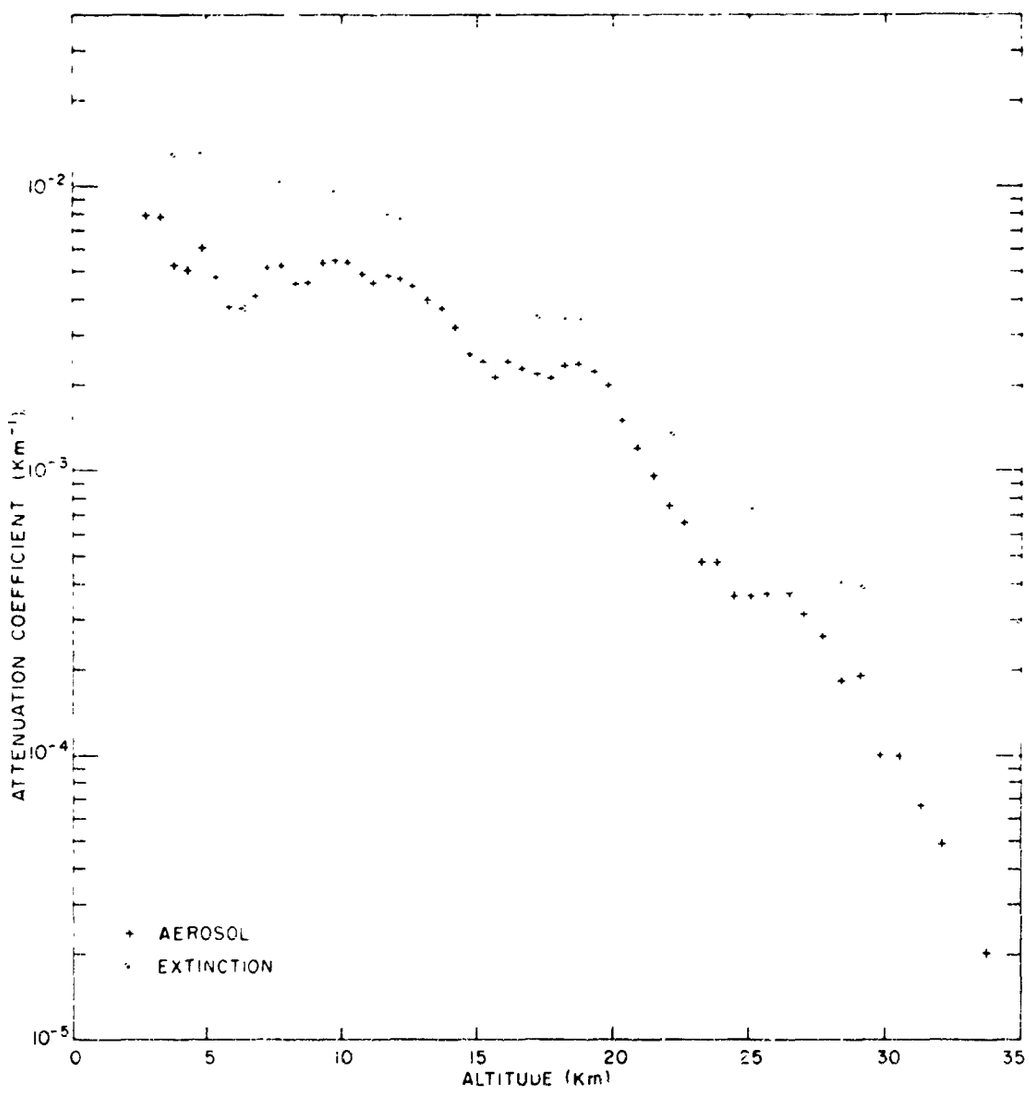

Profile 44. 9 April 1964. Time 01:54

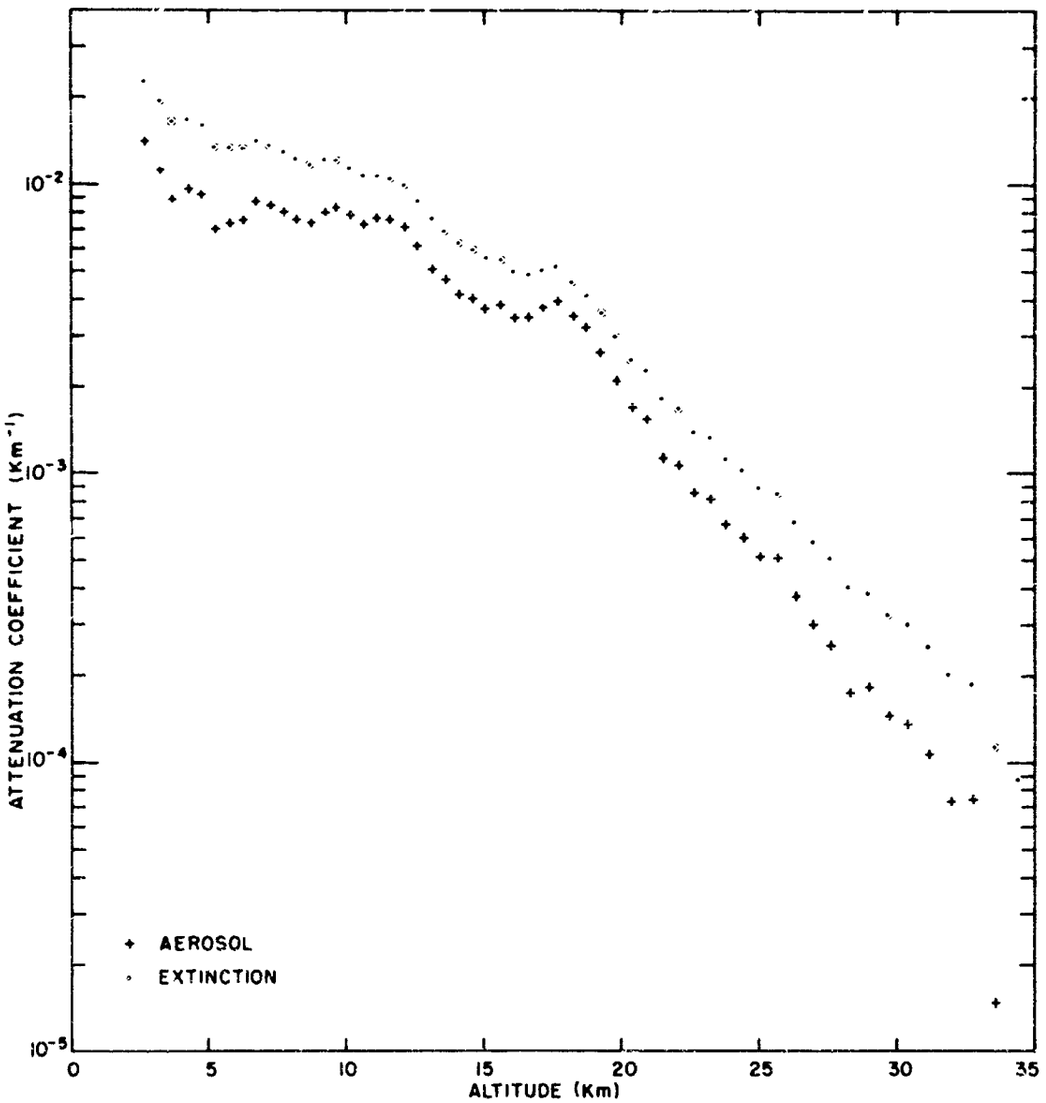

Profile 45. 9 April 1964. Time 02:50

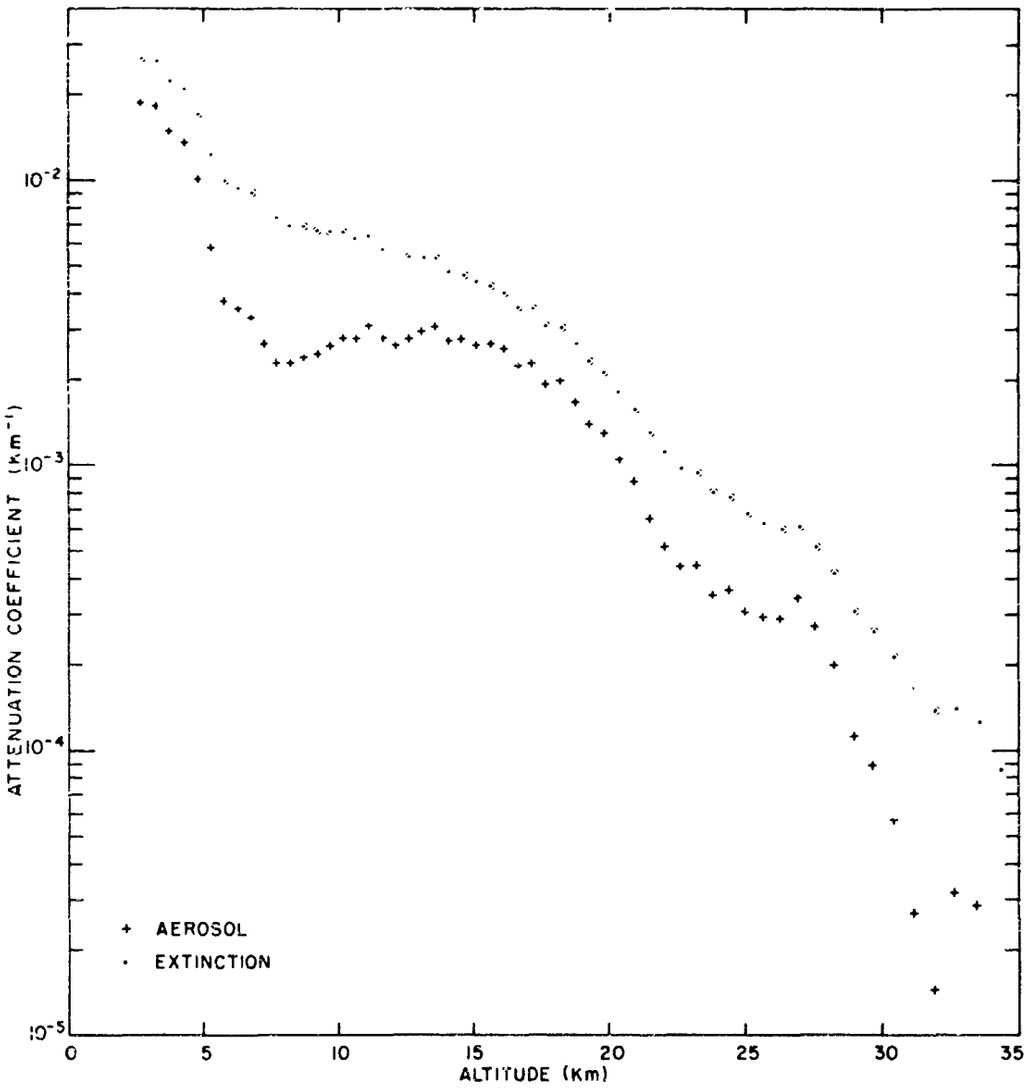

Profile 46. 10 April 1964. Time 20:33

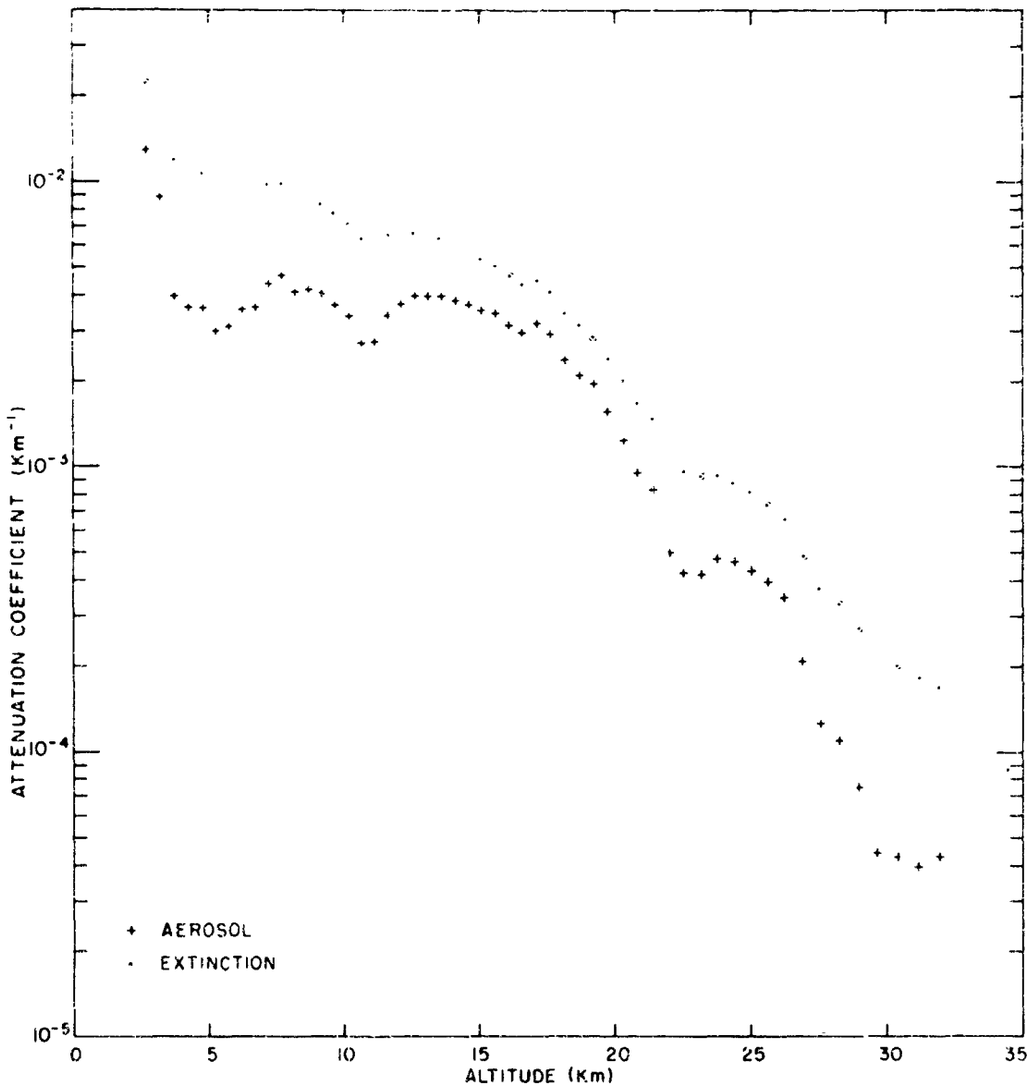

Profile 47. 11 April 1964. Time 02:00

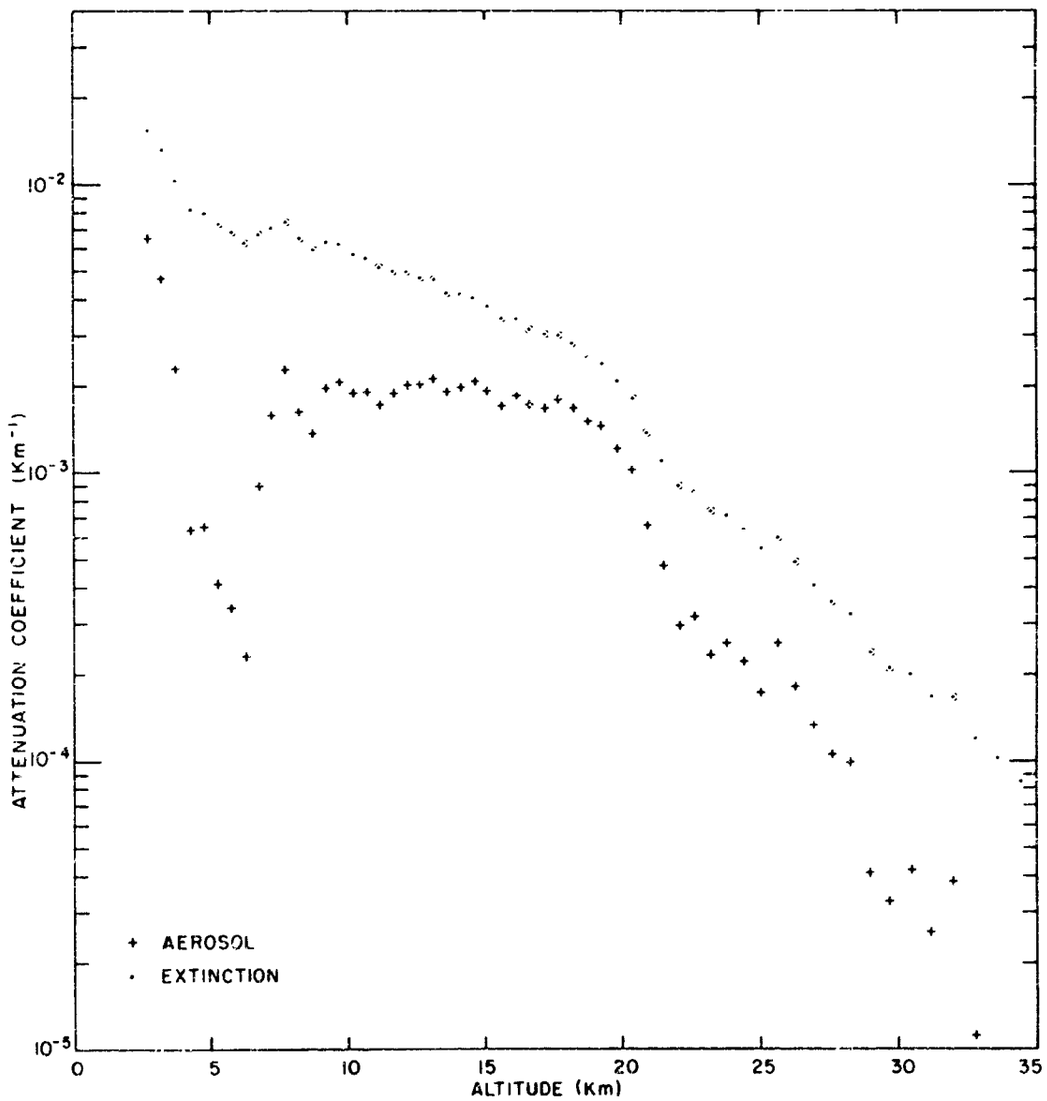

Profile 48. 11 April 1964. Time 02:53

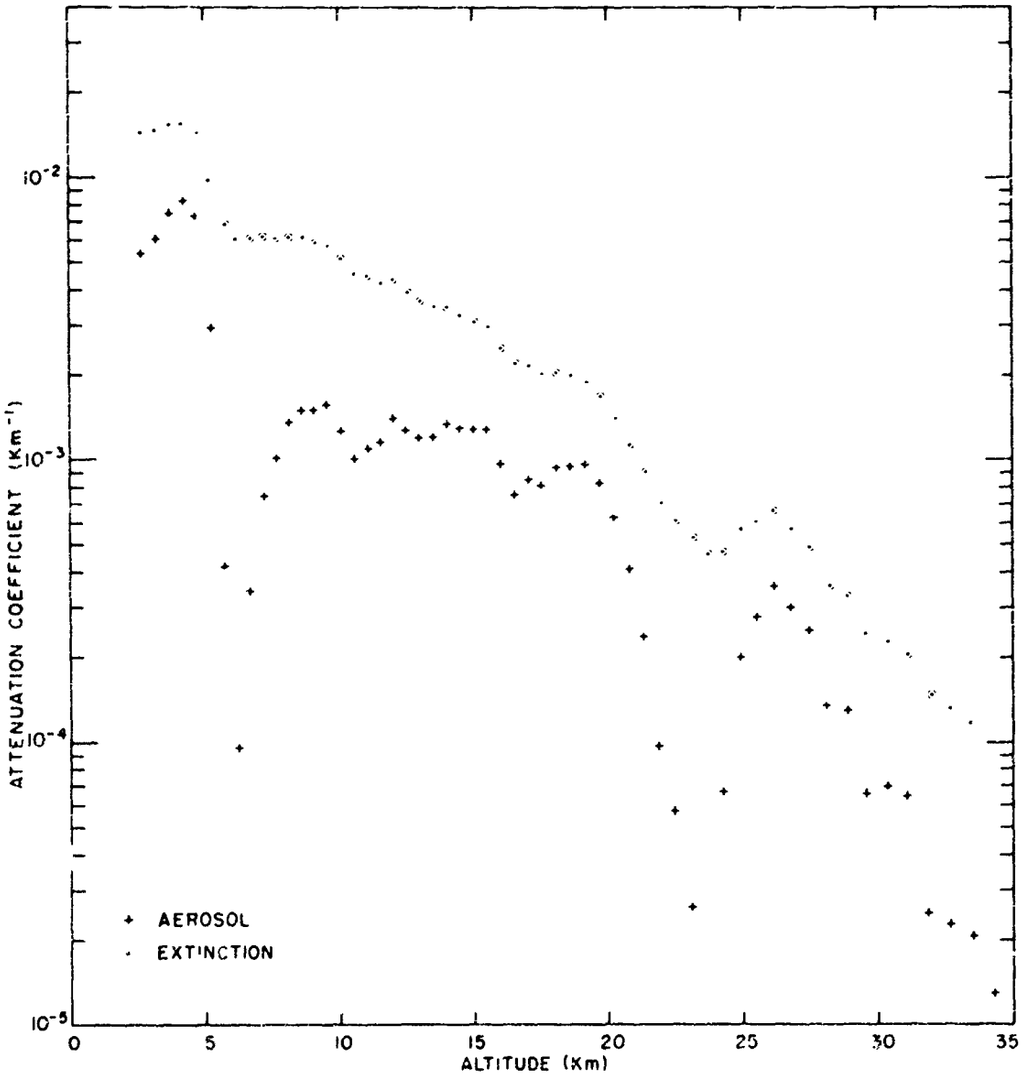

Profile 40. 12 April 1964. Time 20·08

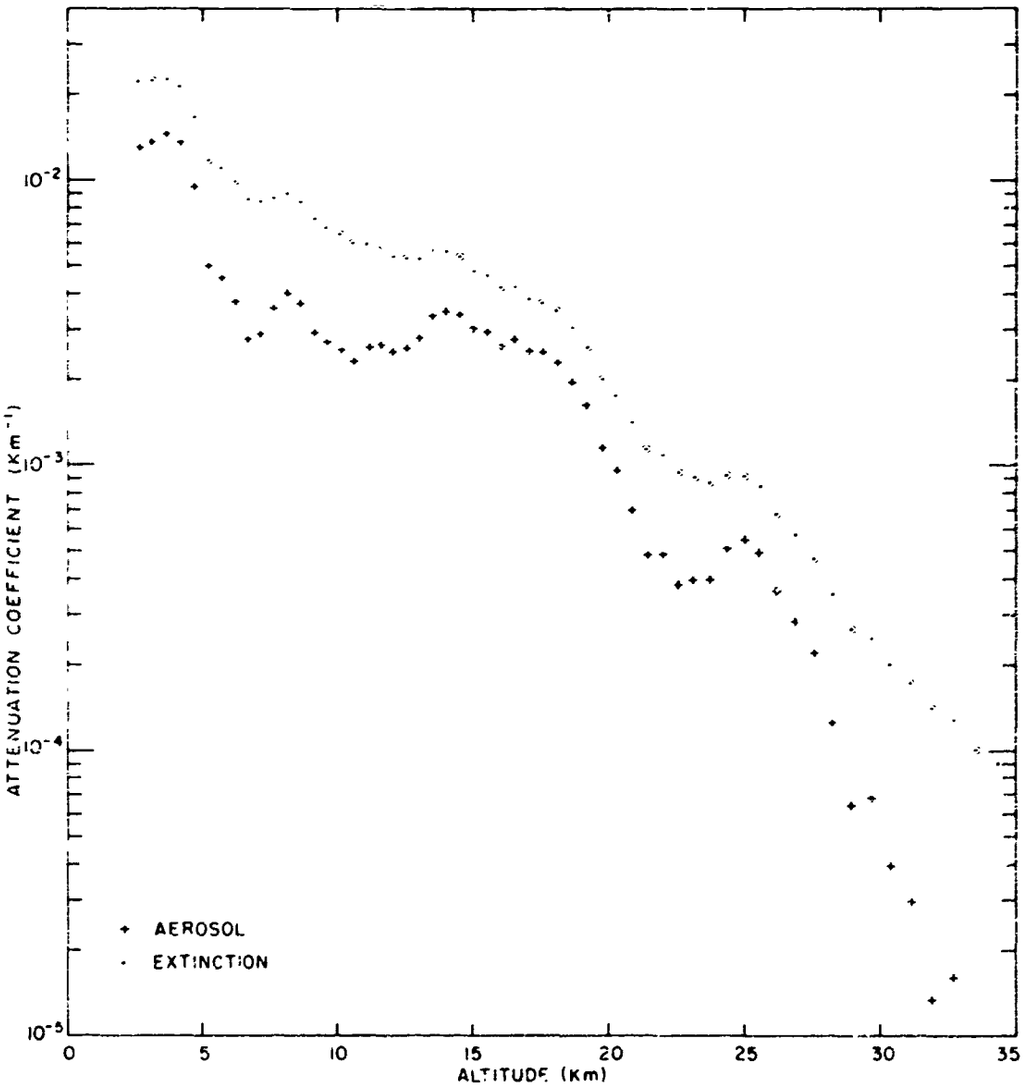

Profile 50. 12 April 1964. Time 21:10

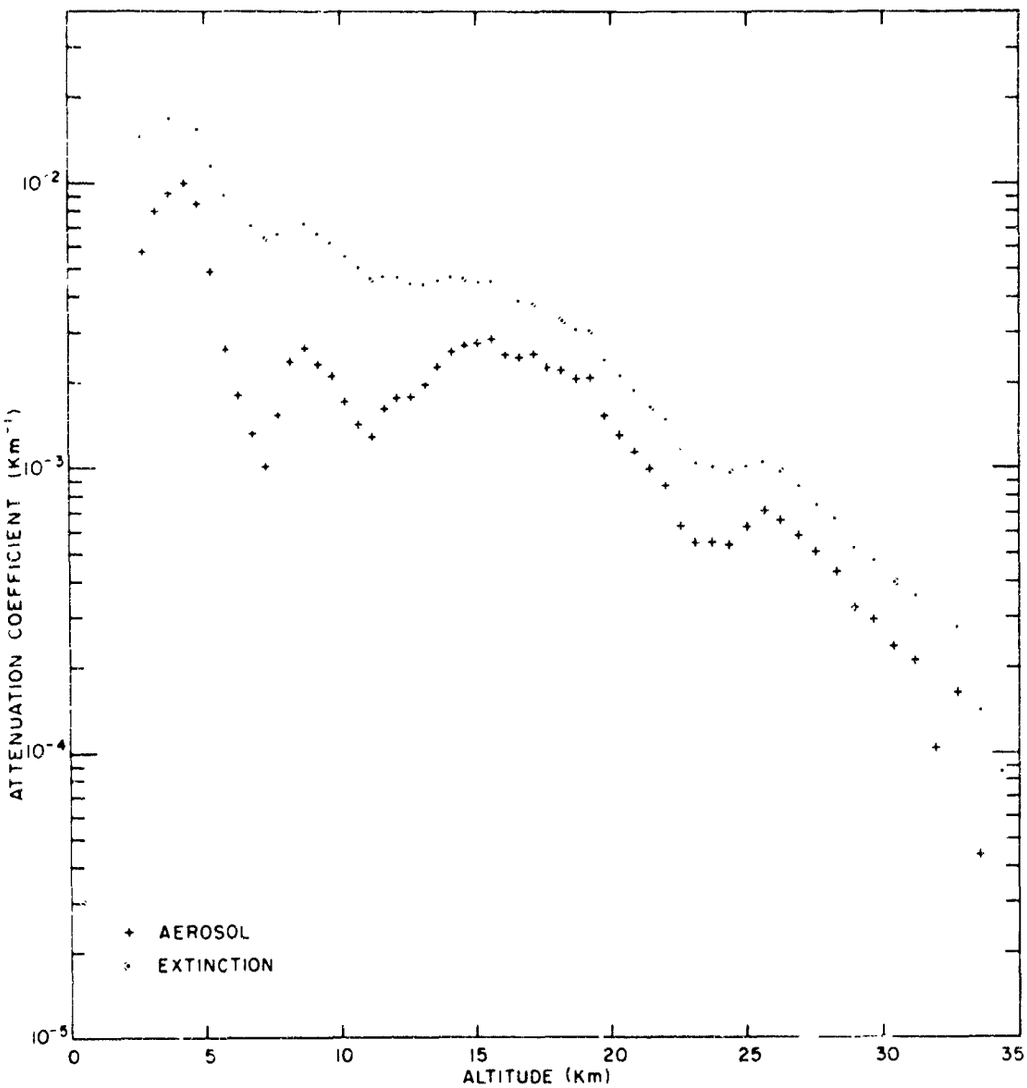

Profile 51. 12 April 1964. Time 22·14

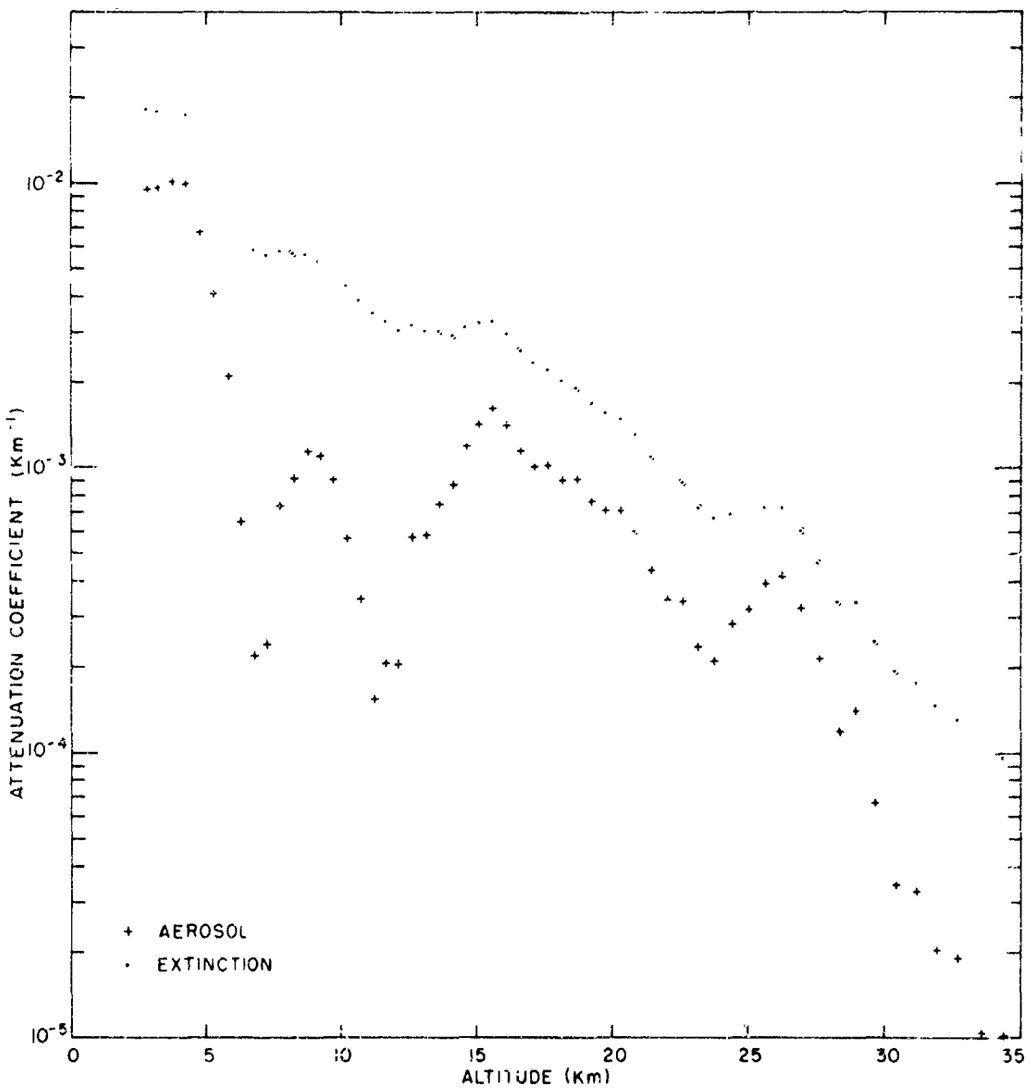

Profile 52. 13 April 1964. Time 00:18

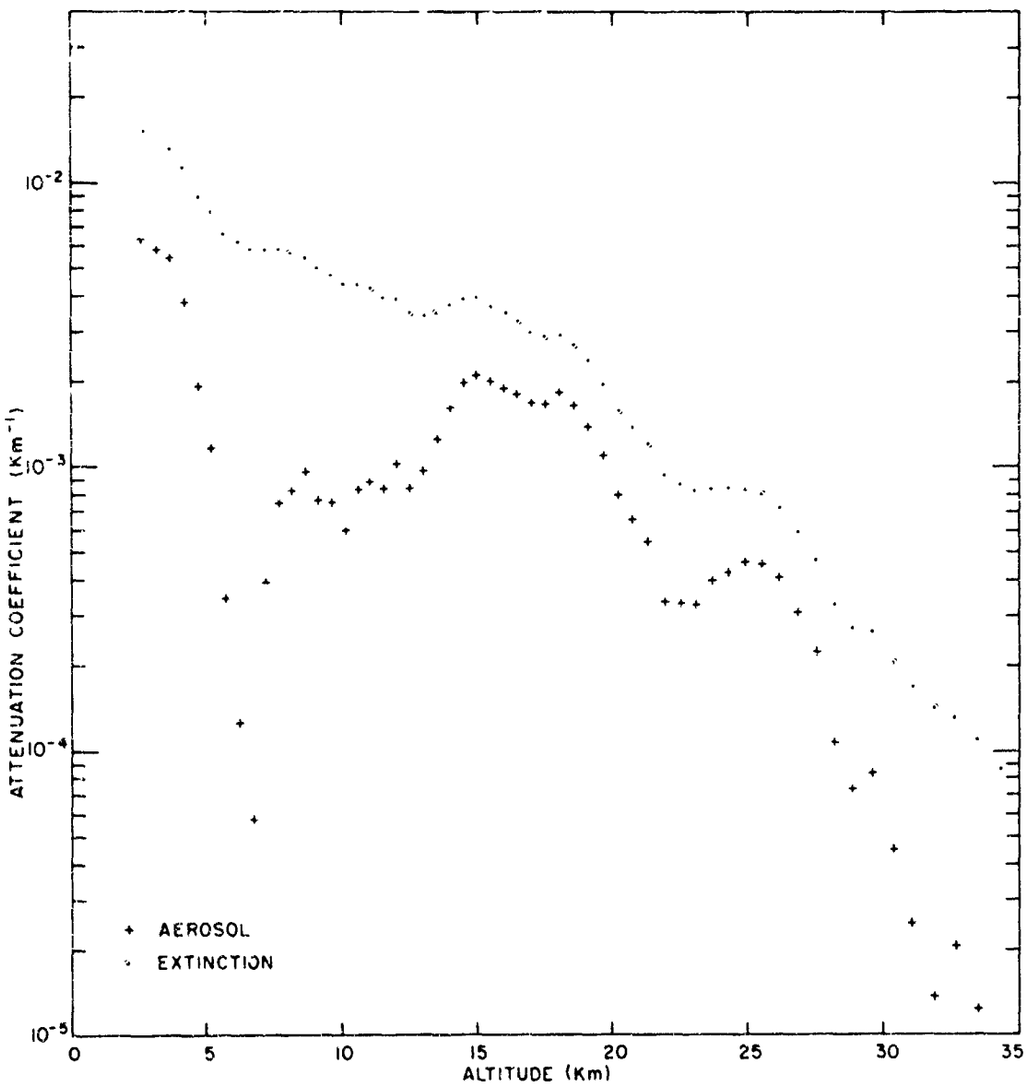

Profile 53. 13 April 1964. Time 00·58

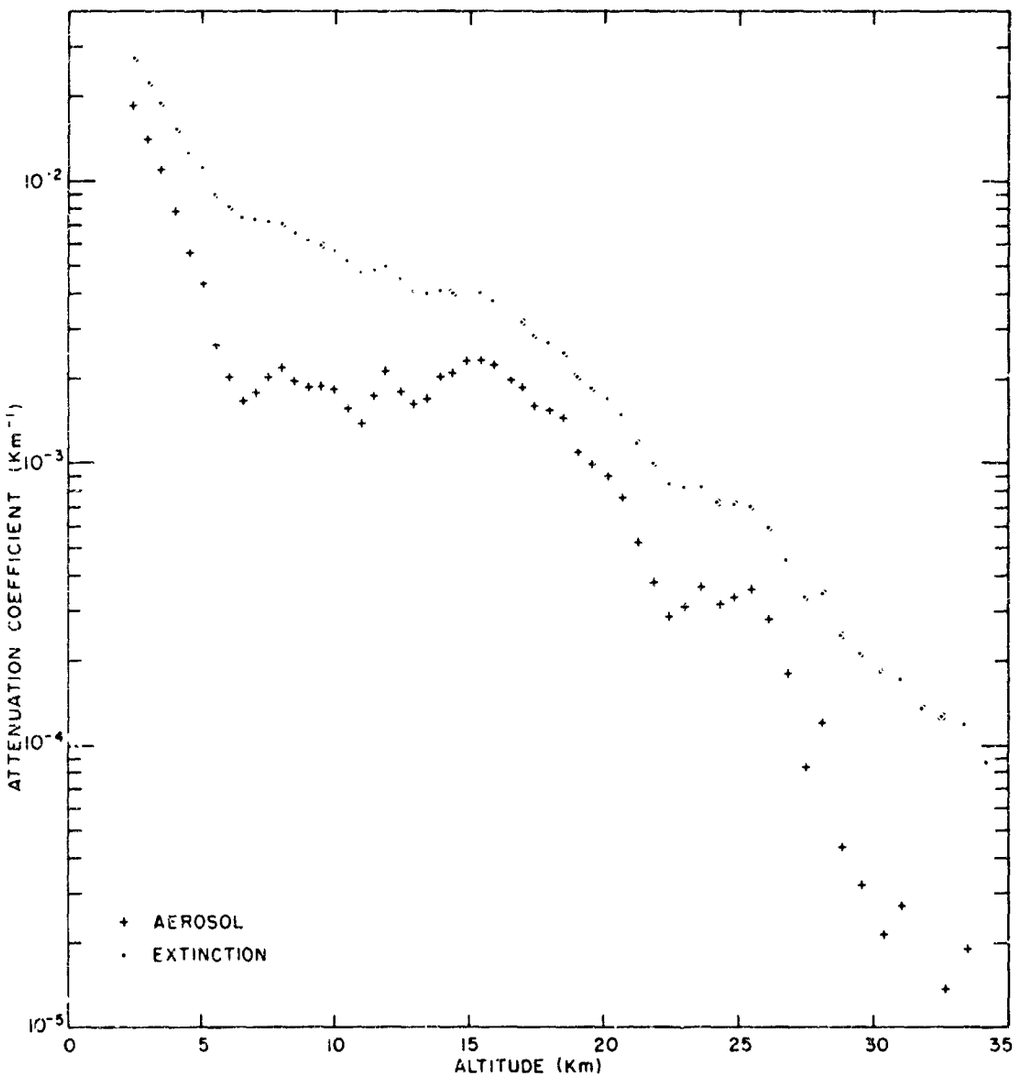

Profile 54. 13 April 1964. Time 02:19

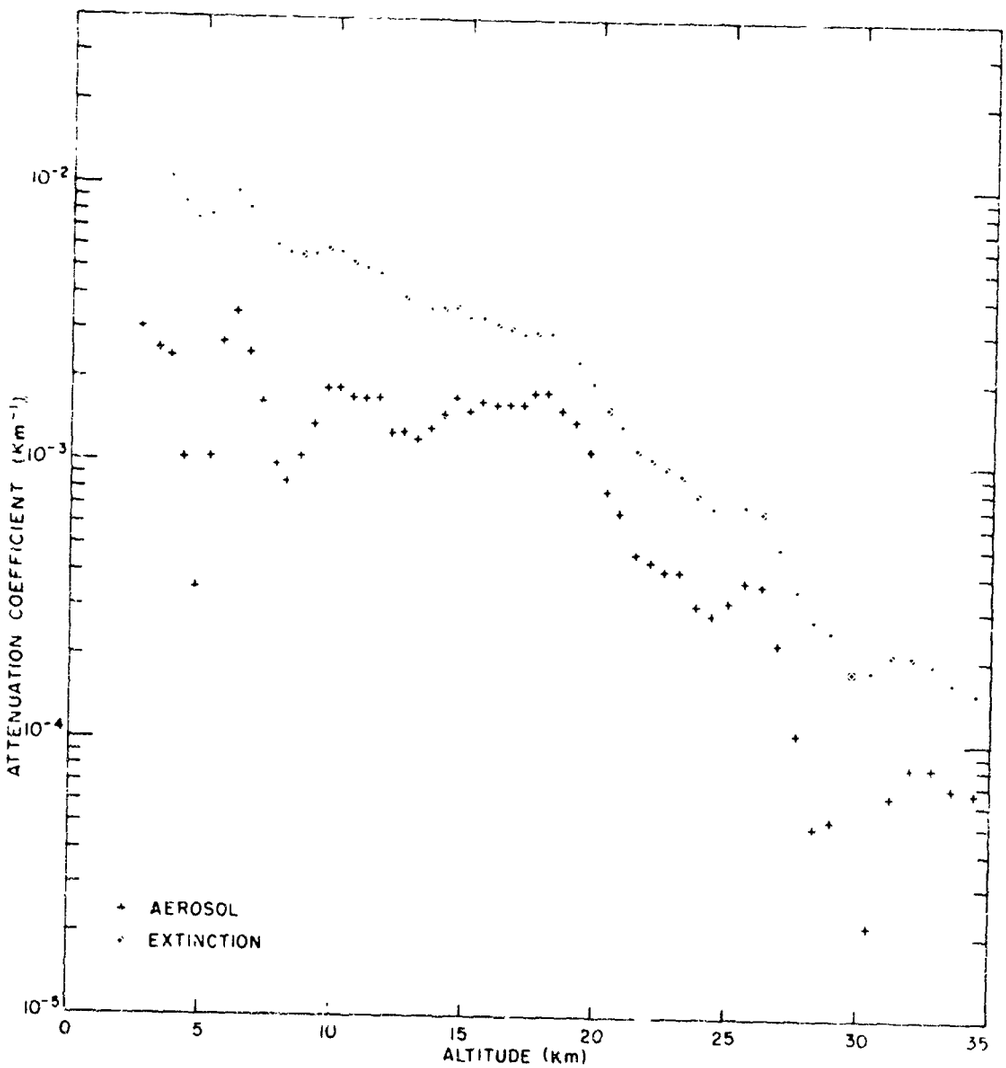

Profile 55. 13 April 1964. Time 03.20

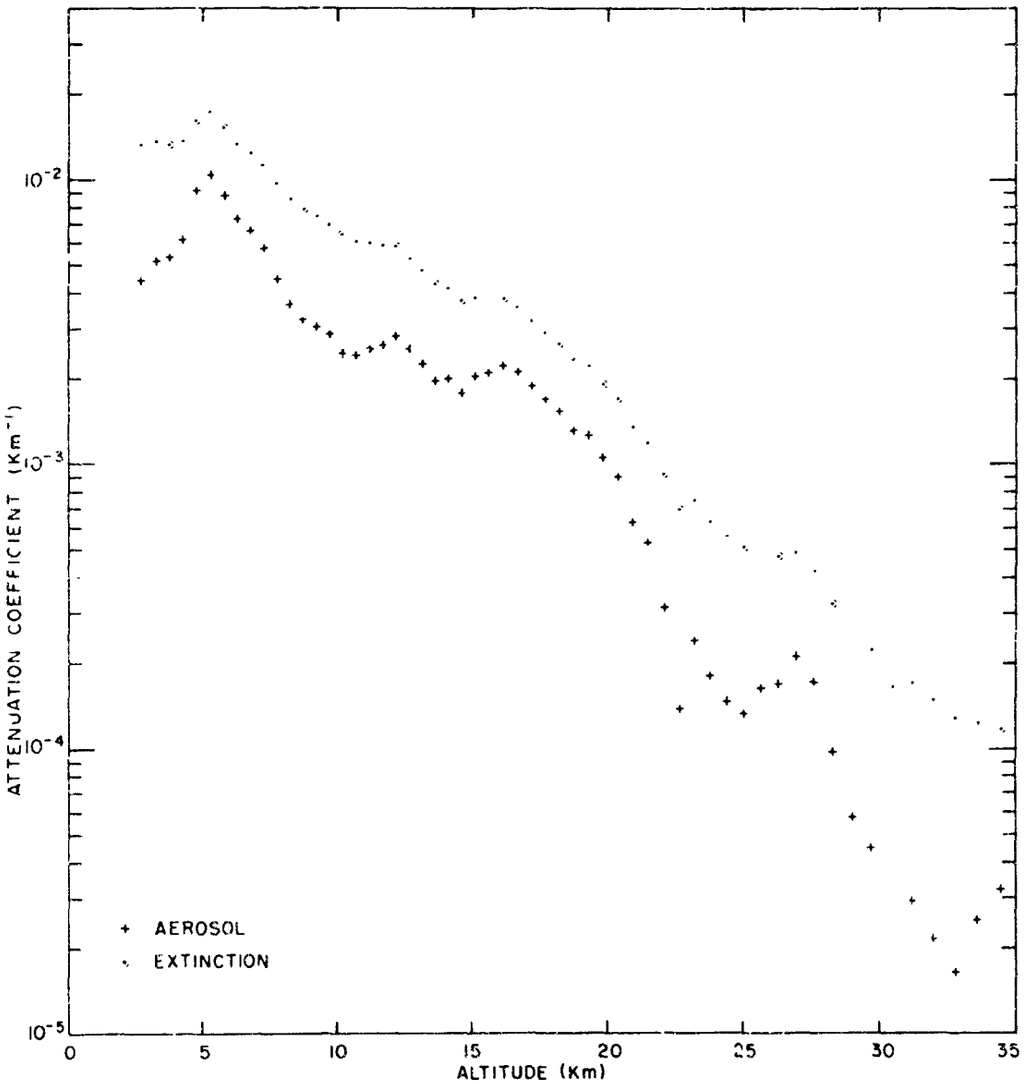

Profile 56. 13 April 1964. Time 22·15

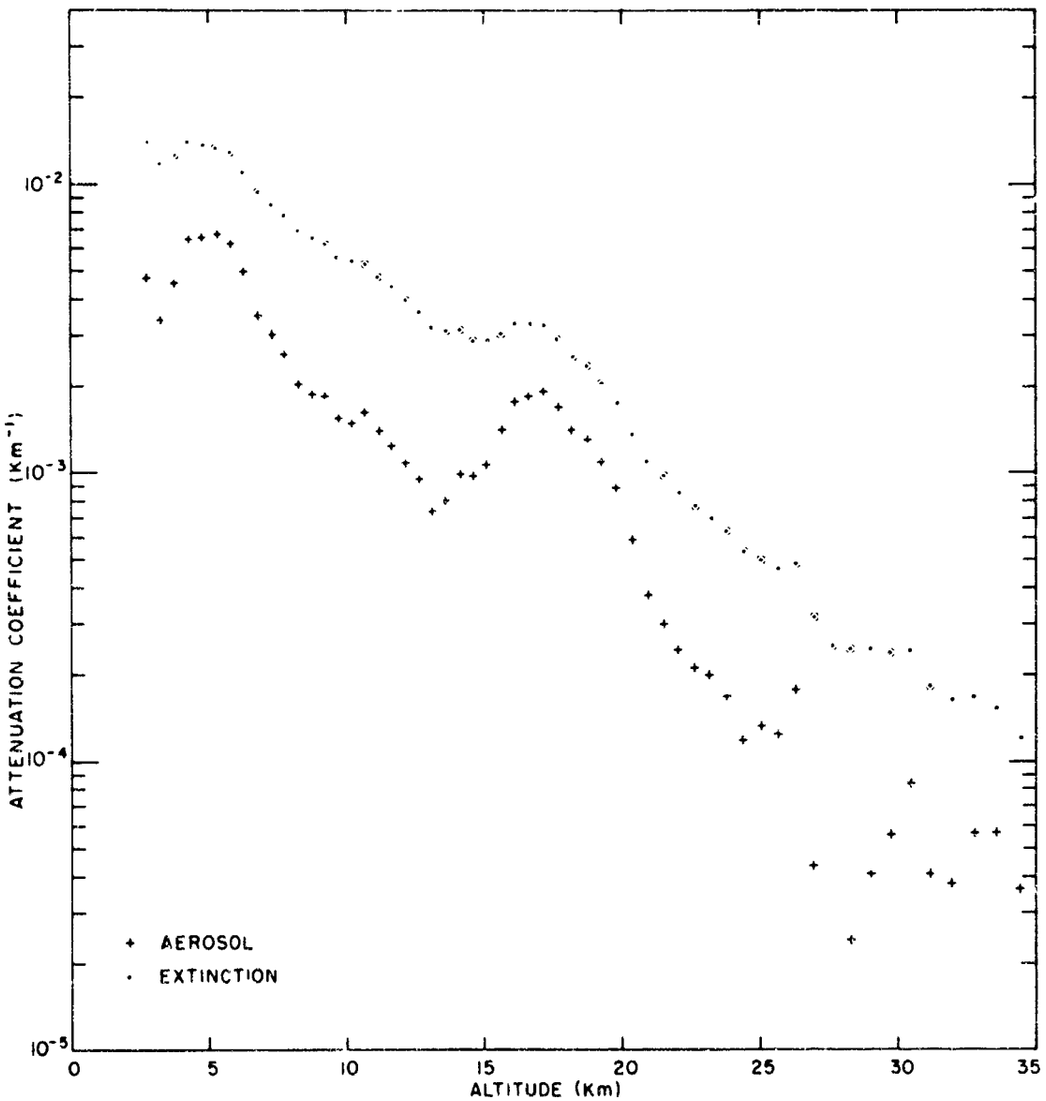

Profile 57. 13 April 1964. Time 23:15

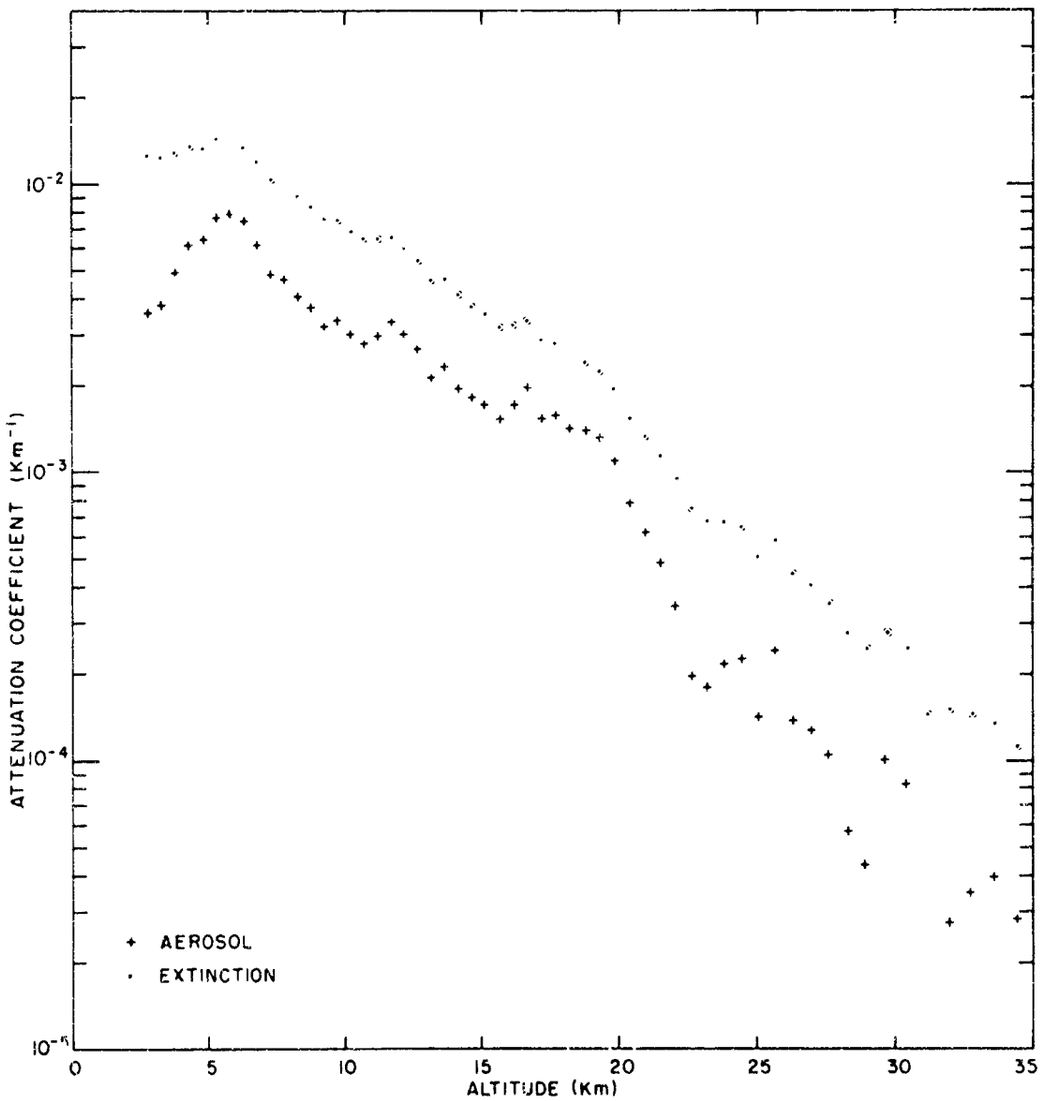

Profile 58. 14 April 1964. Time 00:20

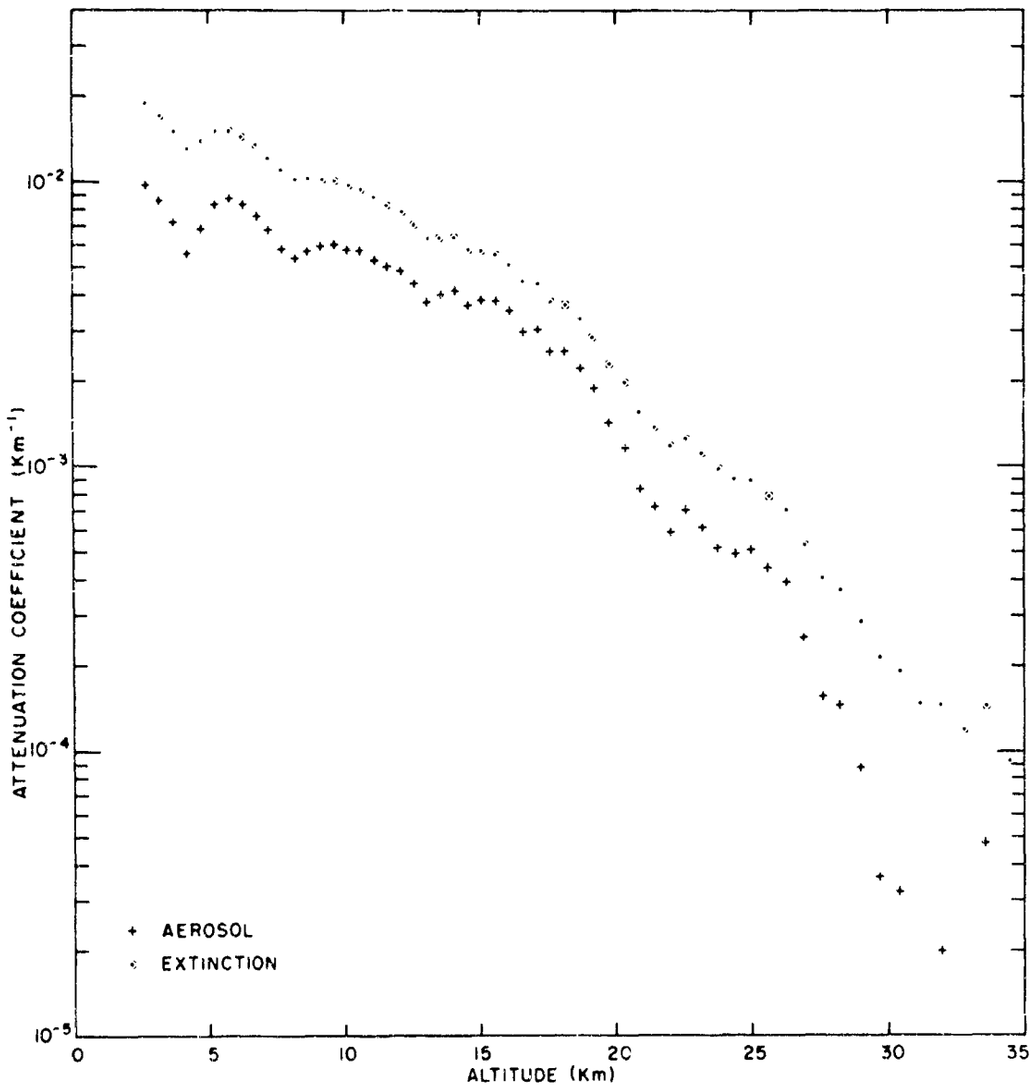

Profile 59, 14 April 1964. Time 01·25

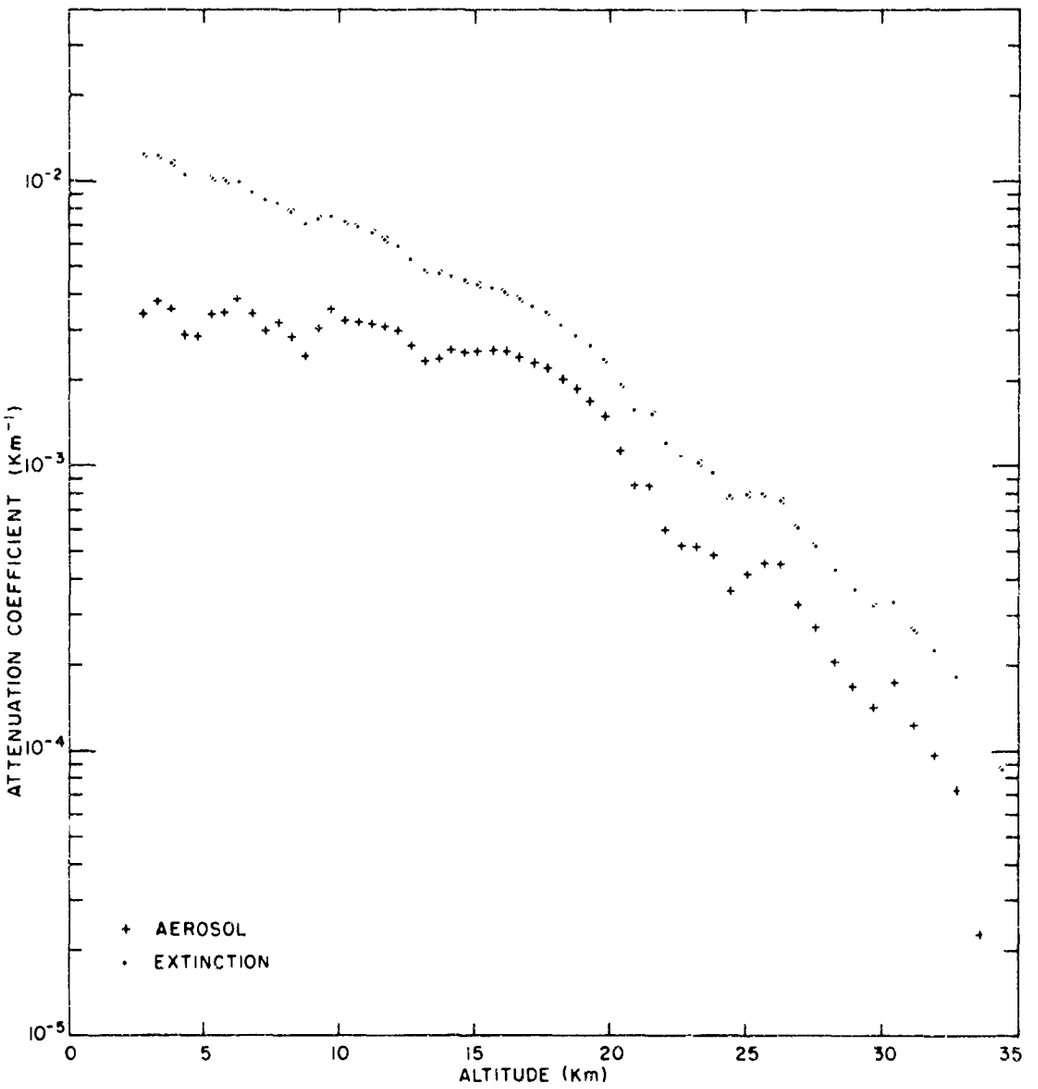

Profile 60. 14 April 1964. Time 02·32

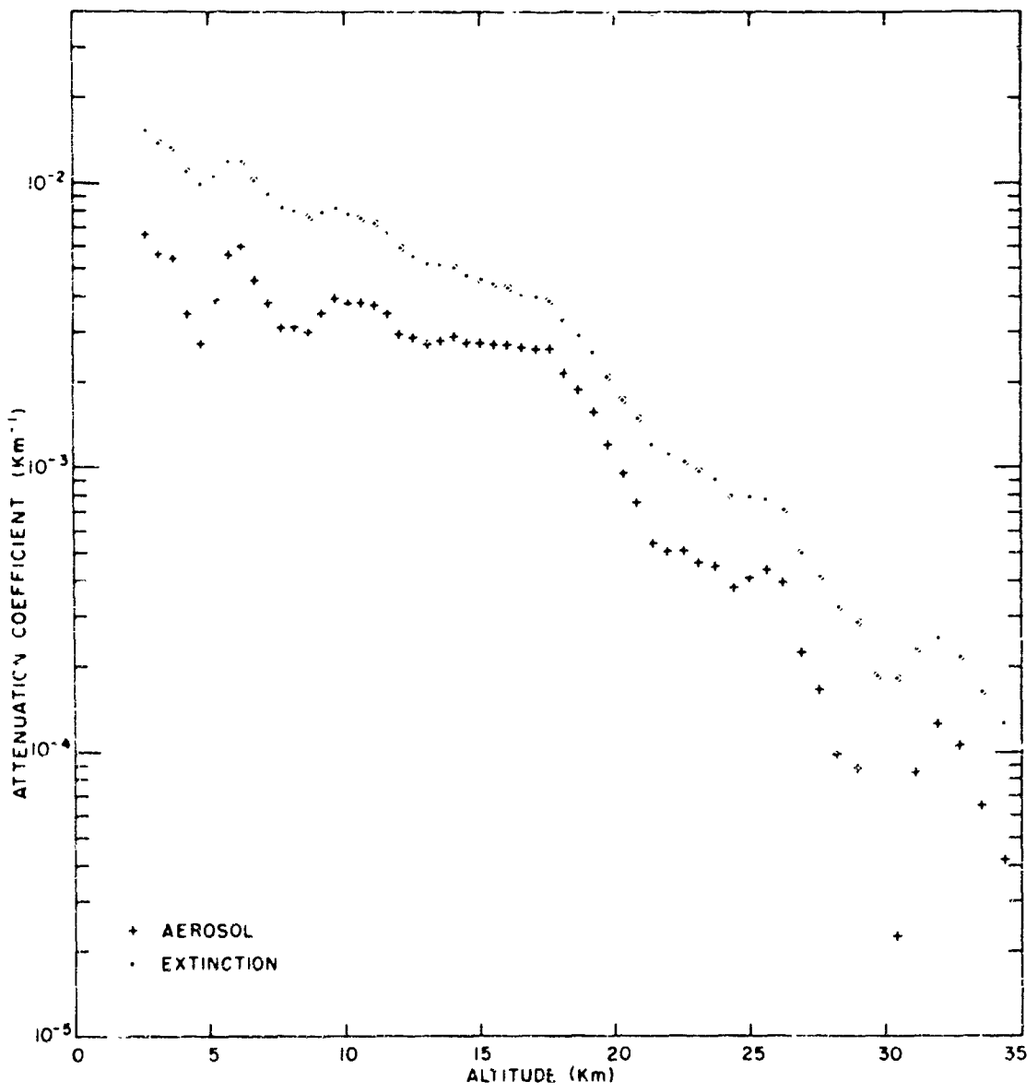

Profile 61. 14 April 1964. Time 03·30

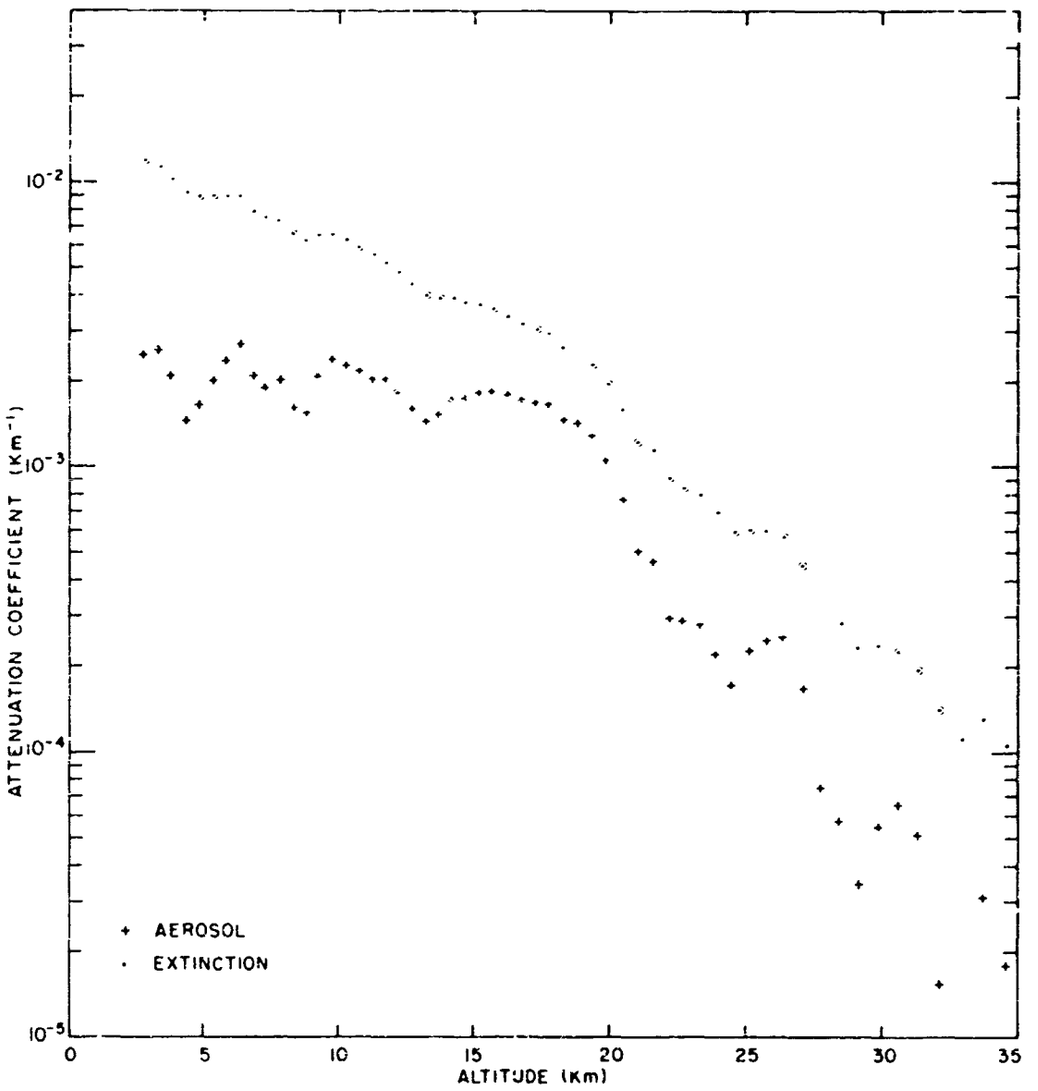

Profile 62. 14 April 1964. Time 20·02

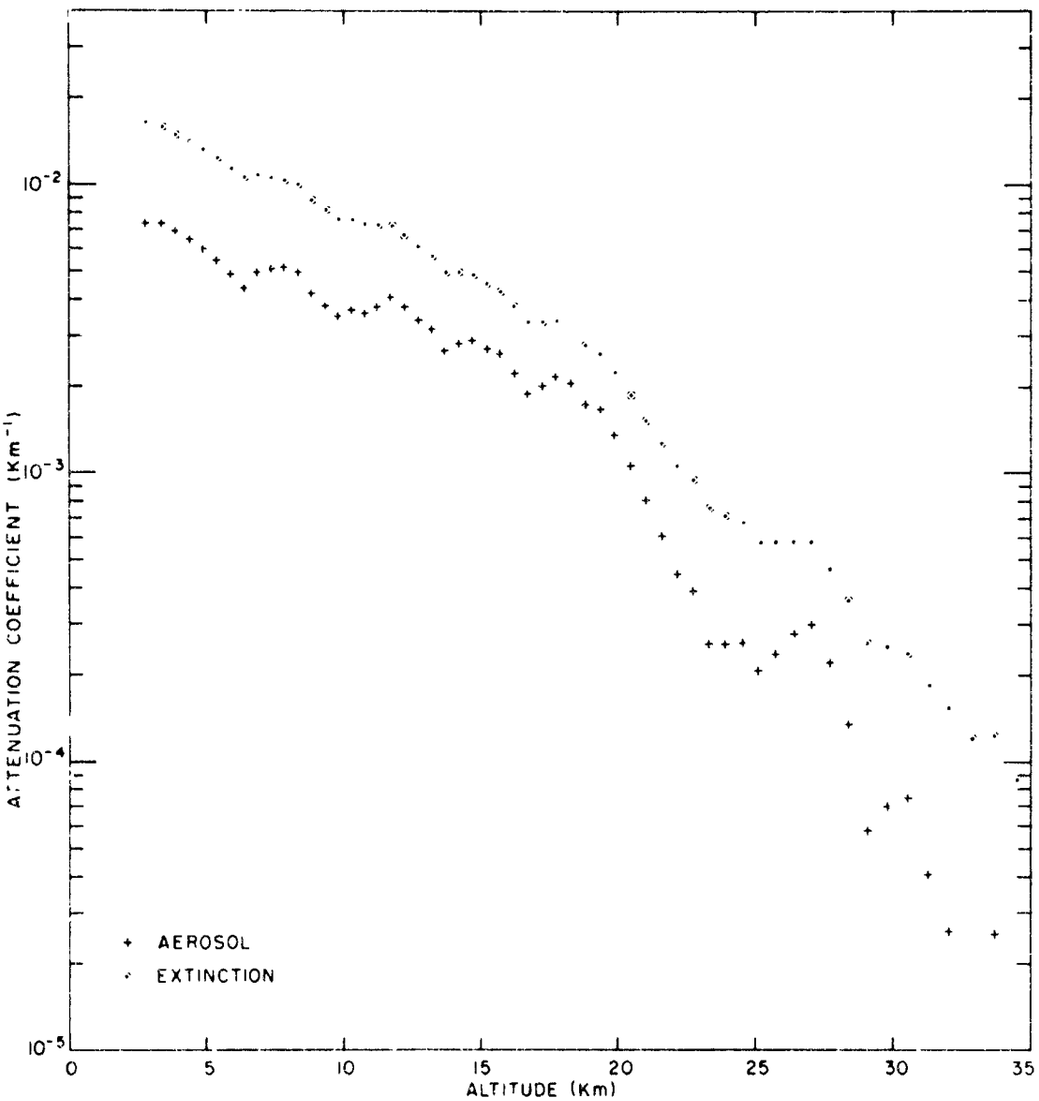

Profile 6, 14 April 1964, Time 23 00

ATTENUATION COEFFICIENT (Km⁻¹)

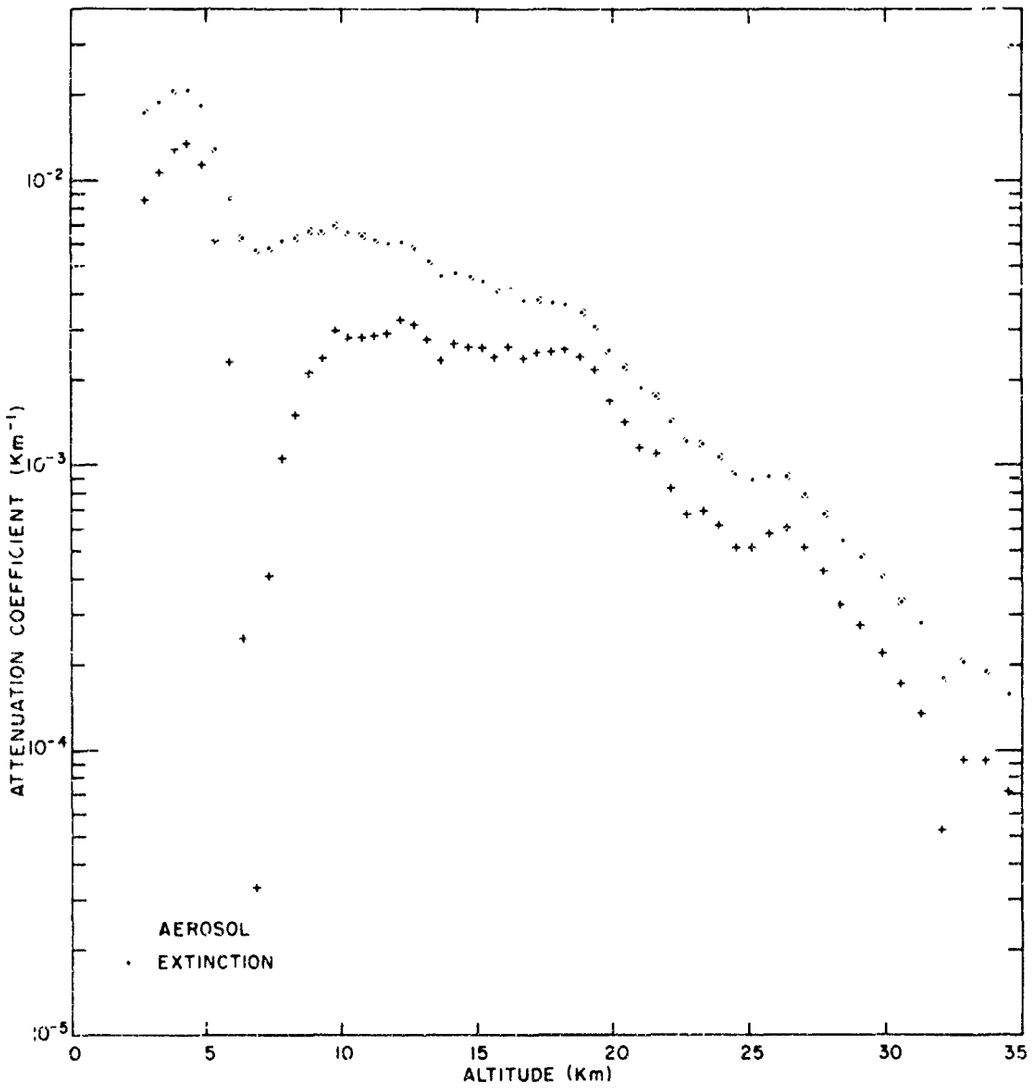

Profile 64. 15 April 1964. Time 22·40

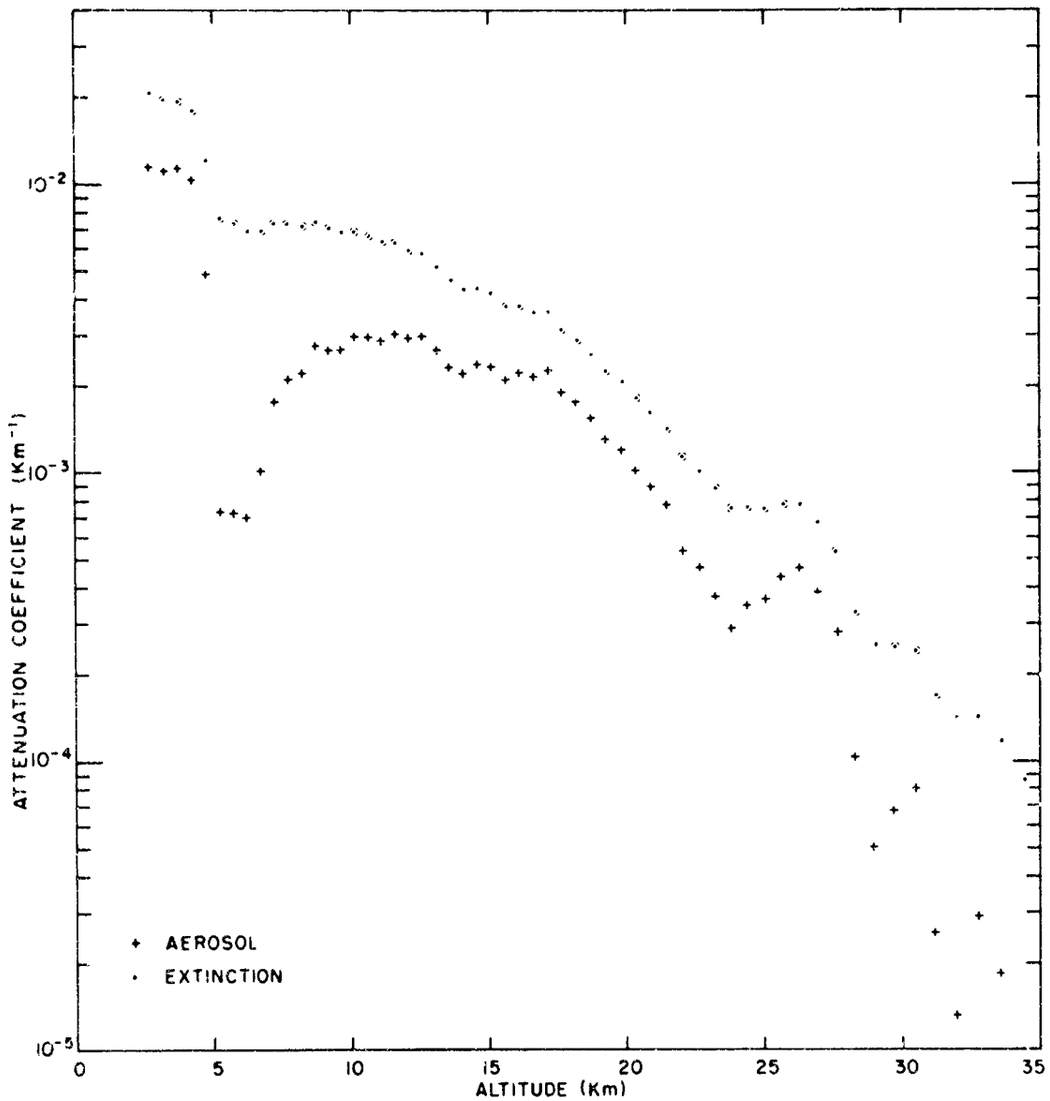

Profile 65. 15 April 1964. Time 23·40

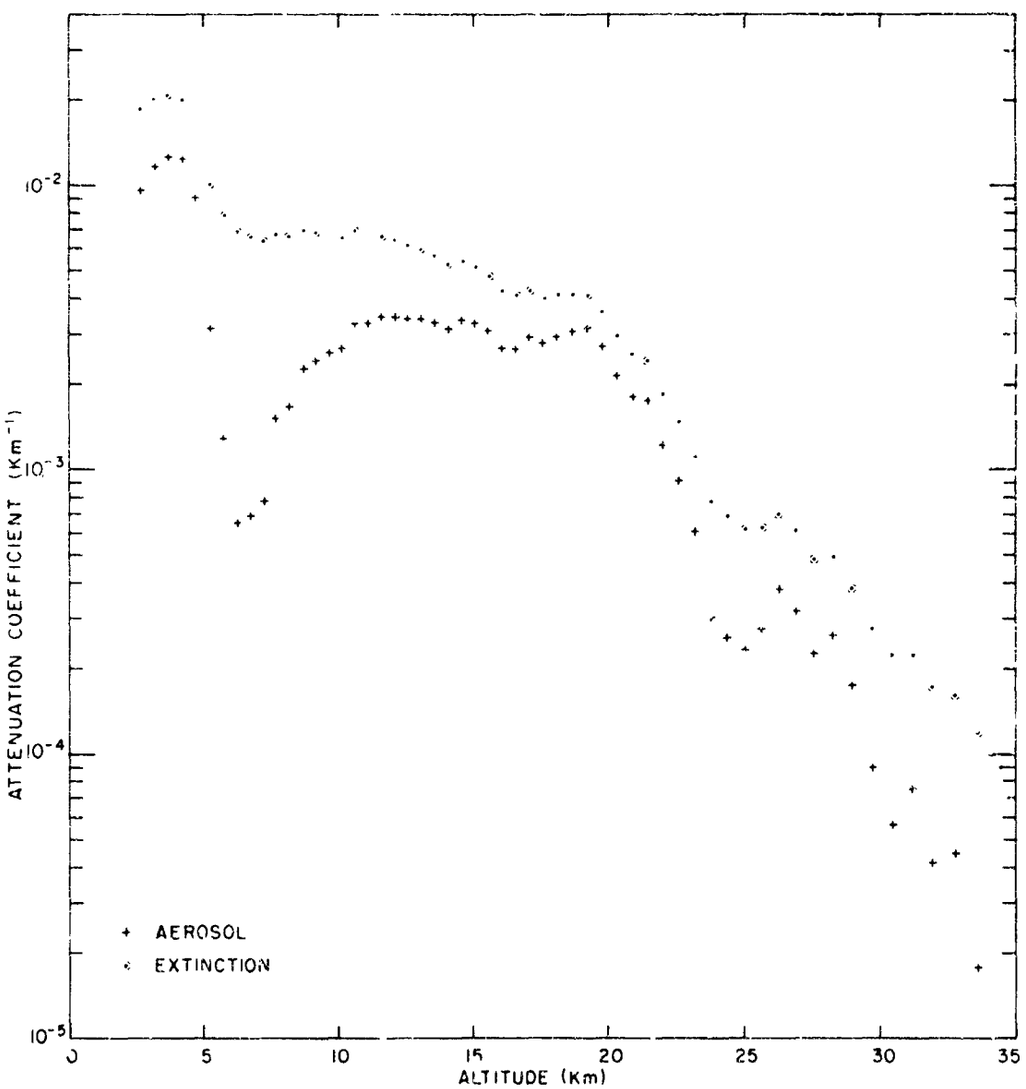

Profile 66. 16 April 1964. Time 00 38

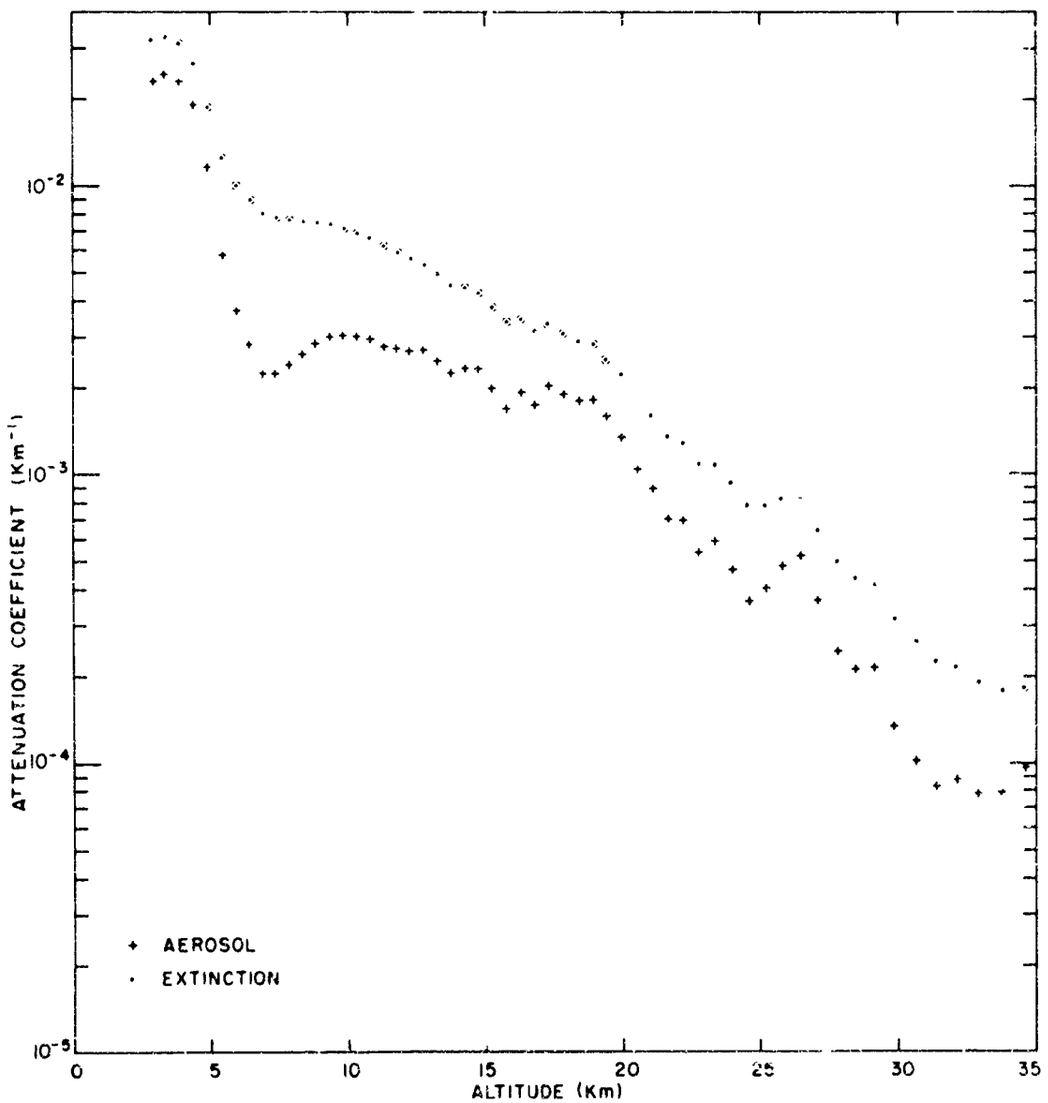

Profile 67. 16 April 1964. Time 01:30

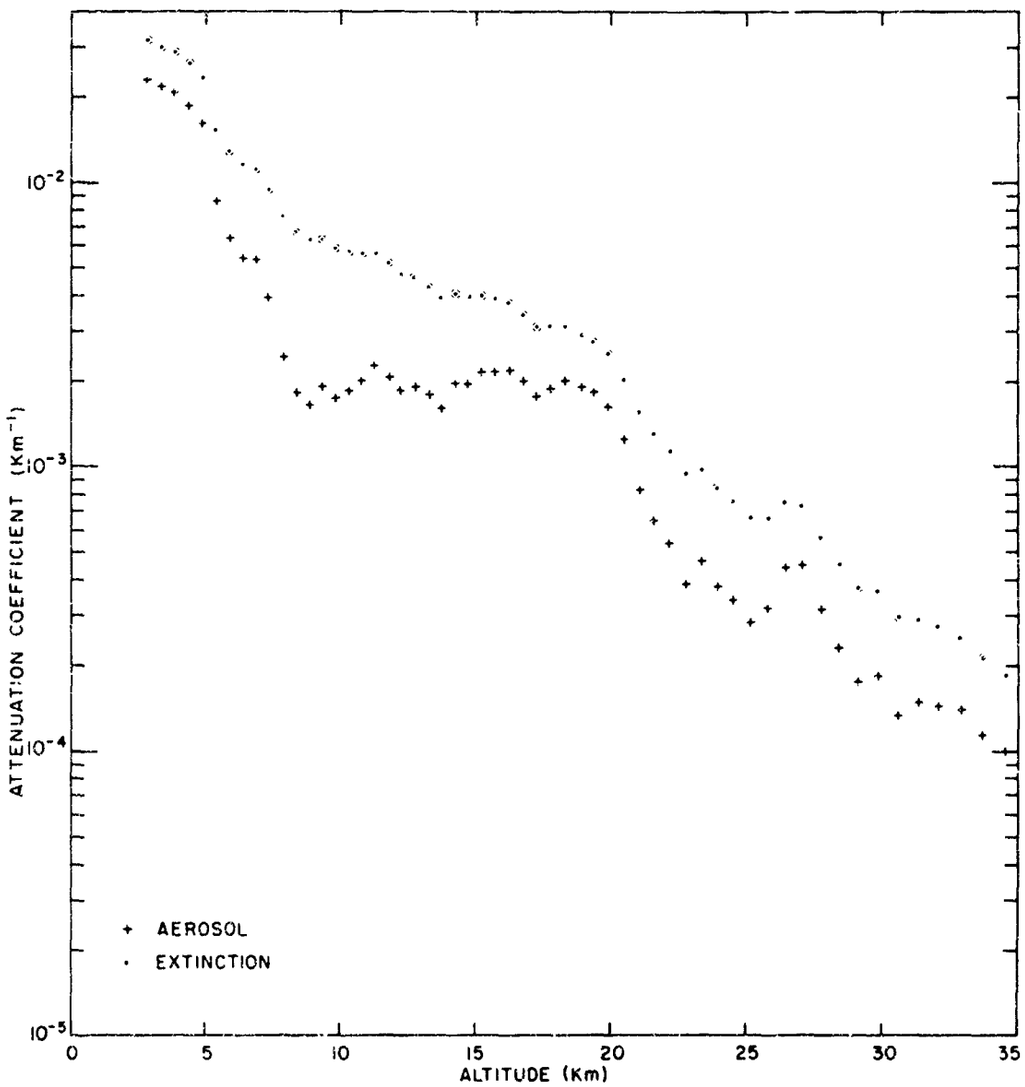

Profile 68. 16 April 1964. Time 02:20

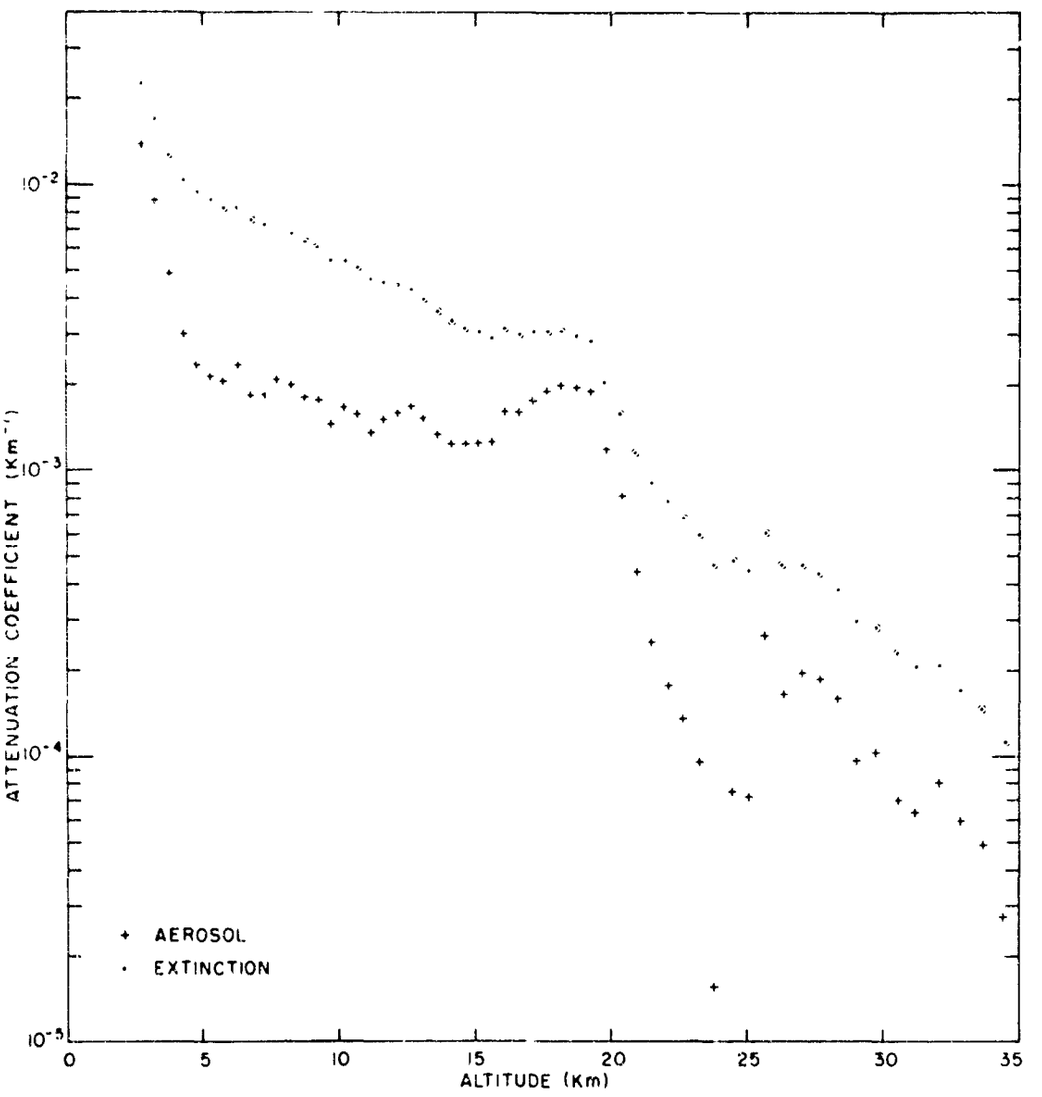

Profile 69. 8 May 1964. Time 02 15

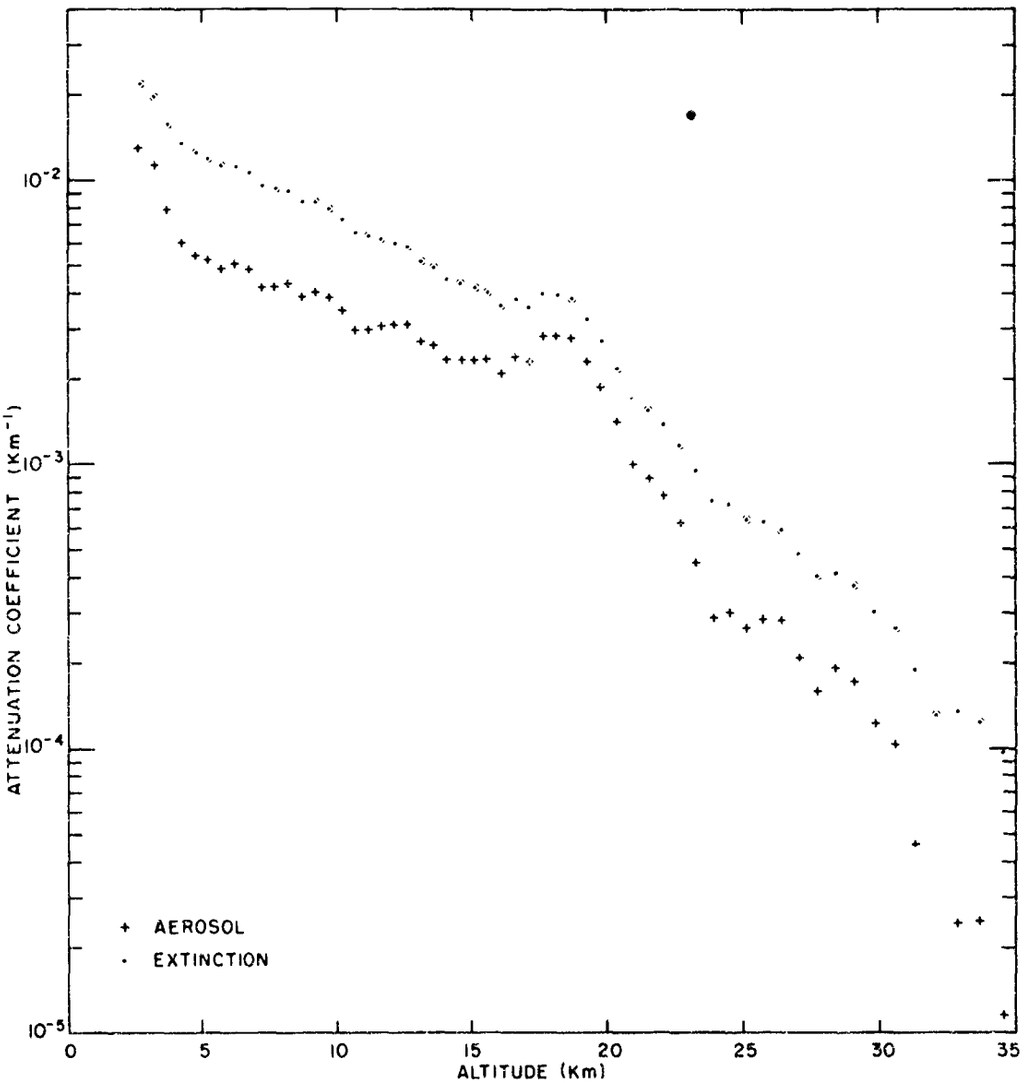

Profile 70, 8 May 64. Time 03·05

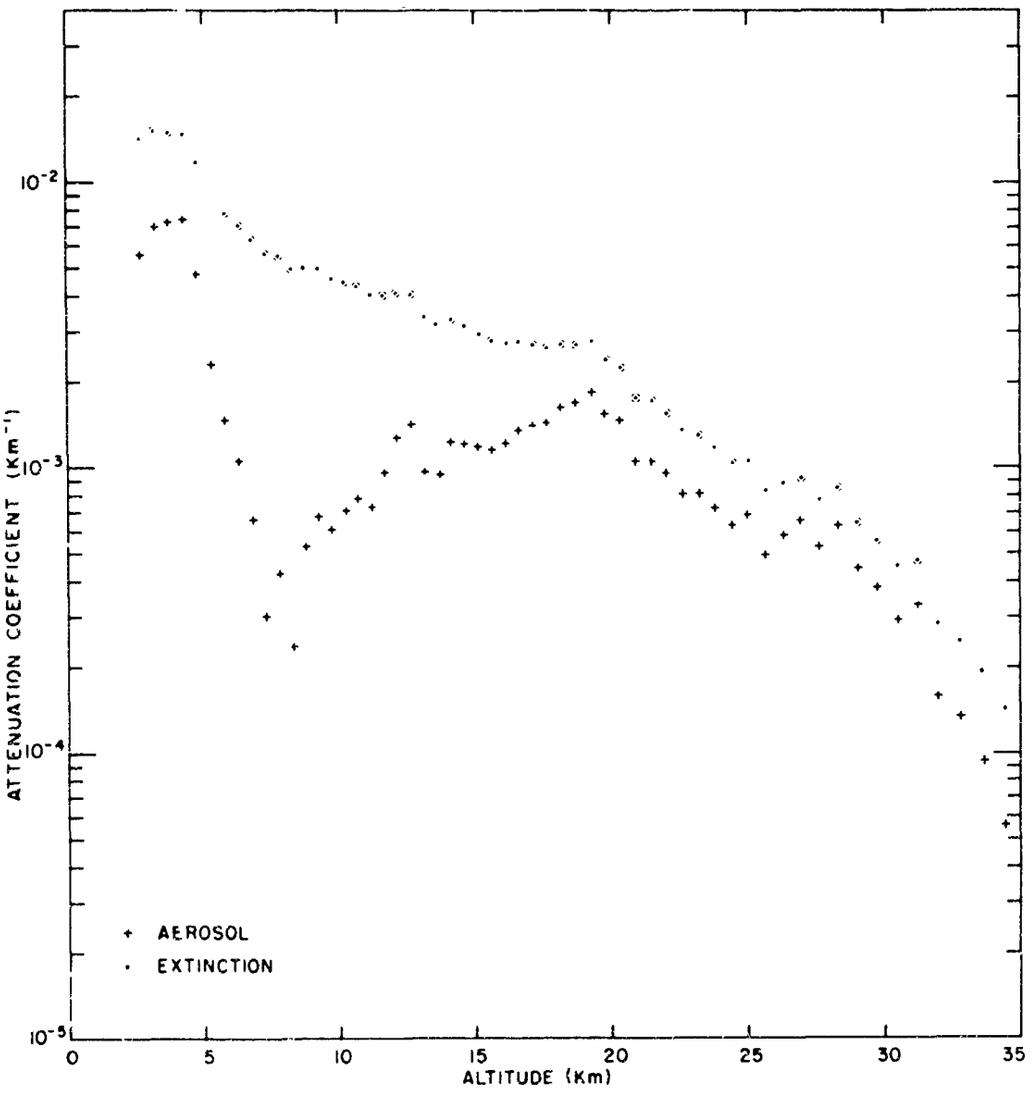

Profile 71. 8 May 1964. Time 21:50

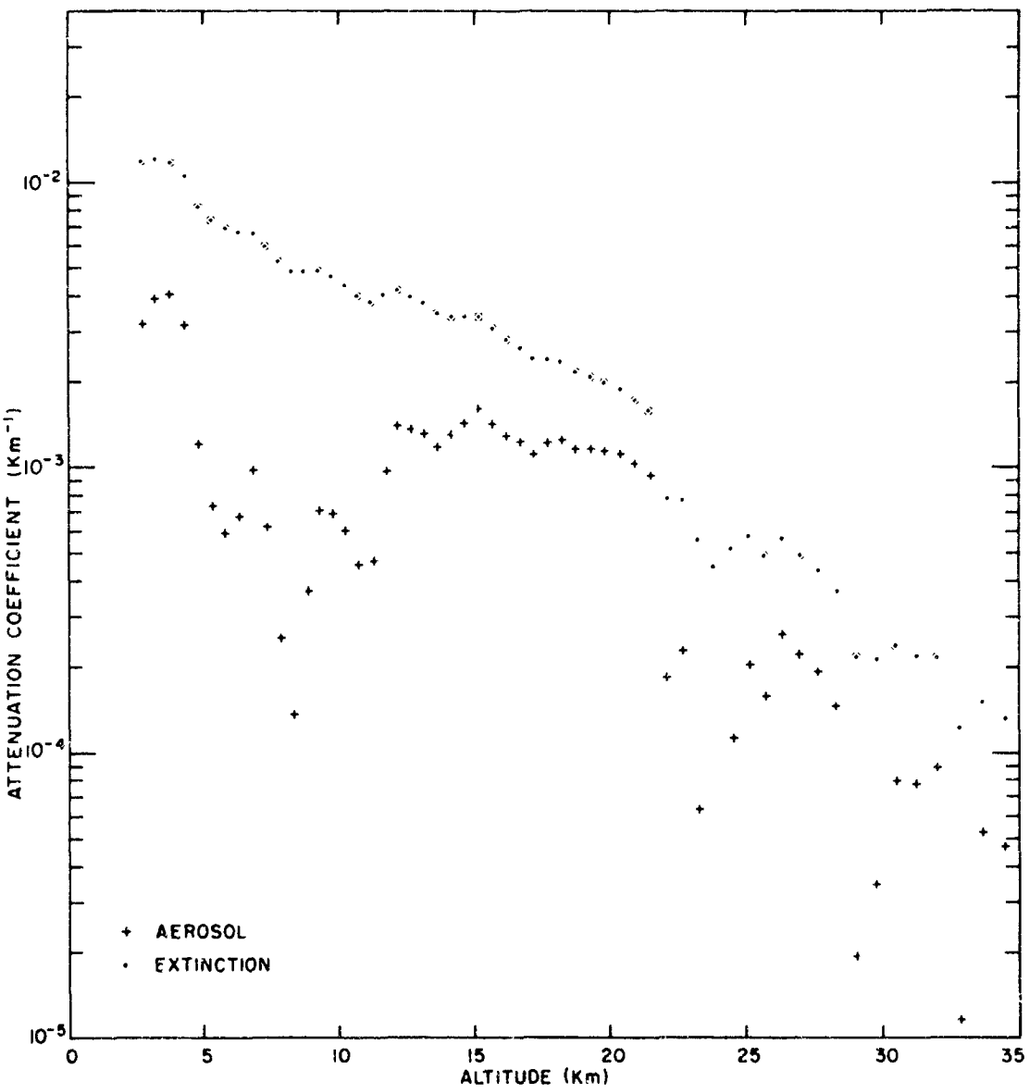

Profile 72. 9 May 1964. Time 00:35

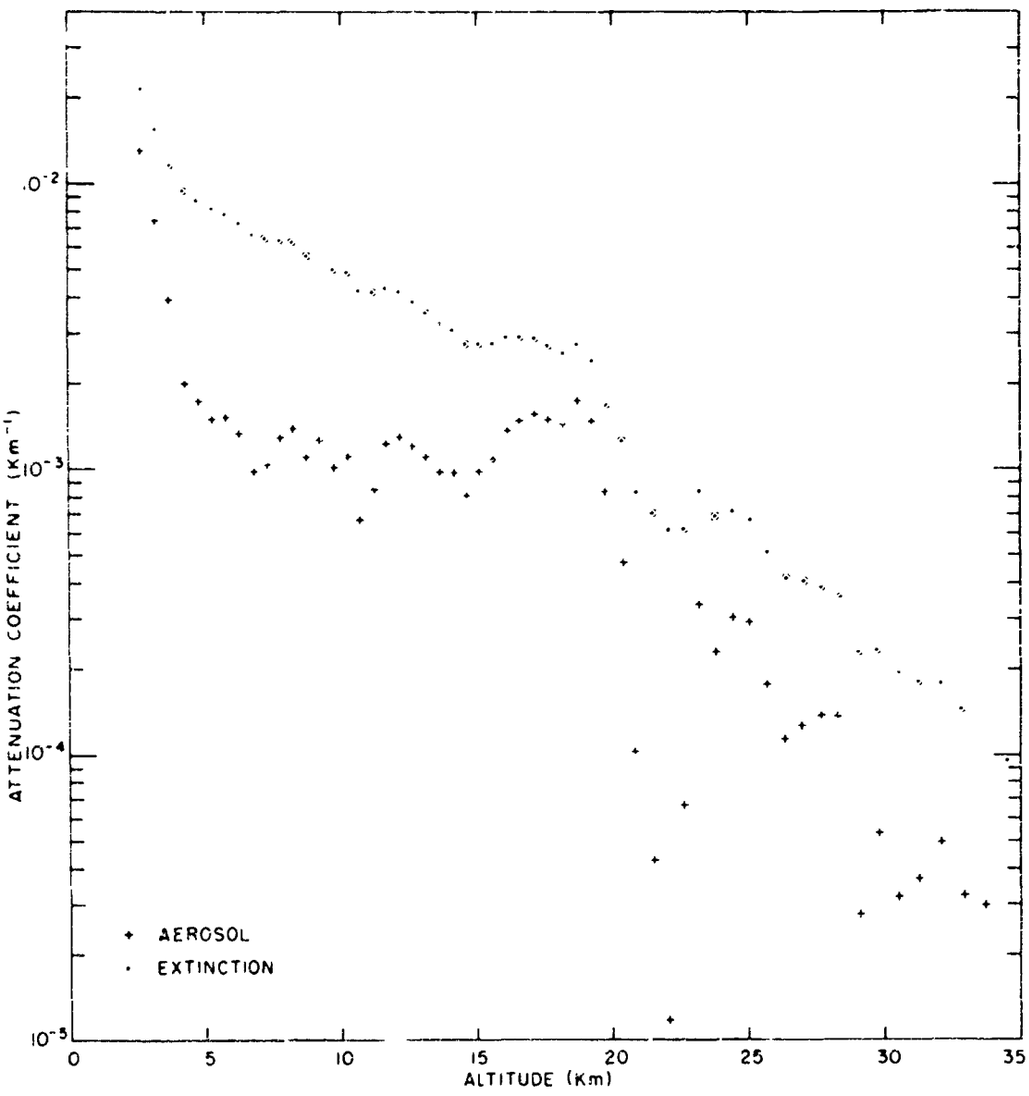

Profile 75. 9 May 1964. Time 02 05

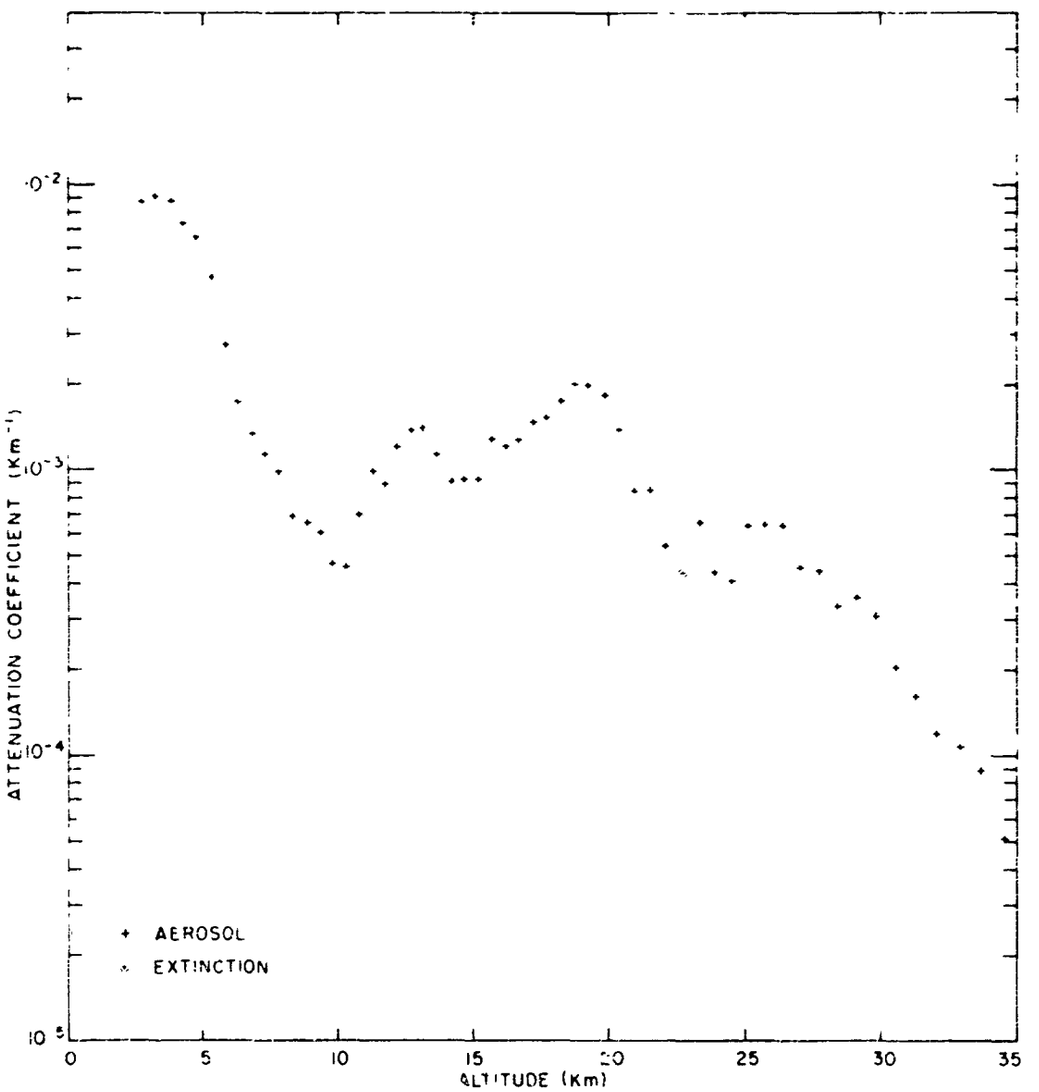

Profile 74. 9 May 1964. Time 21 09

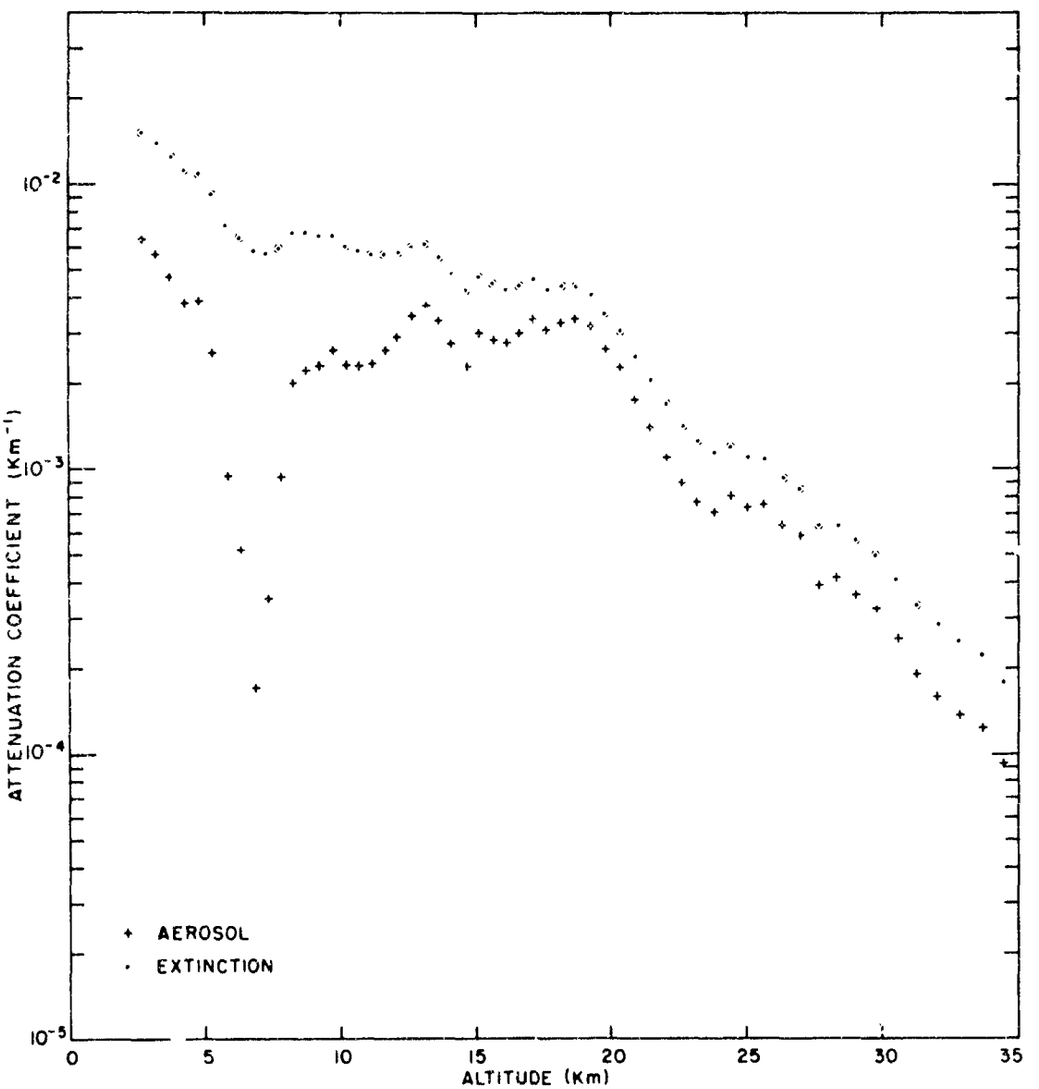

Profile 75. 9 May 1964. Time 22.16

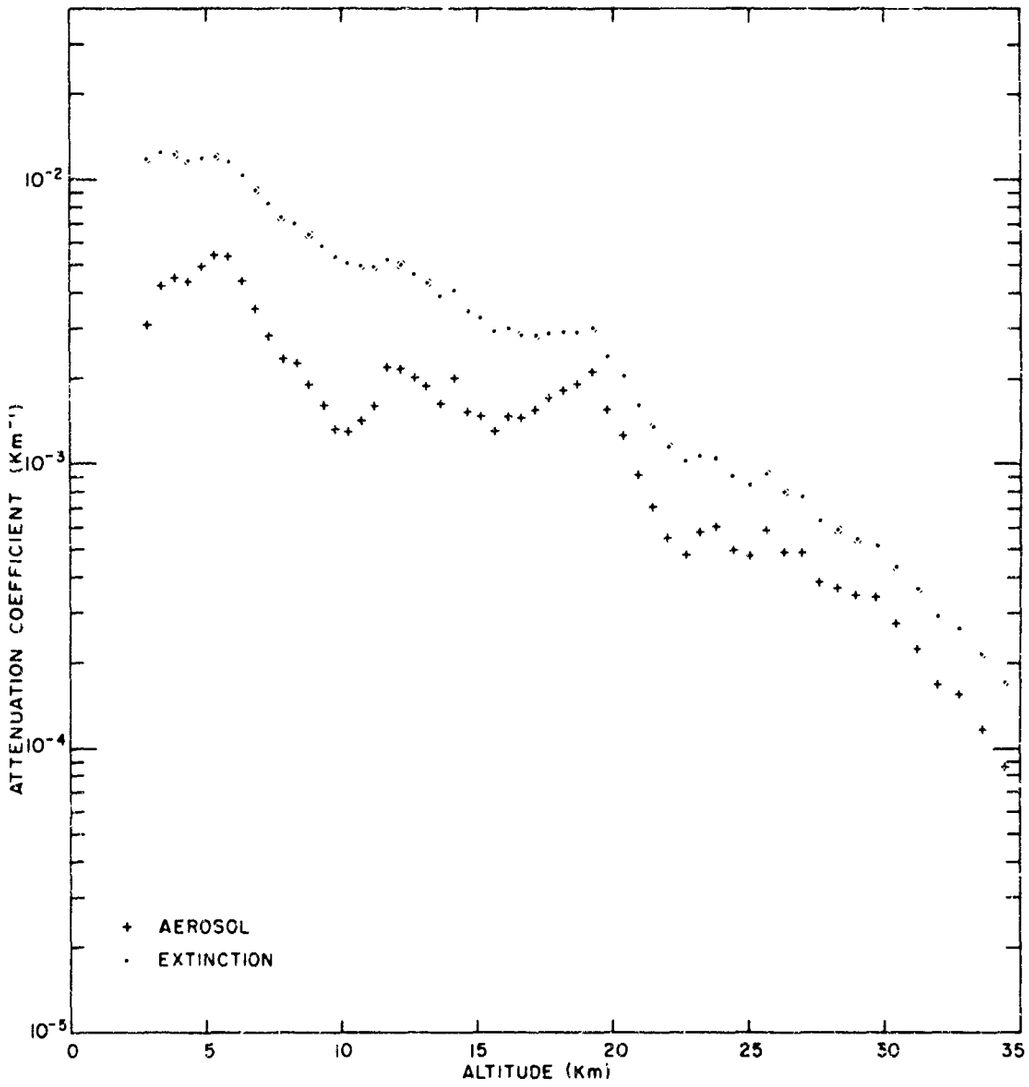

Profile 76. 10 May 1964. Time 03:08

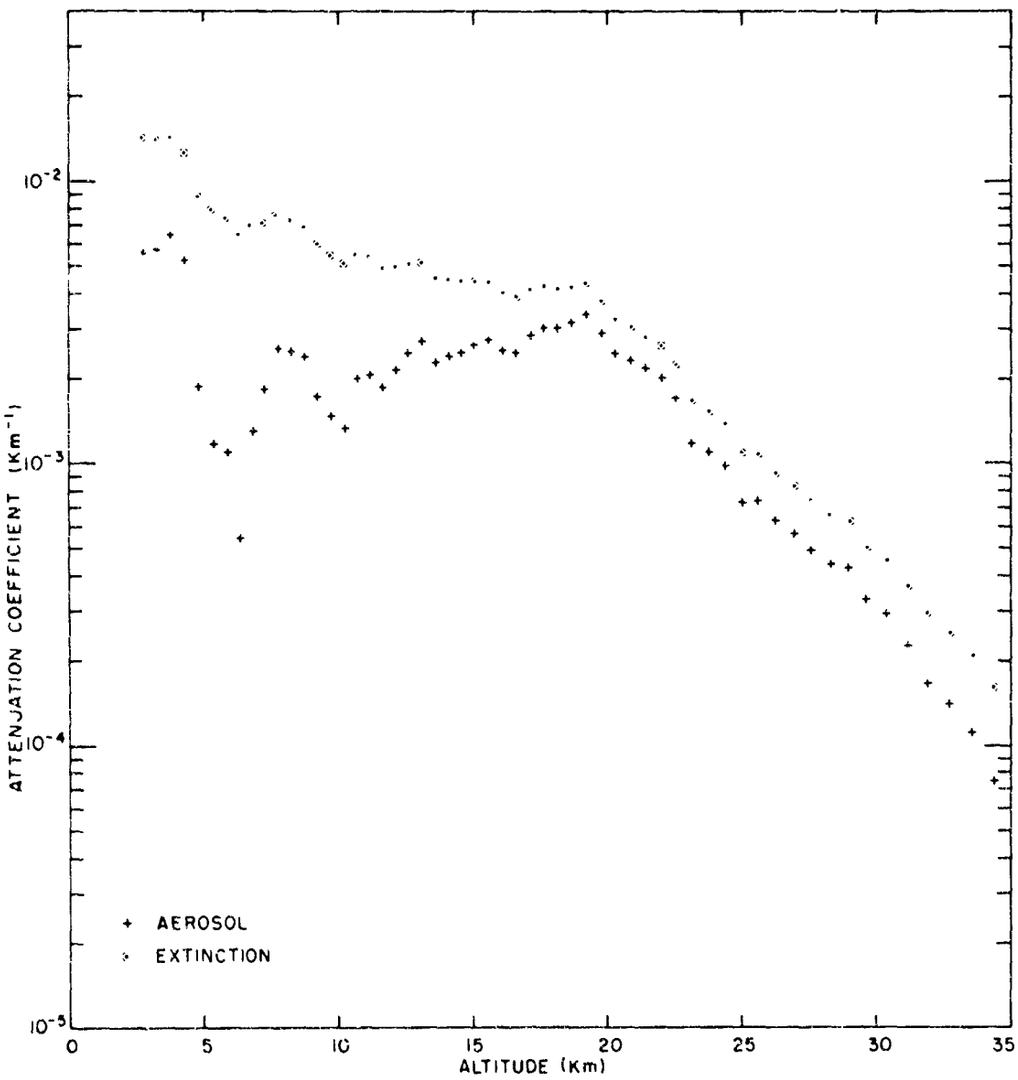

Profile 77. 10 May 1964. Time 23.05

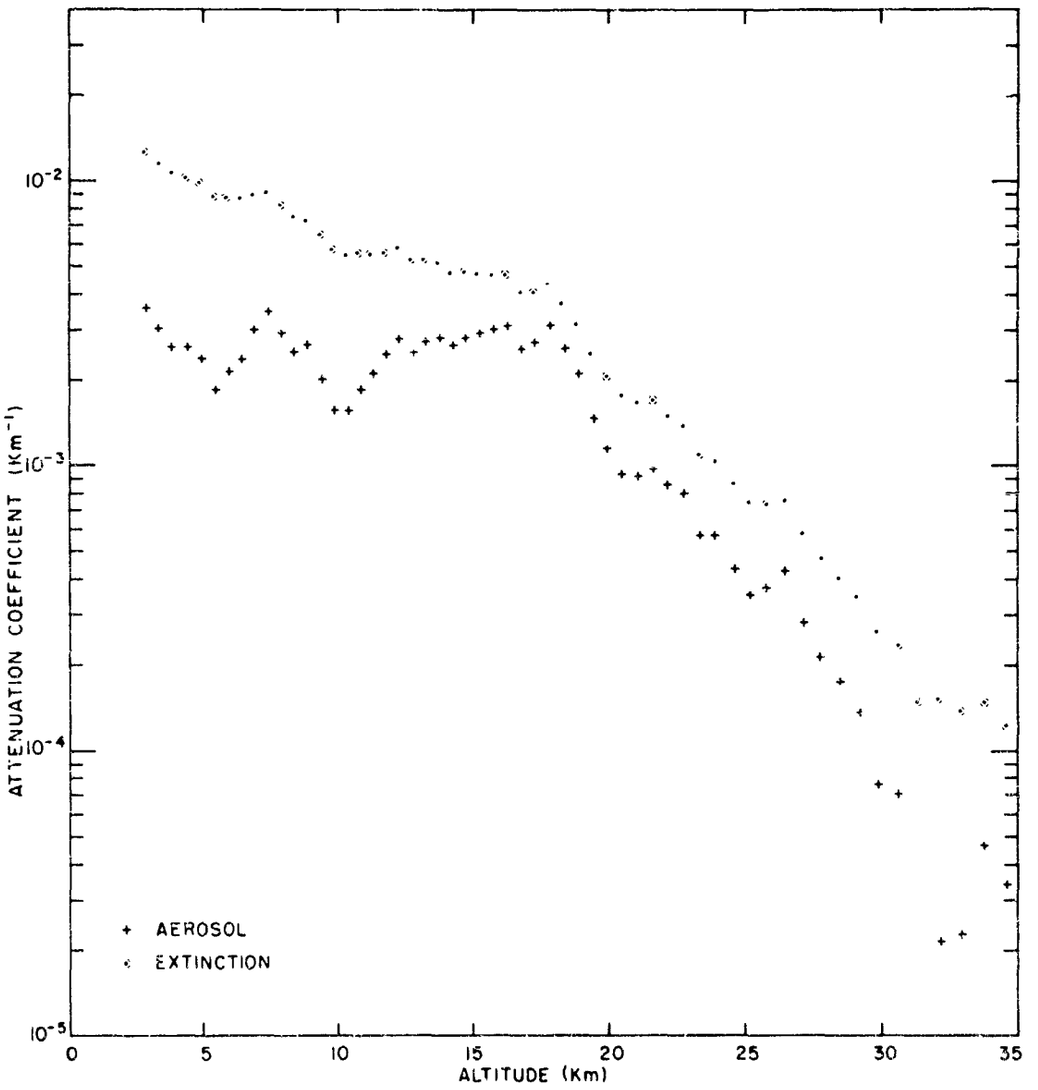

Profile 78. 8 June 1964, Time 22:34

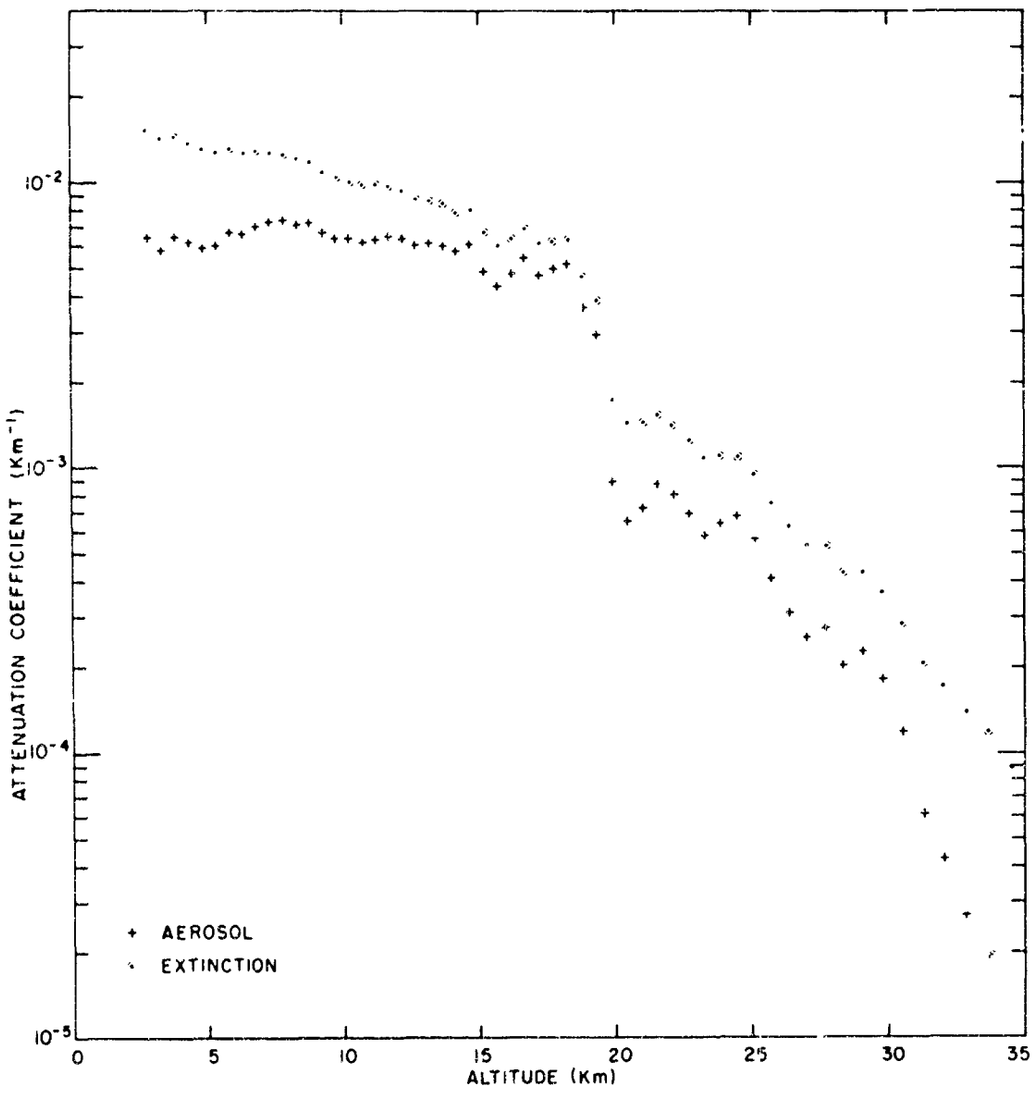

Profile 79. 9 June 1964. Time 01:22

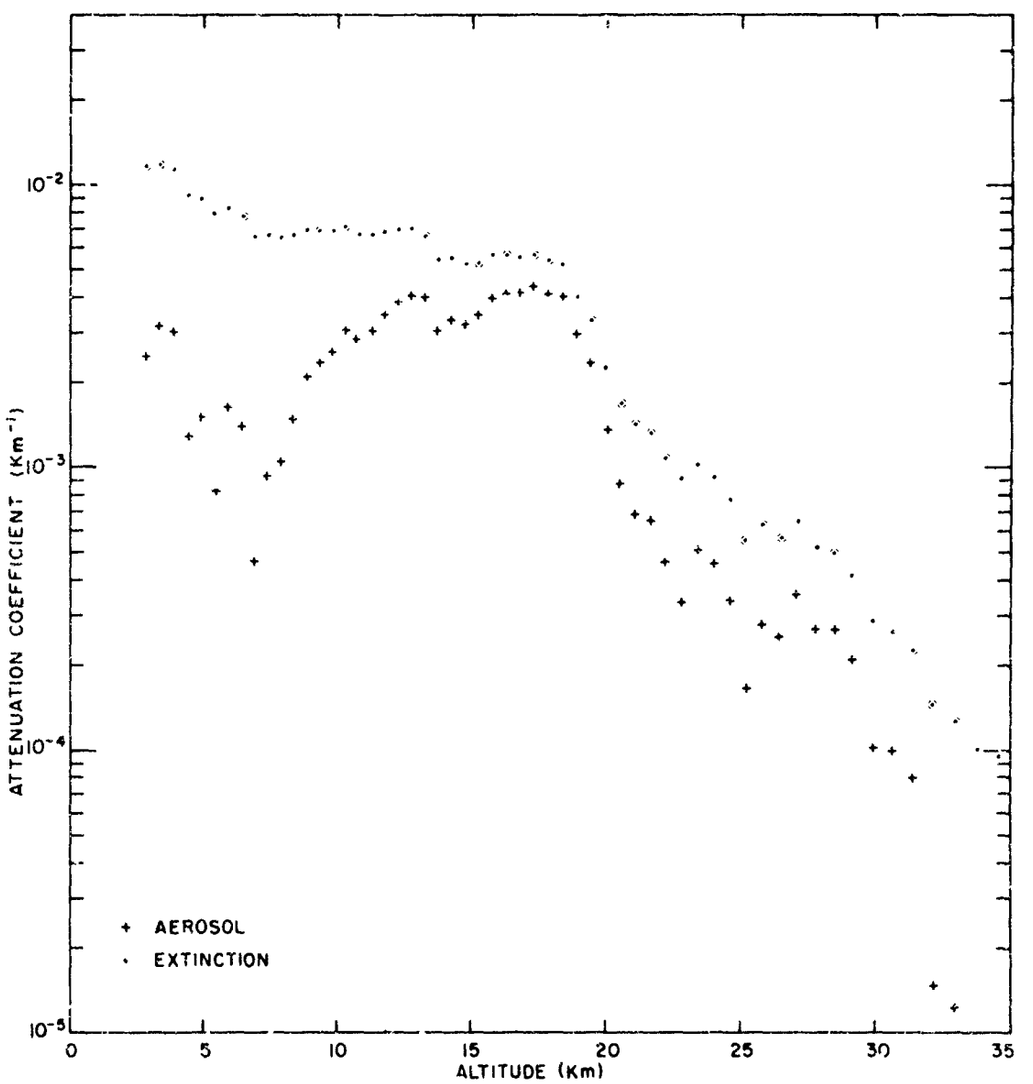

Profile 80. 9 June 1964. Time 02:43

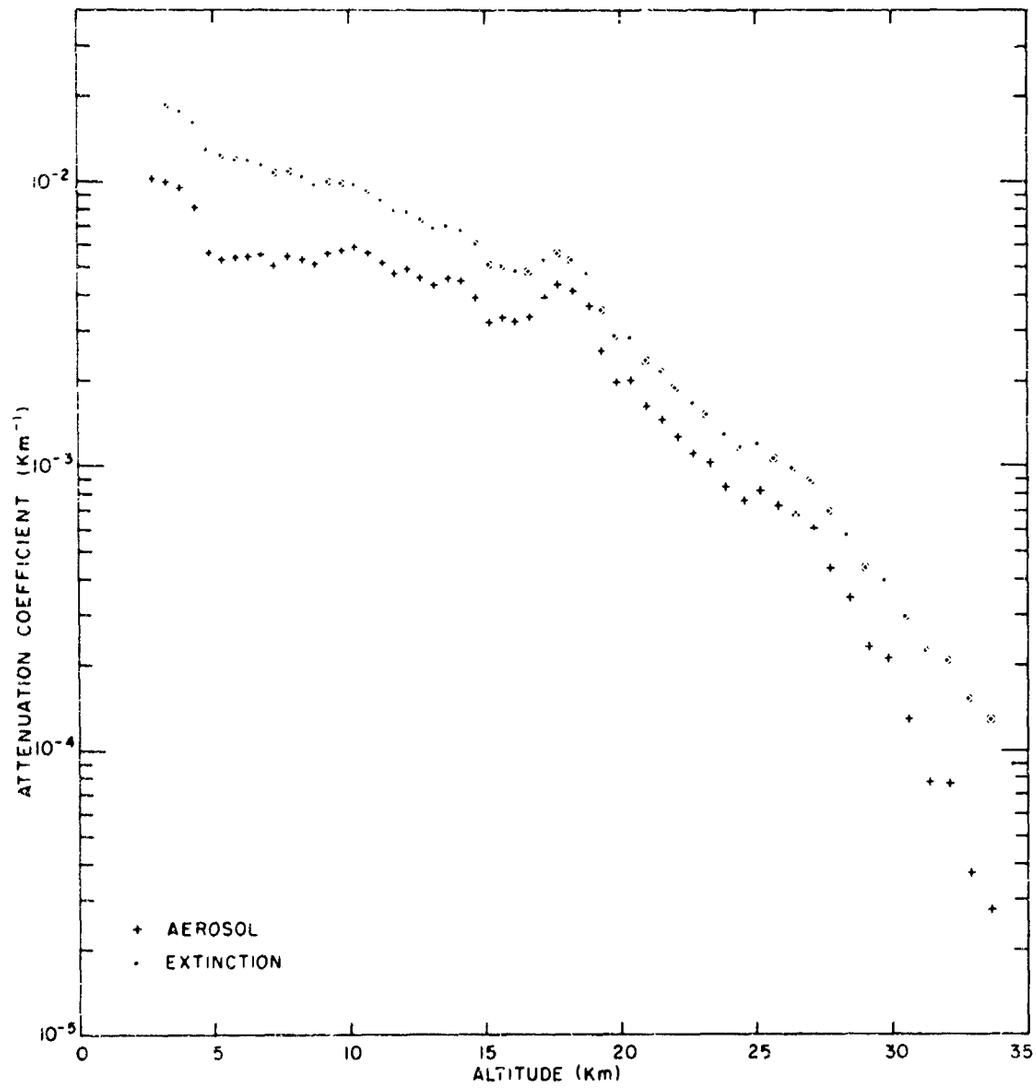

Profile 81. 9 June 1964. Time 20·50

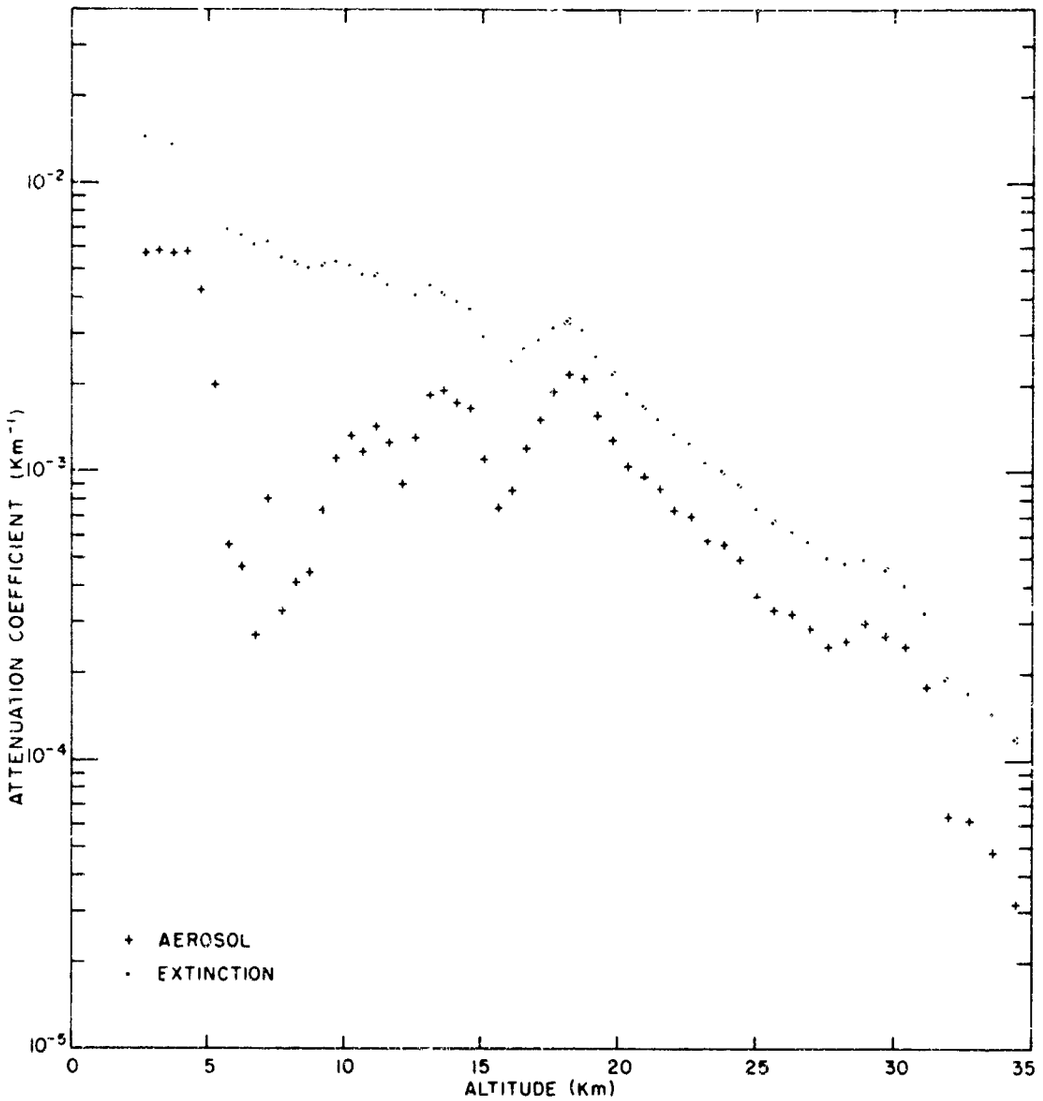

Profile 82, 9 June 1964, Time 22·00

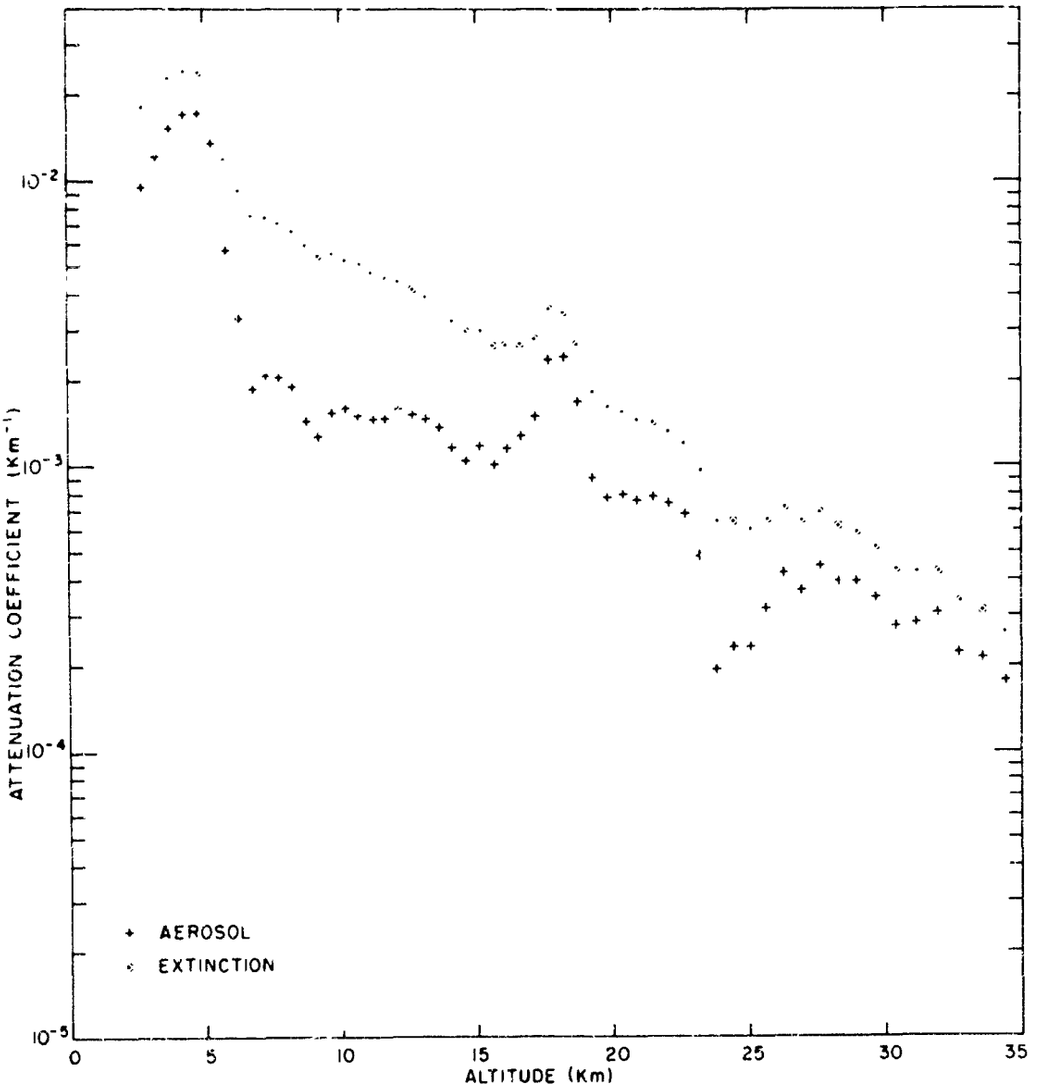

Profile 83, 11 June 1964, Time 00·03

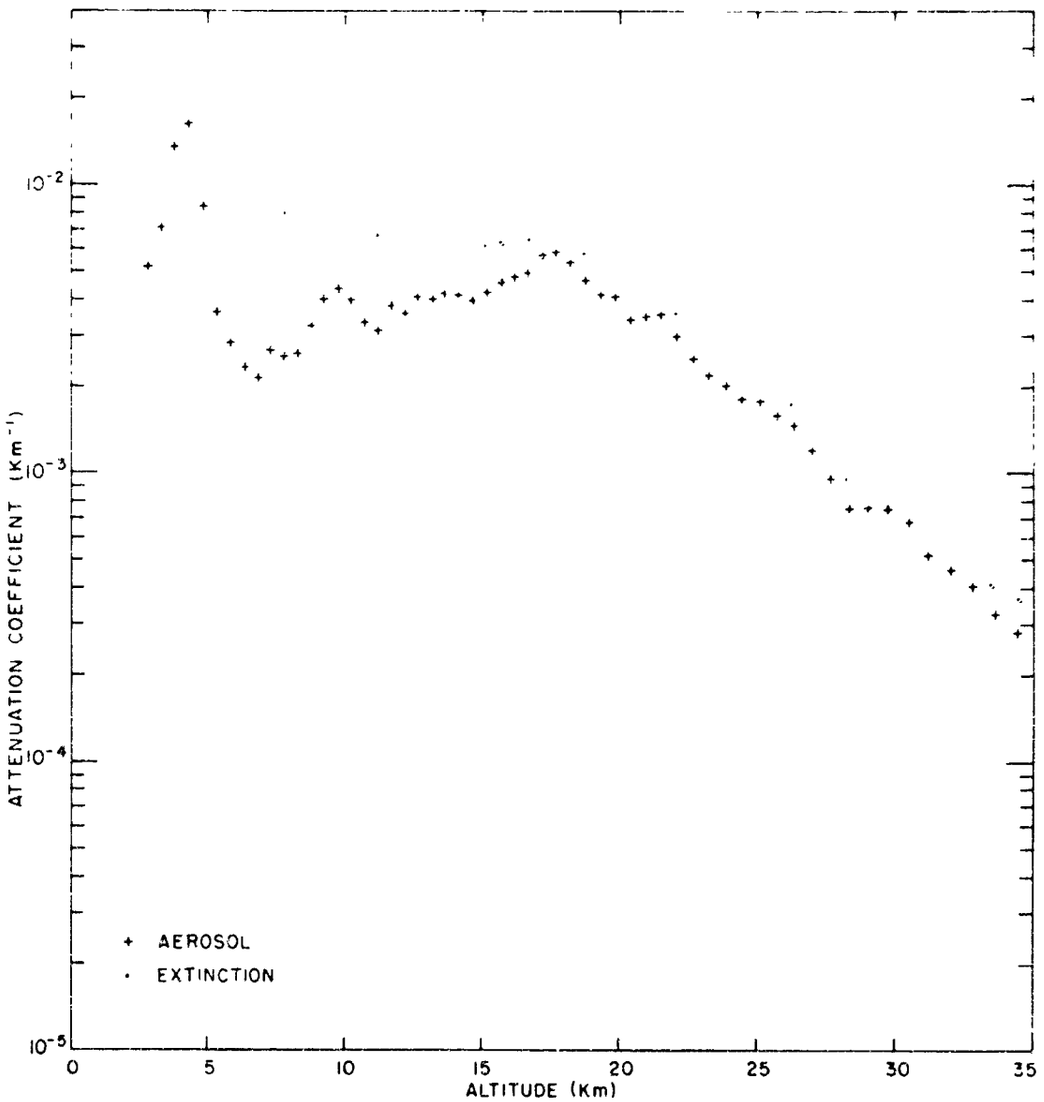

Profile 84. 11 June 1964, Time 21 00

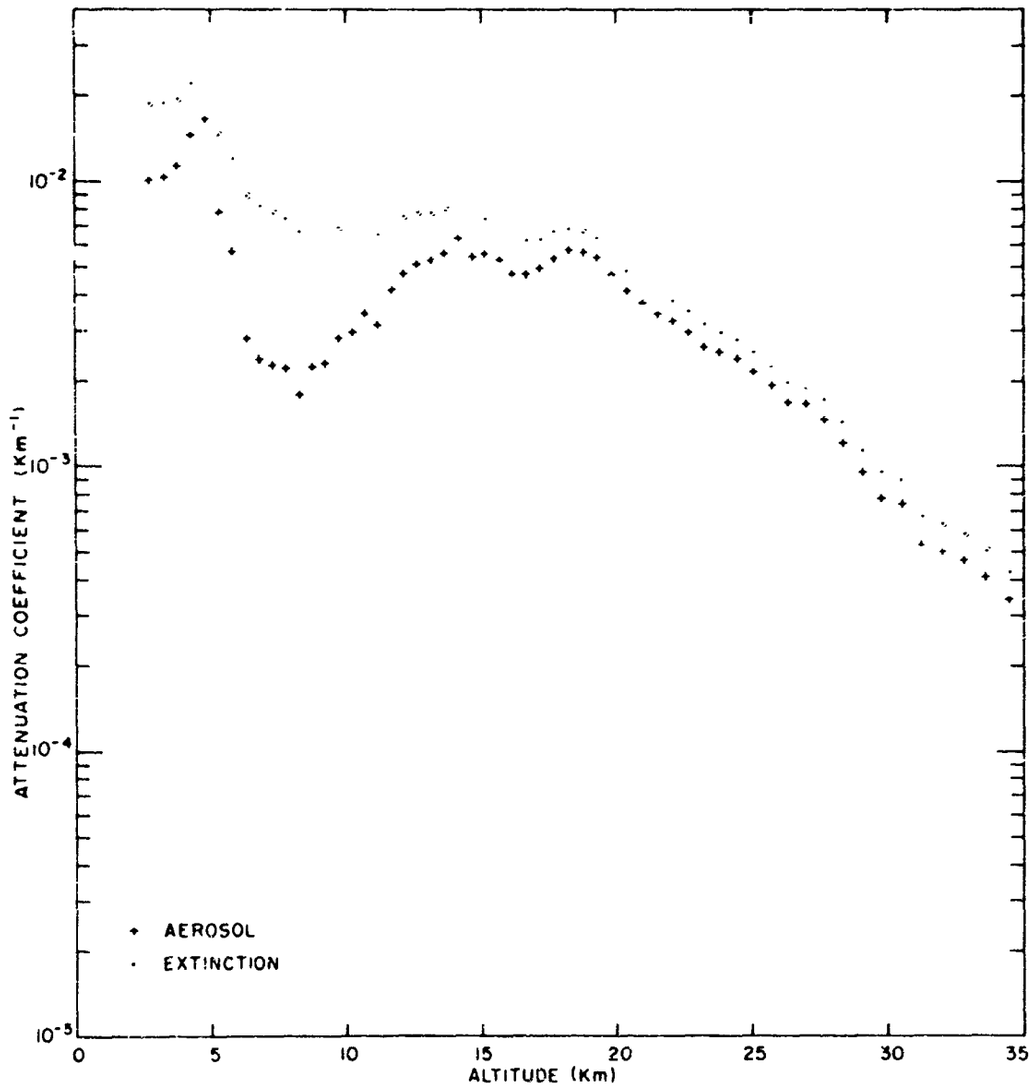

Profile 85. 11 June 1964. Time 23·25

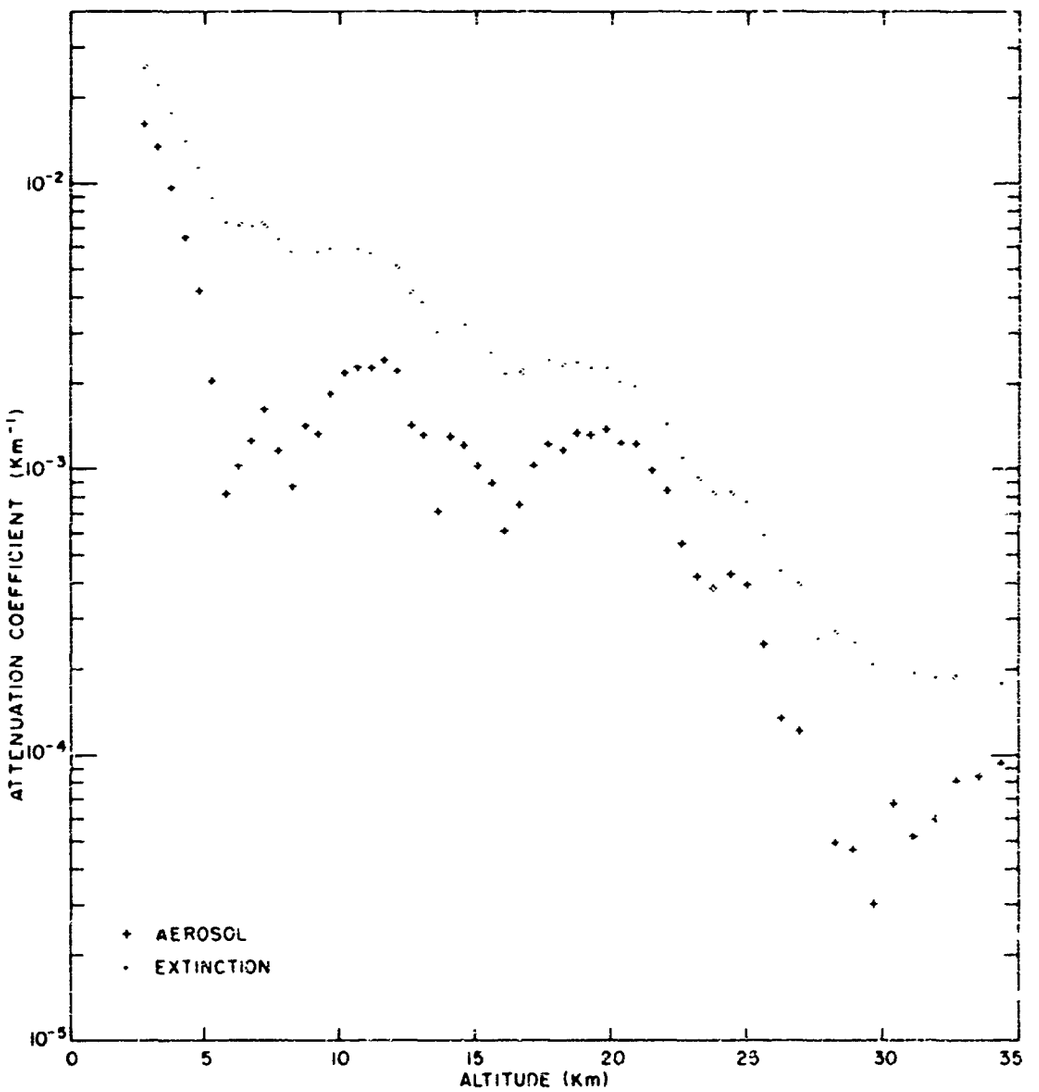

Profile 86. 6 July 1964. Time 01 45

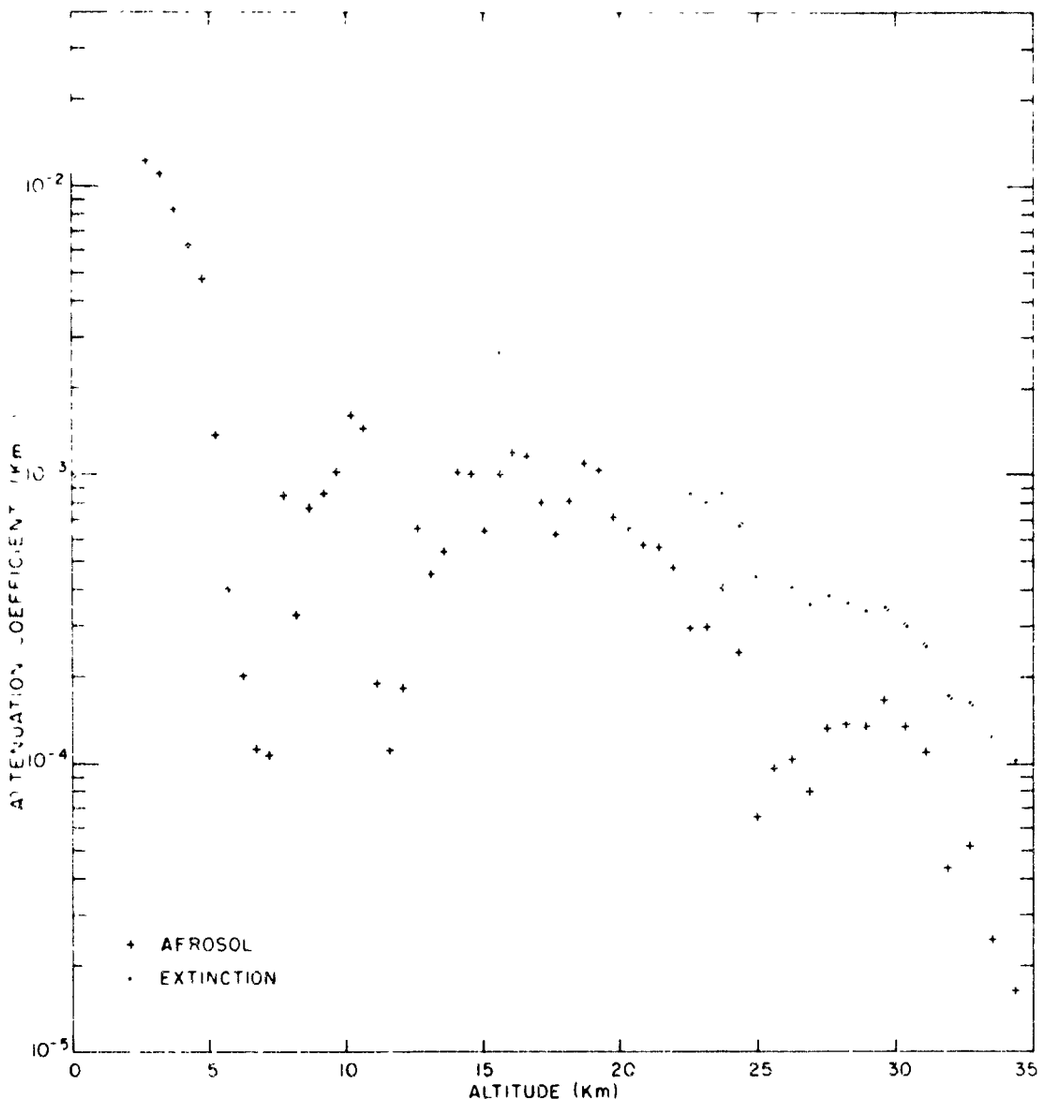

Profile 87$_c$ 6 July 1964. Time 03:05

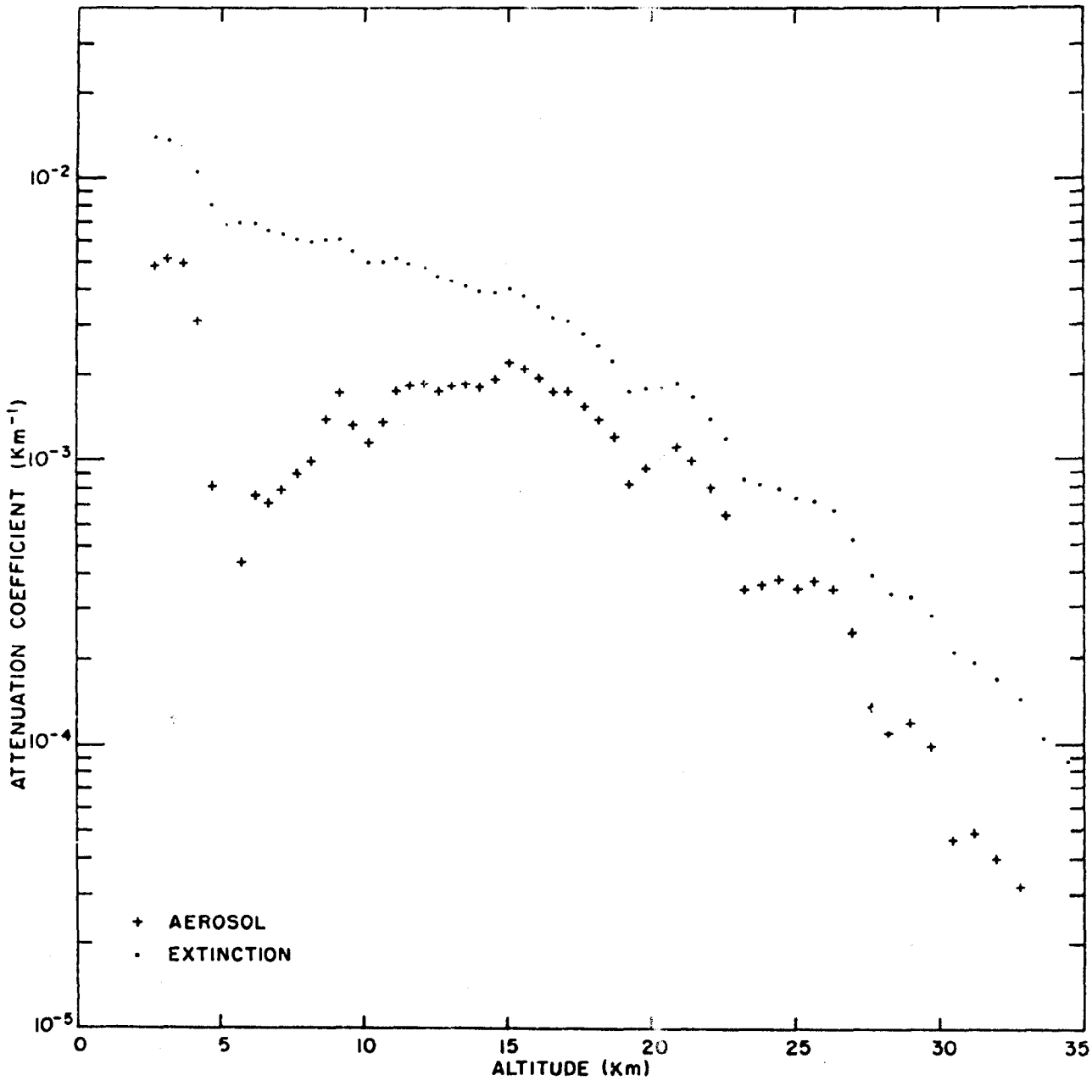

Profile 88. 6 July 1964. Time 22:31

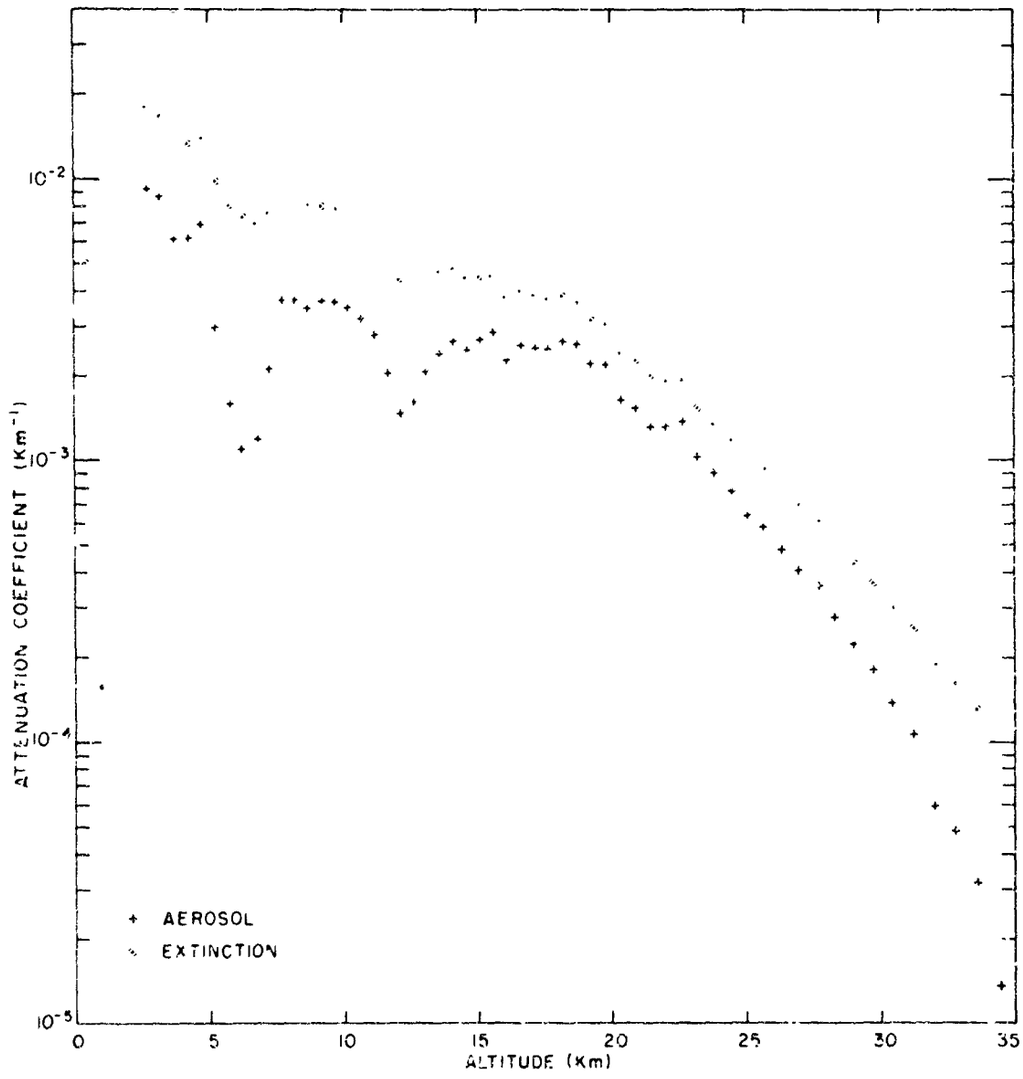

Profile 39, 3 September 1964, Time 00:46

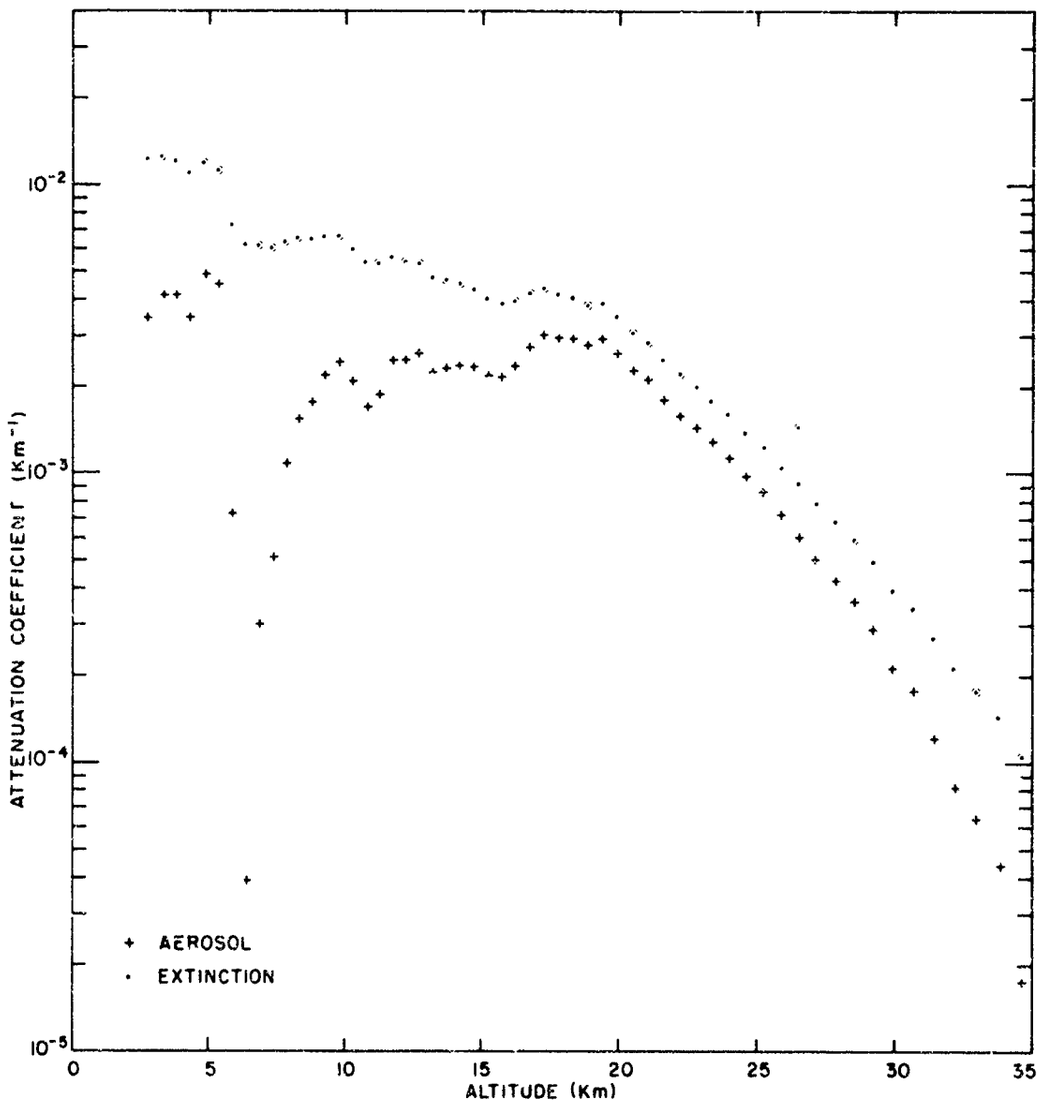

Profile 90. 3 September 1964. Time 01:38

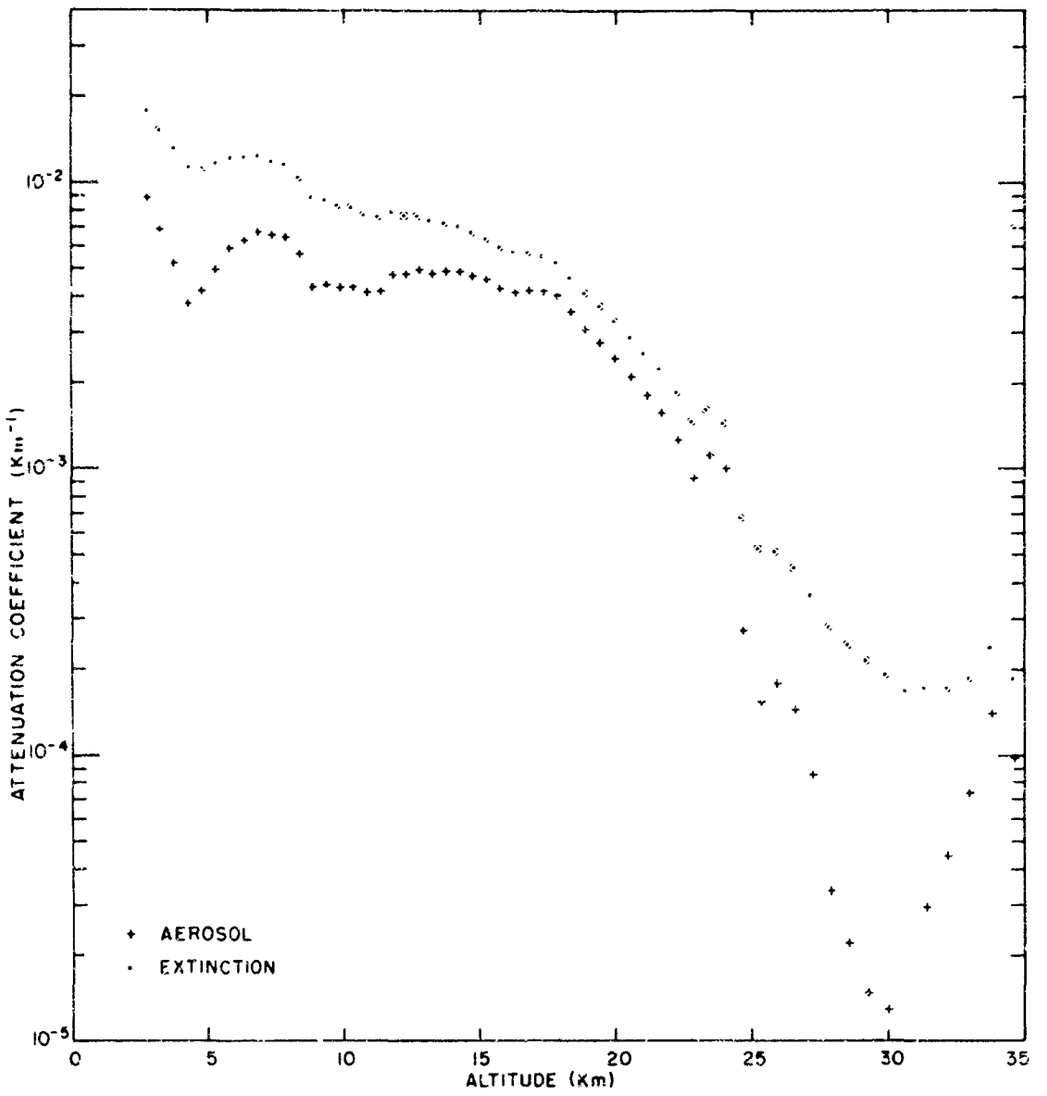

Profile 91. 2 October 64. Time 20:40

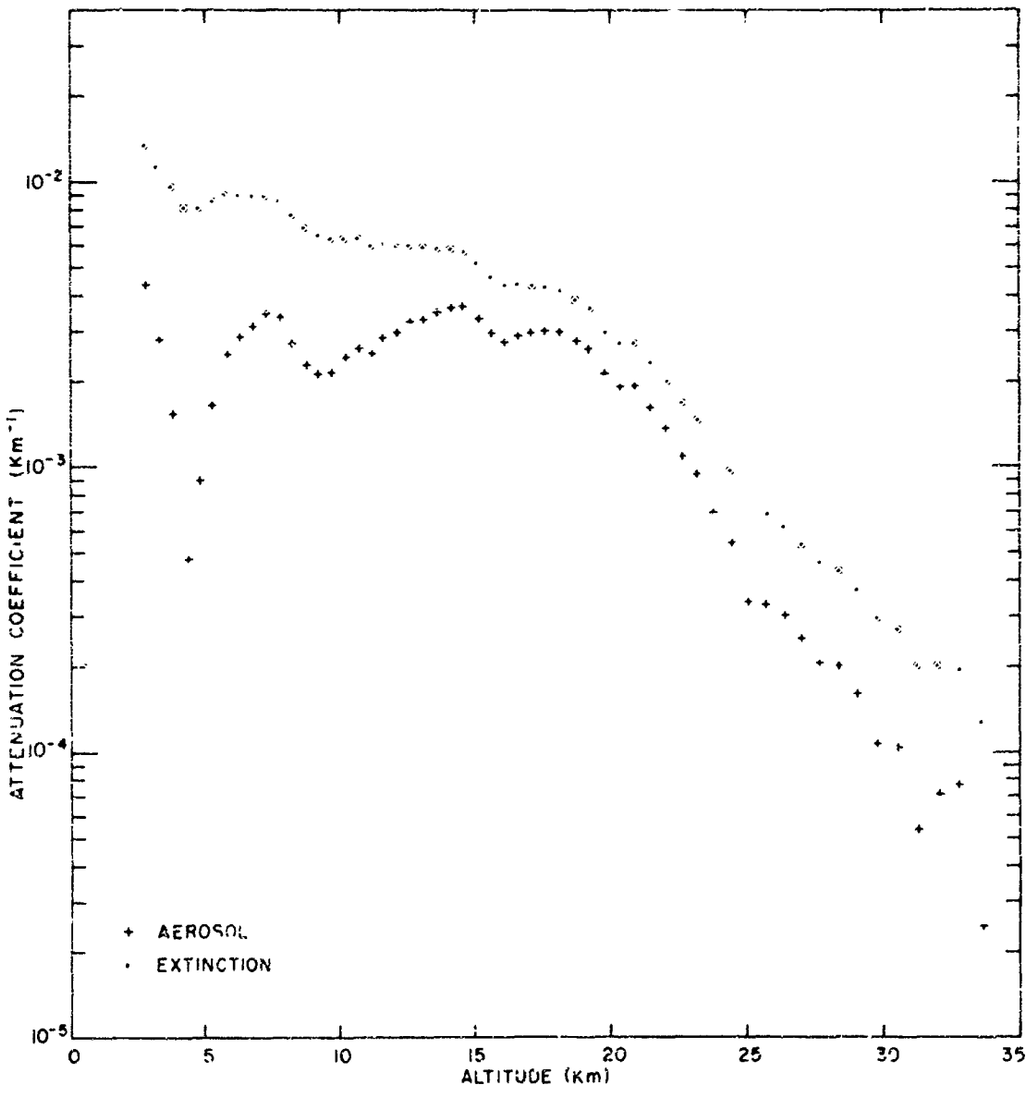

Profile 92. 2 October 1964. Time 22:17

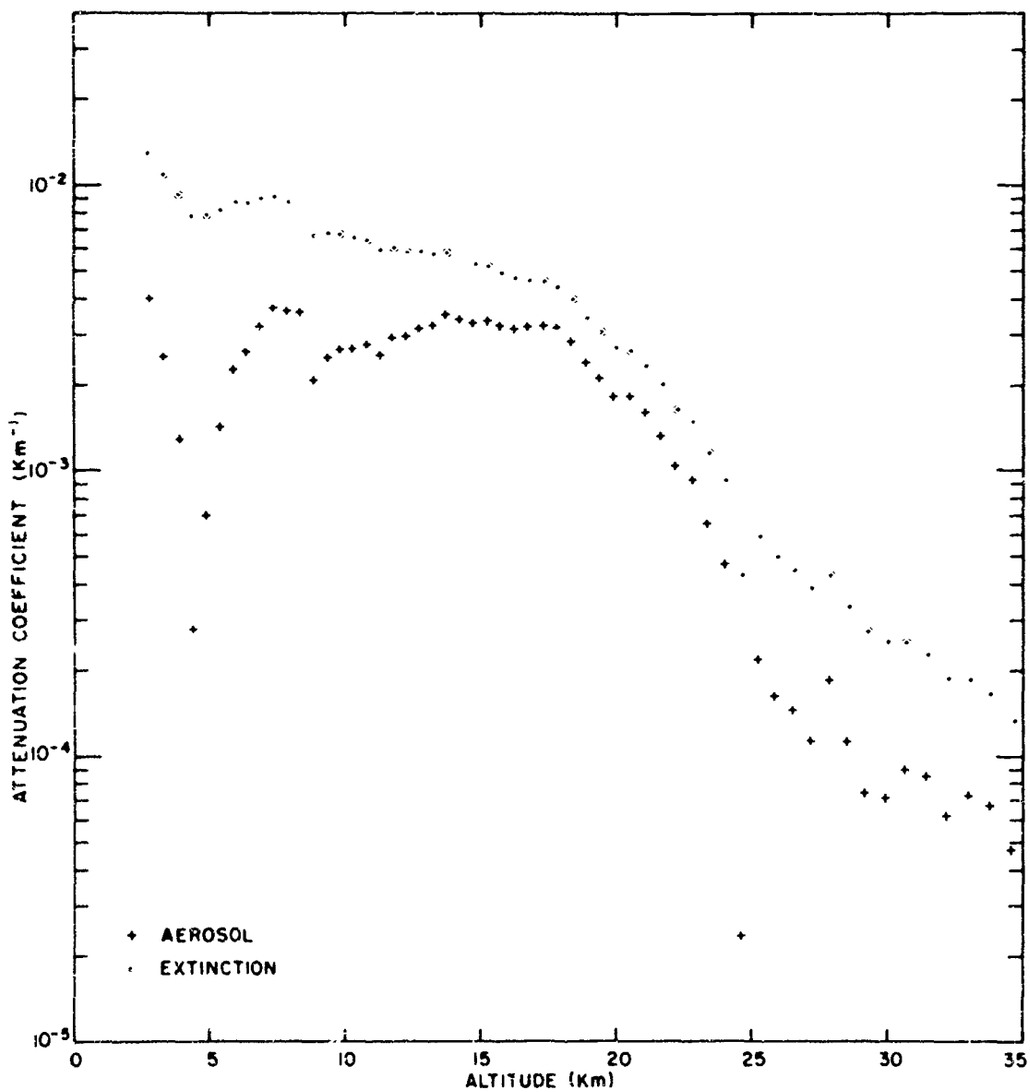

Profile 93. 2 October 1964. Time 23:47

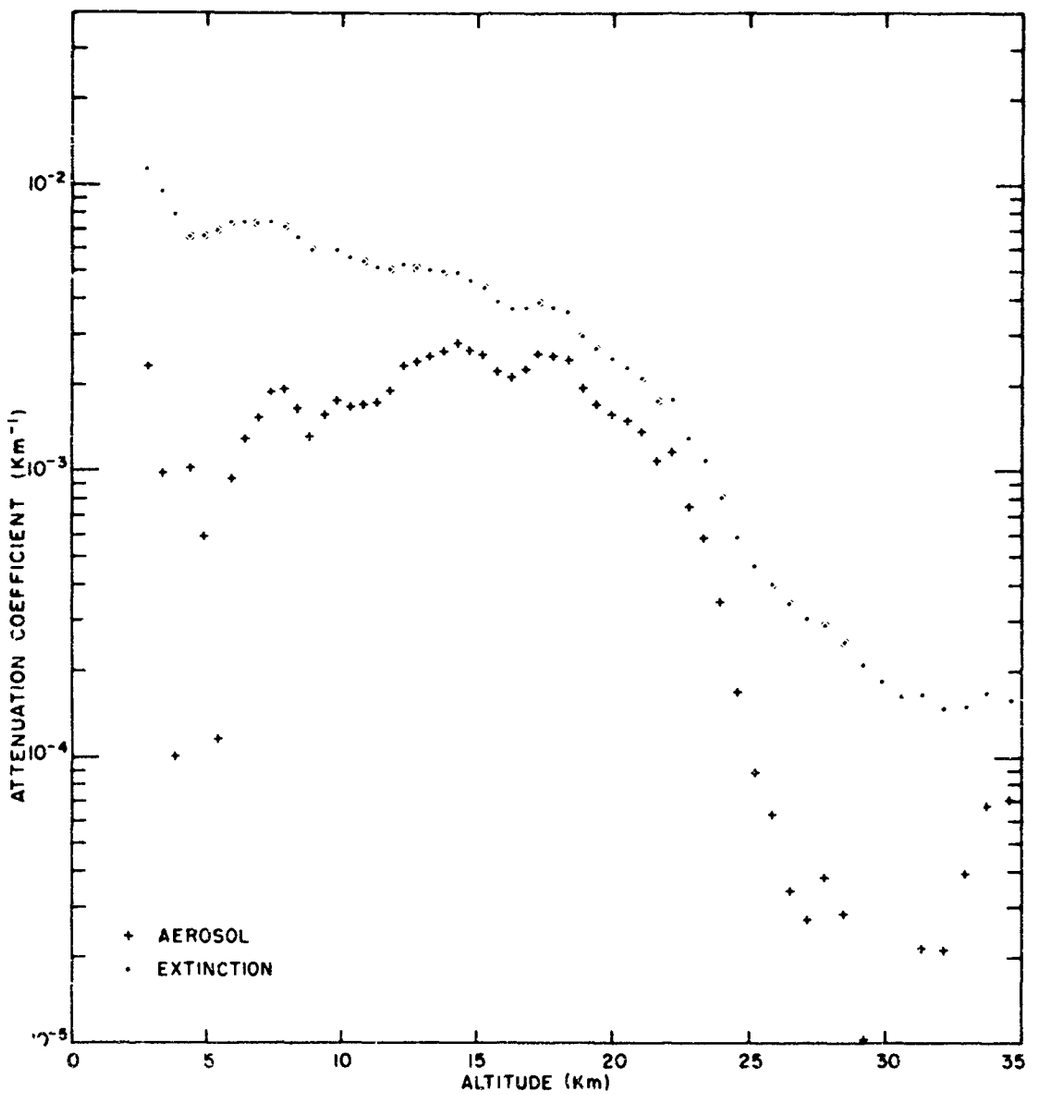

Profile 94. 3 October 1964. Time 01.42

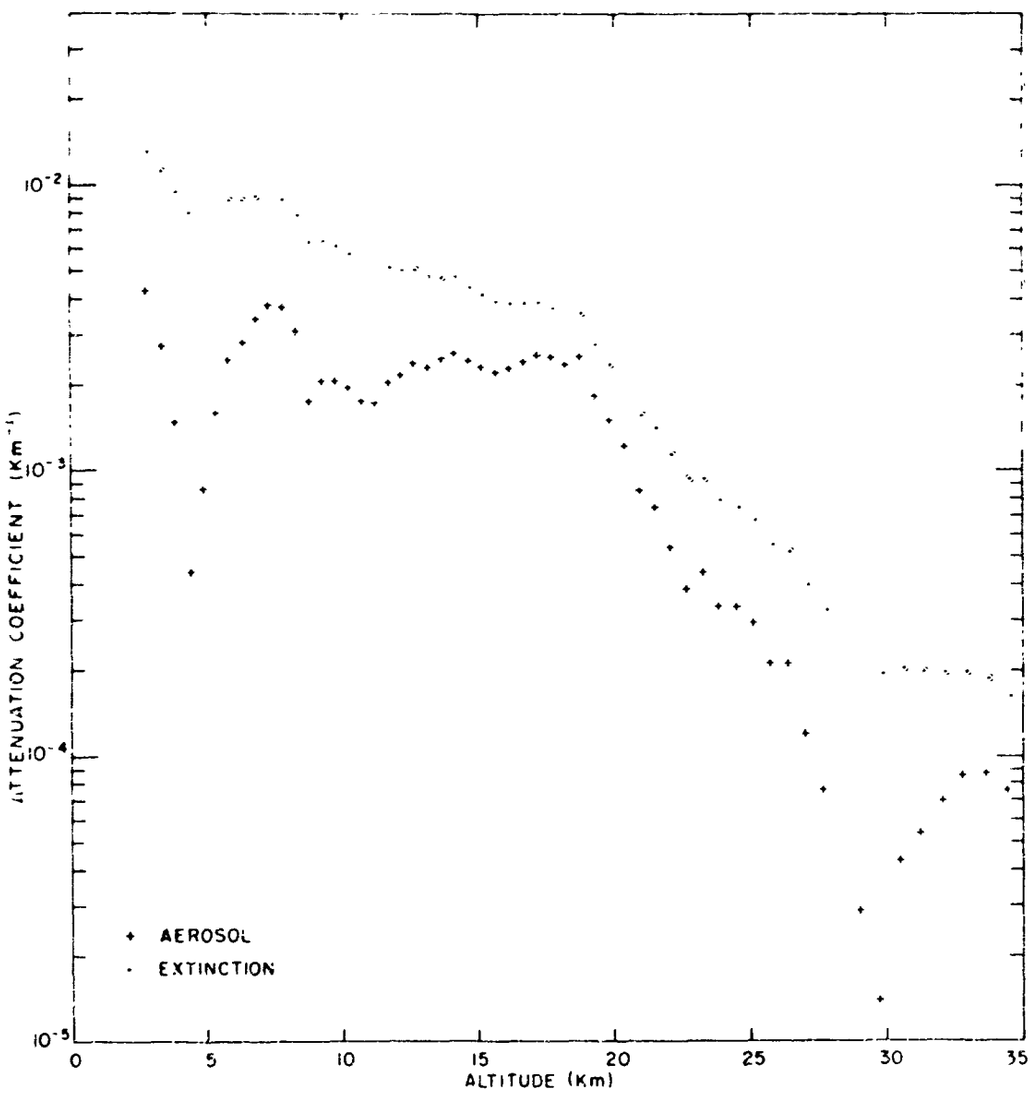

Profile 95, 3 October 1974, Time 03:03

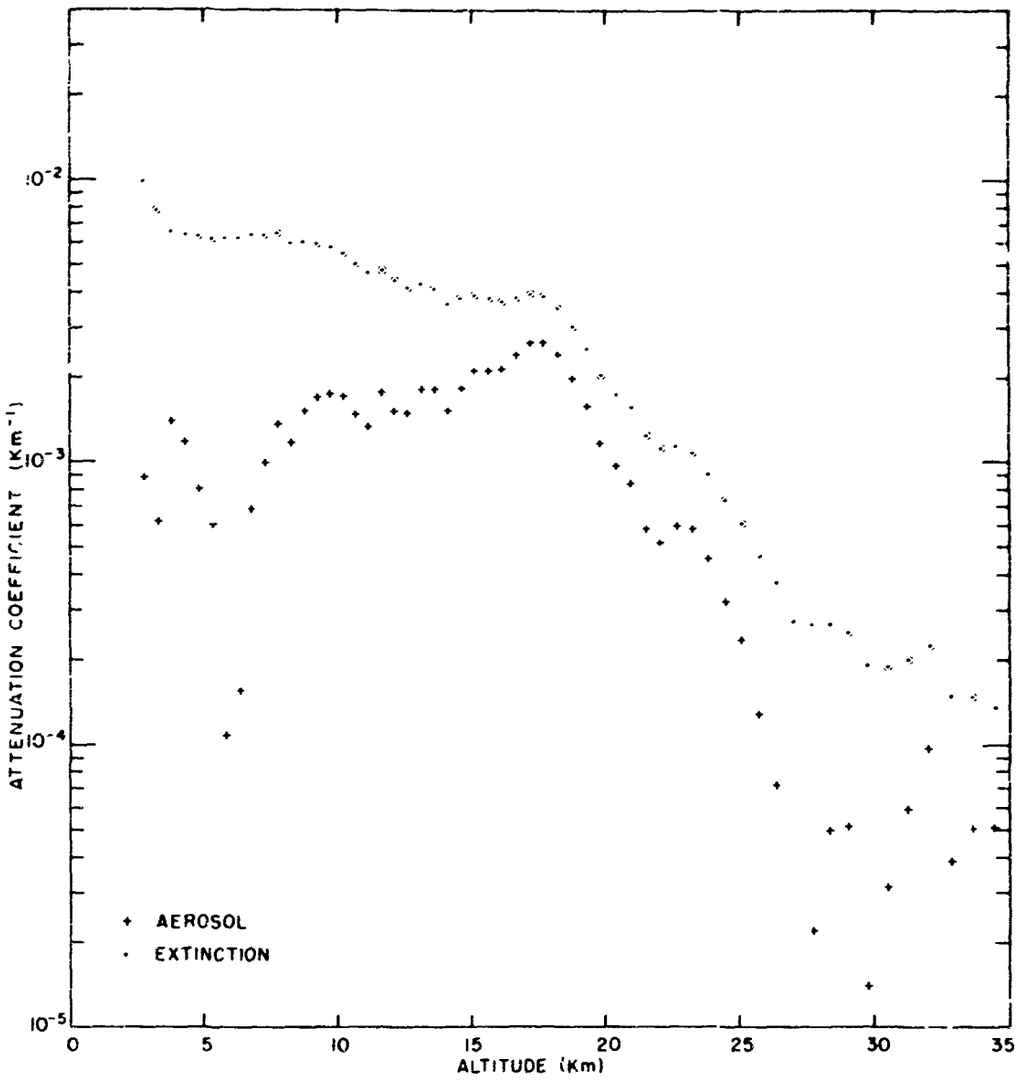

Profile 96. 5 October 1964. Time 19·45

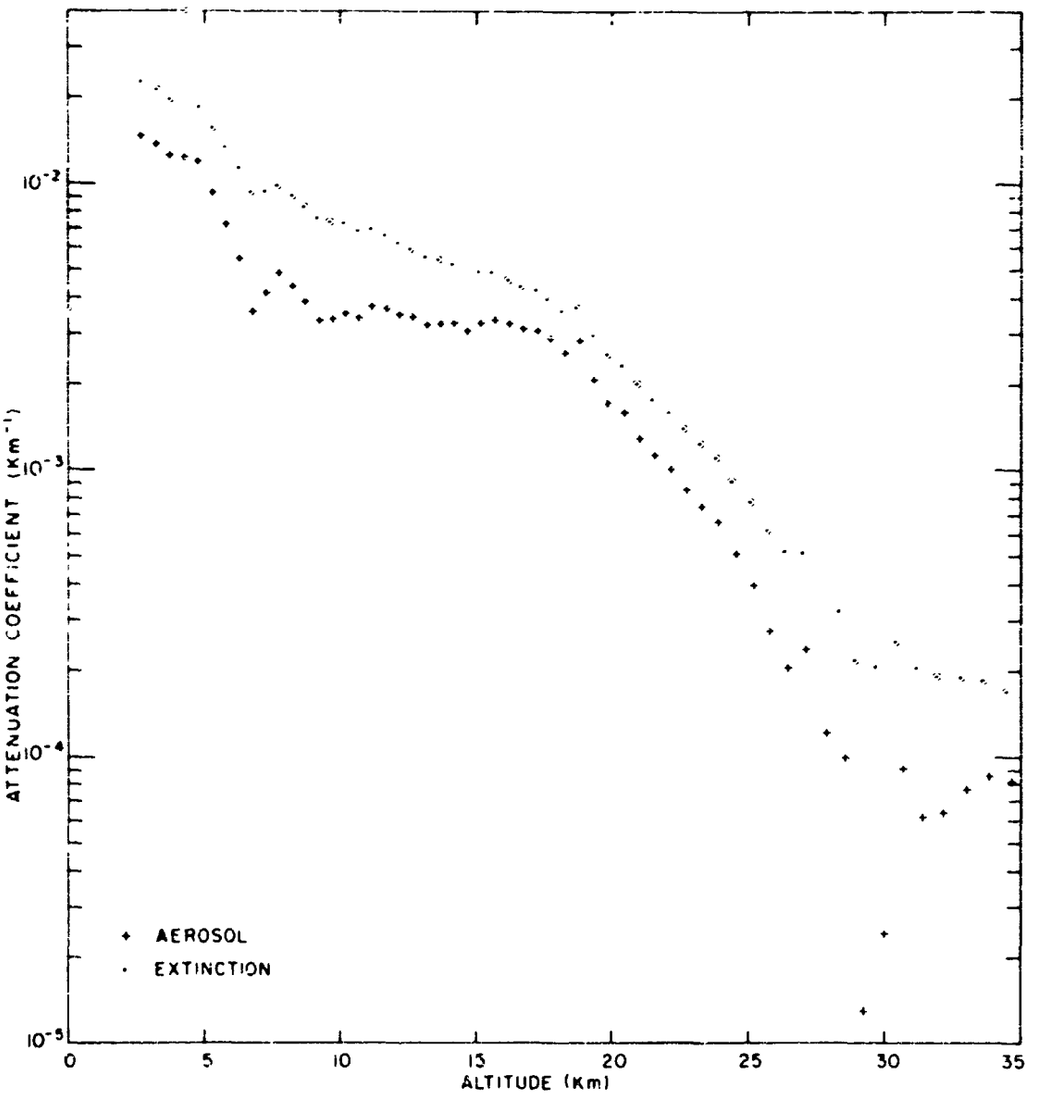

Profile 97, 4 November 1964. Time 02 30

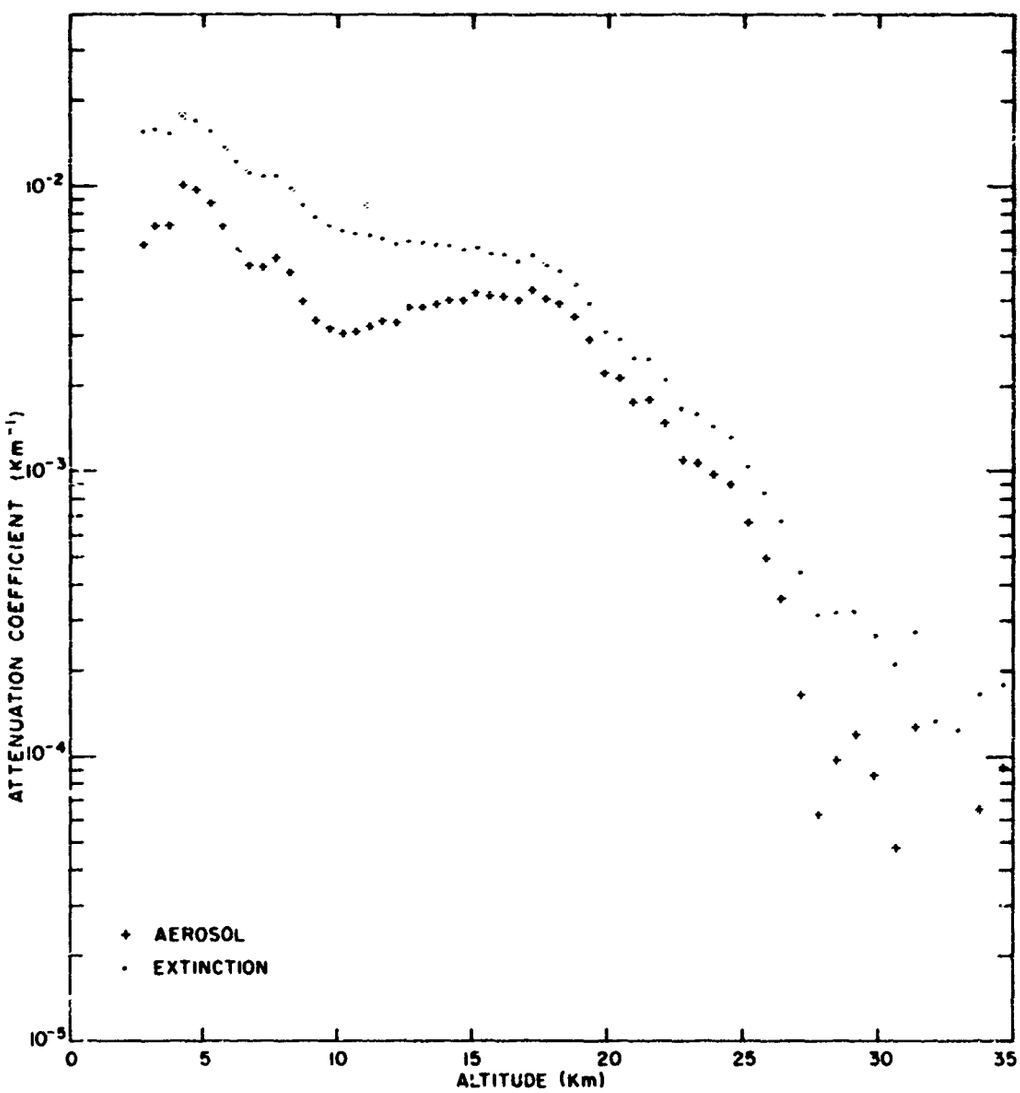

Profile 98. 4 November 1964. Time 04:19

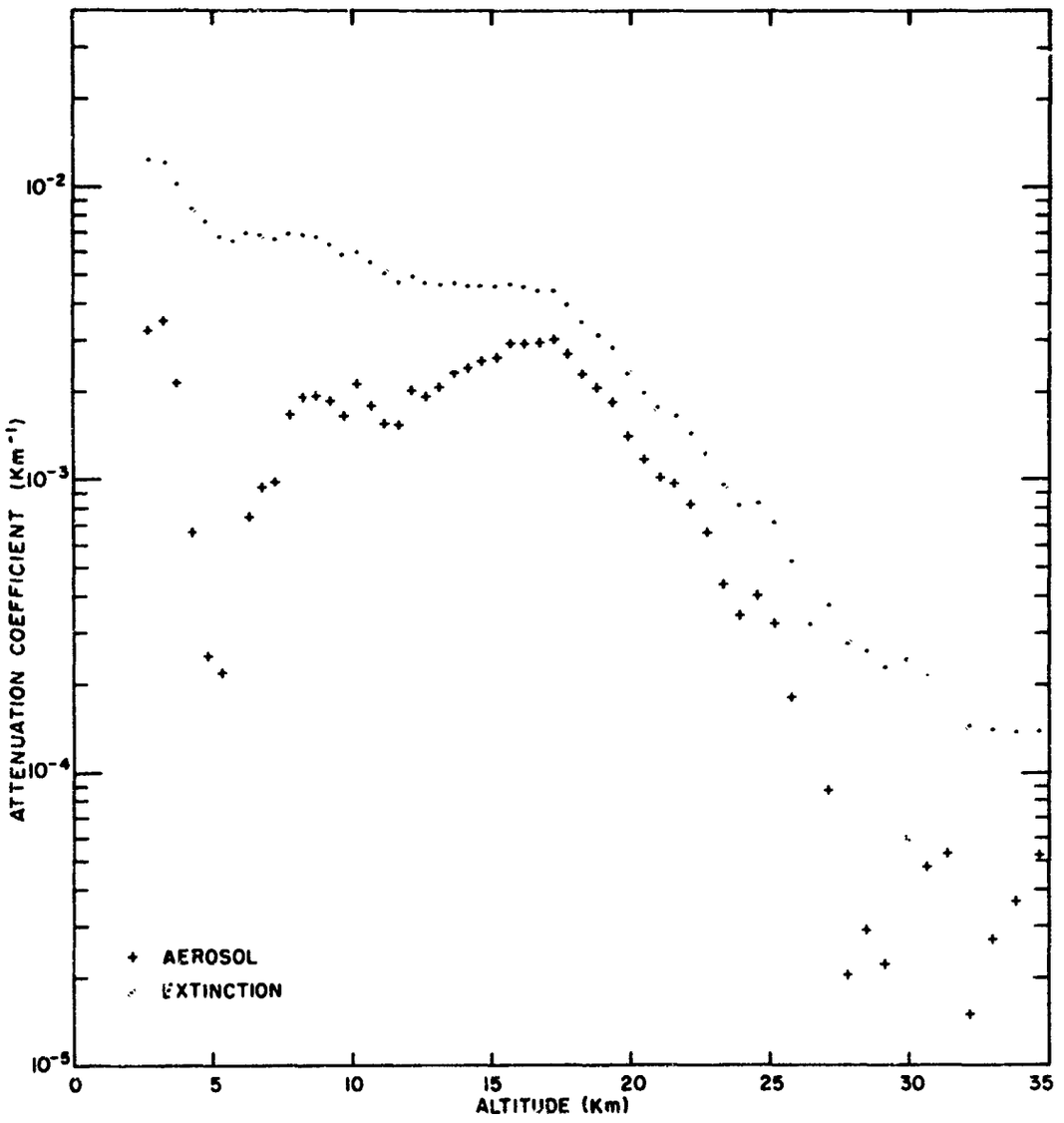

Profile 99. 5 November 1964. Time 22:41

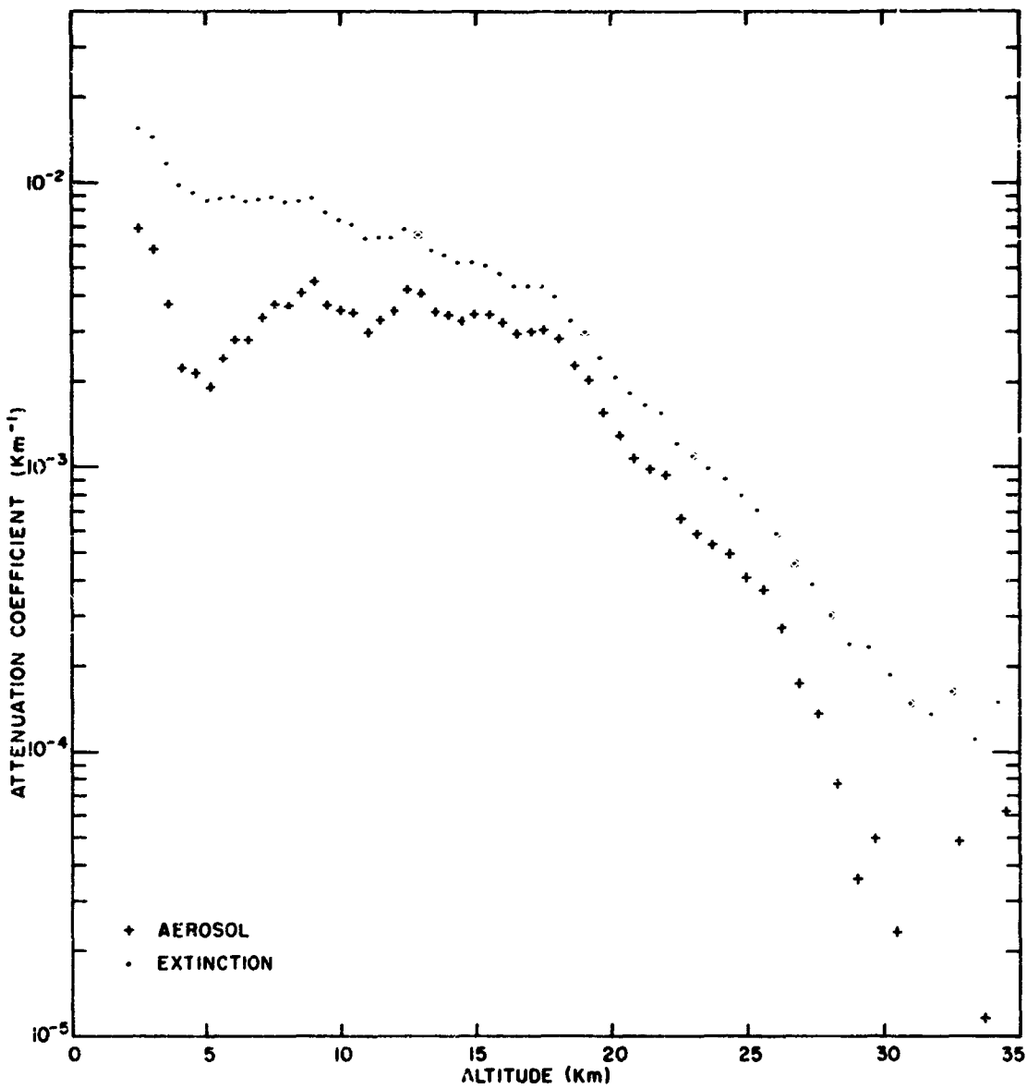

Profile 100. 6 November 1964. Time 00:28

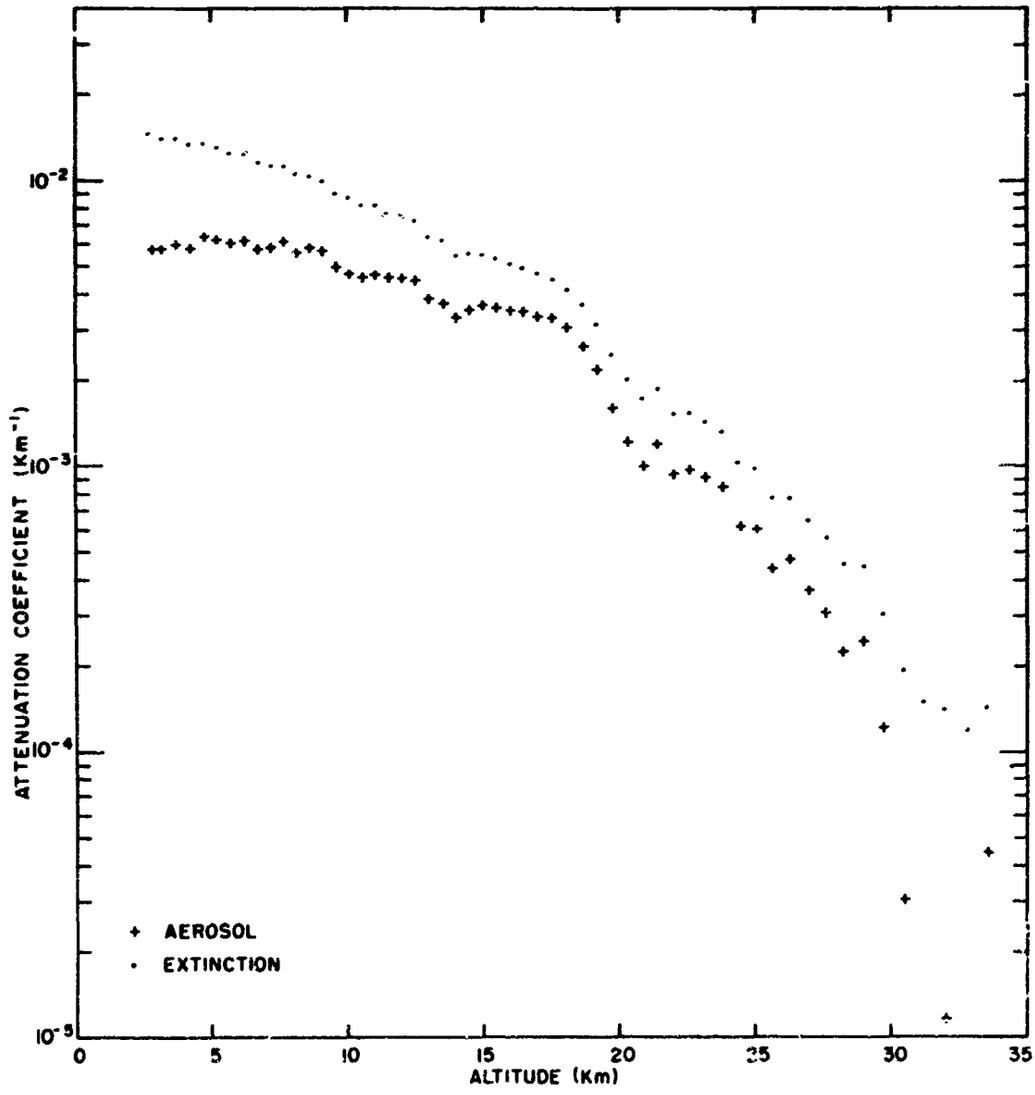

Profile 101. 10 December 1964. Time 22:40

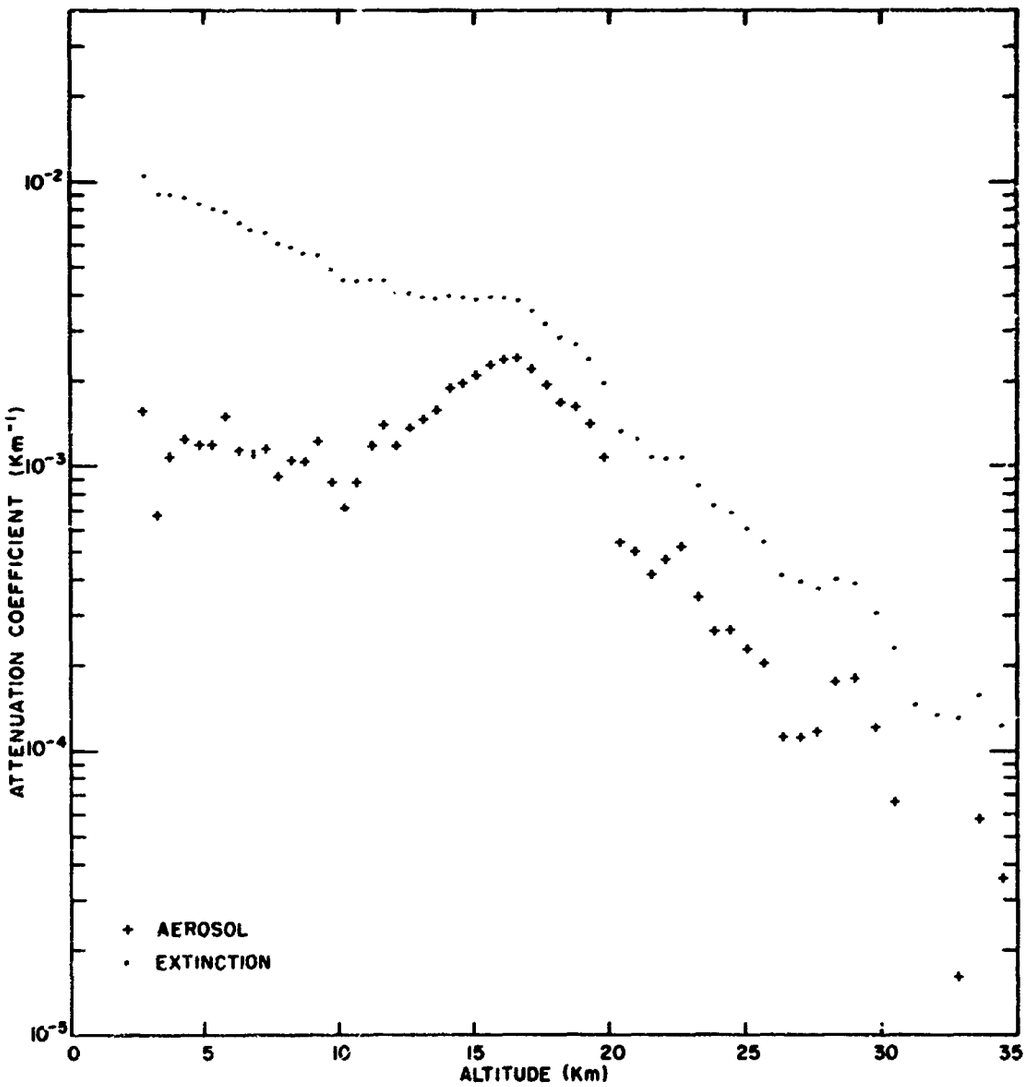

Profile 102. 12 December 1964. Time 00:23

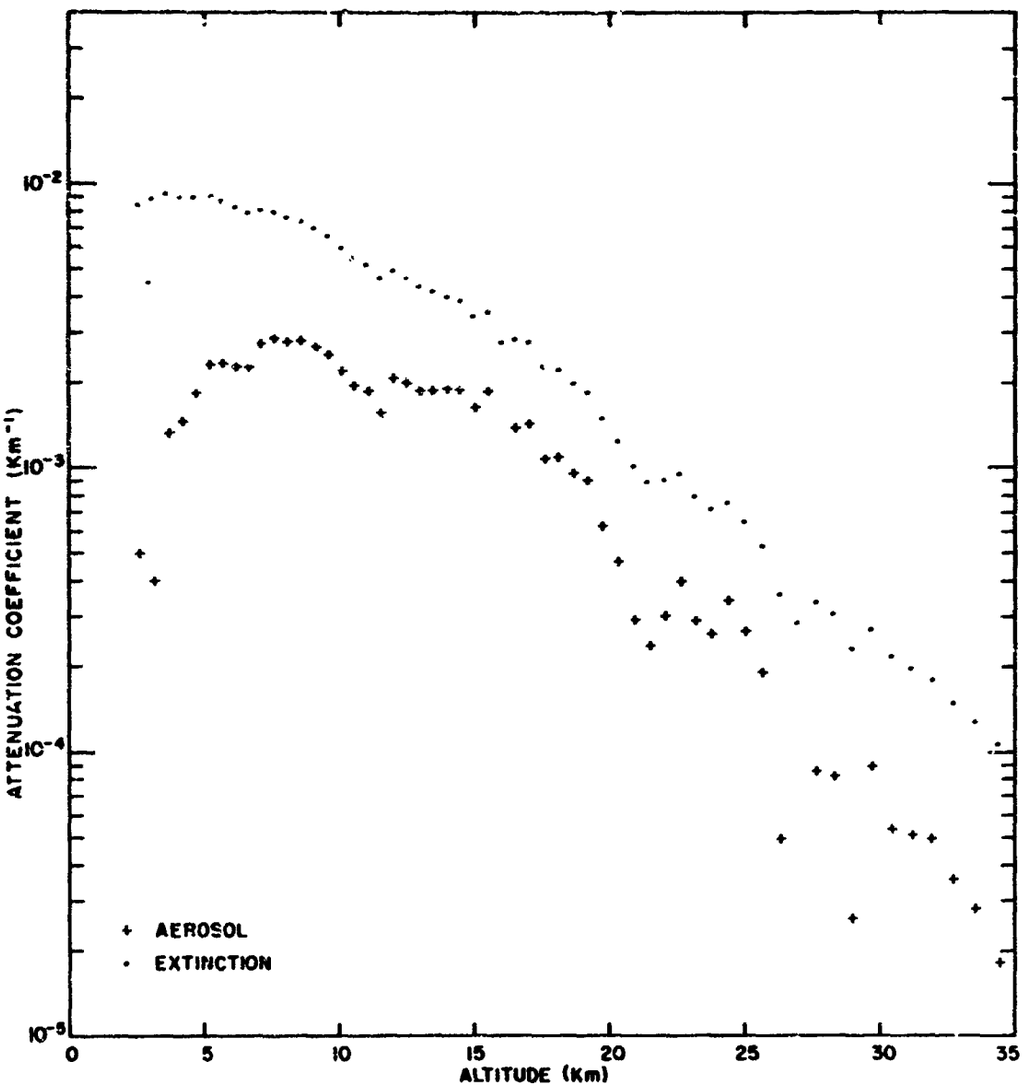

Profile 103. 12 December 1964. Time 02:00

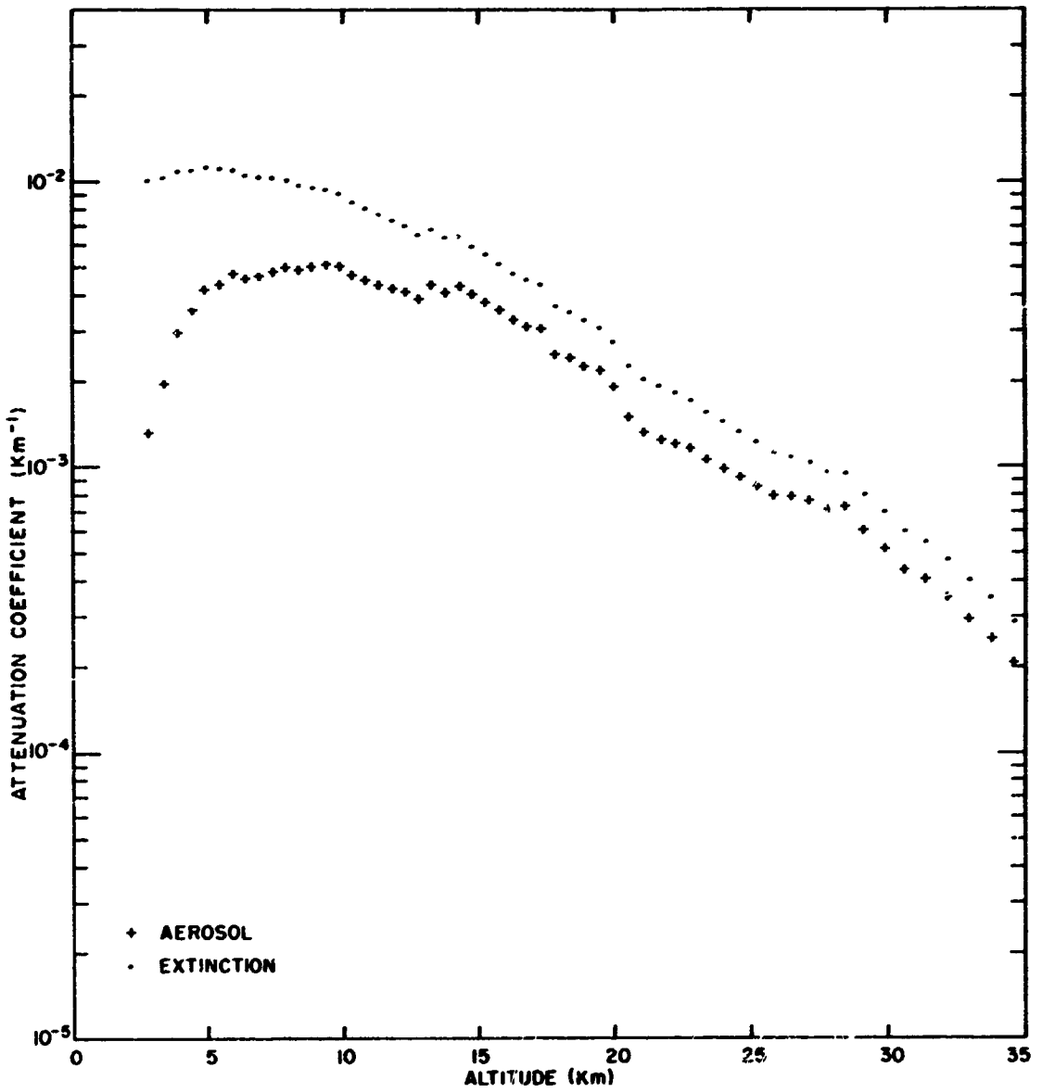

Profile 104. 12 December 1964. Time 03:00

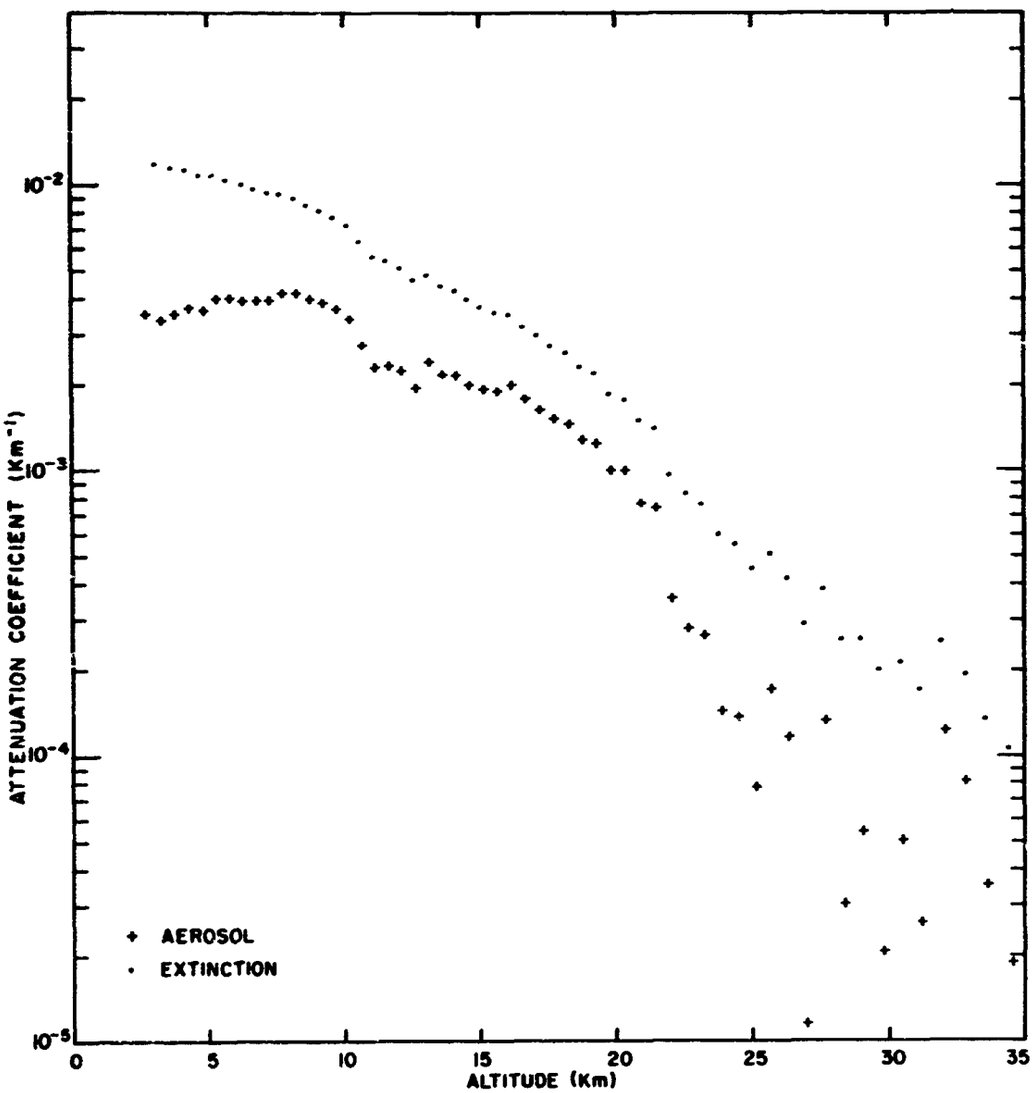

Profile 105. 12 December 1964. Time 03:58

Unclassified
Security Classification

DOCUMENT CONTROL DATA - R&D

(Security classification of title, body of abstract and indexing annotation must be entered when the overall report is classified)

1. ORIGINATING ACTIVITY (Corporate author)
Hq AFCRL, OAR (CRO)
United States Air Force
Bedford, Massachusetts 01730

2a. SECURITY CLASSIFICATION
Unclassified

2b. GROUP
-

3. REPORT TITLE
An Atlas of Aerosol Attenuation and Extinction Profiles for the Troposphere and Stratosphere

4. DESCRIPTIVE NOTES (Type of report and inclusive dates)
Scientific Report. Interim.

5. AUTHOR(S) (Last name, first name, initial)
ELTERMAN, L.

6. REPORT DATE	7a. TOTAL NO. OF PAGES	7b. NO. OF REFS
December 1966	140	13

8a. CONTRACT OR GRANT NO.	9a. ORIGINATOR'S REPORT NUMBER(S)
b. PROJECT AND TASK NO. 7670-04	AFCRL-66-828 ERP No. 241
c. DOD ELEMENT 62405394	9b. OTHER REPORT NO(S) (Any other numbers that may be assigned this report)
d. DOD SUBELEMENT 681000	AFCRL-66-828

10. AVAILABILITY LIMITATION NOTICES
Distribution of this document is unlimited.

11. SUPPLEMENTARY NOTES	12. SPONSORING MILITARY ACTIVITY
	Hq, AFCRL, OAR (CRO) United States Air Force Bedford, Massachusetts 01730

13. ABSTRACT

Light scattering measurements were carried out to determine the aerosol properties of the atmosphere. First the expression for the aerosol attenuation coefficient is derived, based on the field geometry in conjunction with Rayleigh and aerosol scattering considerations. Then the results derived from the measurements are discussed. The paper concludes with an atlas of 105 profiles for altitudes to about 35 km (the data does not exclude the presence of aerosols with low number density between 35 to 70 km). These profiles consist of aerosol attenuation and extinction coefficients as a function of altitude. Since the coefficients are proportional to aerosol number density, the profiles yield information concerning aerosol stratification. A plot for the computed mean of the 105 vertical profiles is included.

DD FORM 1 JAN 64 1473

Unclassified
Security Classification